



## Durham E-Theses

---

### *Penetration of Surfactant Solutions into Capillaries*

DUDGEON, ALEXANDER,PAUL

#### How to cite:

---

DUDGEON, ALEXANDER,PAUL (2011) *Penetration of Surfactant Solutions into Capillaries*, Durham theses, Durham University. Available at Durham E-Theses Online: <http://etheses.dur.ac.uk/585/>

#### Use policy

---

The full-text may be used and/or reproduced, and given to third parties in any format or medium, without prior permission or charge, for personal research or study, educational, or not-for-profit purposes provided that:

- a full bibliographic reference is made to the original source
- a [link](#) is made to the metadata record in Durham E-Theses
- the full-text is not changed in any way

The full-text must not be sold in any format or medium without the formal permission of the copyright holders.

Please consult the [full Durham E-Theses policy](#) for further details.

Department of Chemistry, University of Durham

# Penetration of Surfactant Solutions into Capillaries

A thesis submitted in partial fulfilment of the requirements for the  
degree of Master of Science at the University of Durham



Durham  
University

Alexander Paul Dudgeon  
January 2011

## **Preface**

Please note, a list of nomenclature and defined terms can be found at the end of this thesis in Appendix A and Appendix B.

## **Abstract**

This investigation studies the processes by which water and surfactant solutions penetrate macroscopic, horizontal, hydrophilic glass capillaries. Additional investigations were conducted on some capillaries that are made hydrophobic by being silanised. A laser is shone along the capillary to illuminate the advancing meniscus, so the meniscus is seen as a dot of light, which is detected by a high-speed camera. An investigation on the effect of the presence and type of surfactant aims to reveal the processes by which penetration occurs. Dissipation in the wedge was investigated as a source of deviation from Lucas-Washburn behaviour. Three theoretical models were compared to the experimental data: (I) The Lucas-Washburn model, (II) A “Young” model and (III) Overflowing cylinder model. All these models are shown to be unable to account for the observed penetration rates. The wedge of liquid near the three-phase contact line is considered as a possible additional dissipative mechanism. Penetration of surfactant solutions into capillaries filled with oil is investigated. Due to the viscosity matching effect of this technique, viscous dissipation is constant.

## **Acknowledgments**

The author would like to thank Professor Colin Bain for his excellent supervision, assistance and knowledge, and for allowing me to take on this project. Thanks also need to go to David Woods and Andy McKeague for their assistance with MATLAB programming, Lisong Yang for her knowledge and surface tension data, and the rest of the Bain Group for their assistance, guidance and enjoyment they provided while completing this project.

## Table of Contents

Preface .....	i
Abstract .....	i
Acknowledgments.....	i
Table of Contents .....	ii
Table of Figures.....	v
Chapter 1 Introduction and Theory .....	1
1.1 Aims of the Project .....	1
1.2 Background.....	1
1.2.1 Wetting, Spreading and Young's Equation.....	2
1.2.2 Roughness and Contact Angle Hysteresis .....	3
1.2.3 Capillary Action .....	5
1.2.4 Lucas-Washburn Equation .....	6
1.2.5 Dynamic Contact Angle .....	9
1.2.6 Limitations of Lucas-Washburn Theory .....	11
1.3 Assumptions.....	12
1.3.2 Vertical Rise.....	14
1.3.3 Horizontal Capillaries .....	14
1.3.4 Hydrophobized Capillaries.....	14
1.3.5 Oil Filled Capillaries.....	18
1.4 Dissipation in the Wedge.....	20
1.5 Surfactants .....	23
1.5.1 Introduction .....	23
1.5.2 Adsorption at the liquid/vapour interface.....	24
1.5.3 Adsorption at the solid/liquid interface.....	25
1.5.4 Calculation of dynamic contact angle.....	26
1.5.5 Surfactant Solutions in capillaries .....	26
Bibliography.....	27

Chapter 2 Experimental .....	30
2.5.1 Data Removal .....	39
2.5.2 Pixel Size Calibration .....	39
Bibliography .....	43
Chapter 3 Results and Discussion .....	44
3.1 Experimental Procedures .....	44
3.2 Varying Radius .....	47
3.3 Varying Humidity .....	49
3.4 Varying Salinity .....	52
3.5 Varying SDS Concentration.....	53
3.6 Varying type of surfactant .....	59
3.6.1 CTAB .....	59
3.6.2 Non-ionic Surfactants.....	61
3.7 Hydrophobic Capillaries .....	62
3.8 Oil Filled Capillaries .....	66
3.9 Further Experiments.....	68
3.10 Conclusion.....	69
Bibliography.....	70
Appendices.....	I
Appendix A    Nomenclature.....	I
Appendix B    Defined Terms .....	II
Capillary Number.....	II
Reynolds Number.....	II
The ratio of inertial to viscous forces .....	II
Capillary Length .....	II
Characteristic length scale of the meniscus due to gravity and surface tension <sup>1</sup> .....	II
Capillary Pressure.....	II
The difference in pressure across the interface between two immiscible liquids.....	II
Capillary Force.....	II

The force by which water penetrates a capillary .....	II
Drag .....	II
Péclet number.....	II
Young-Laplace Equation .....	III
Lucas-Washburn Equation.....	III
Weber Number.....	III
Quére Equation.....	III
Bibliography.....	III
Appendix C    MATLAB Code.....	IV
rulerfft Function.....	IV
imageprocess Function.....	V
lp_filtery Function .....	IX
my_intilt Function .....	IX
getRotation Function.....	XI

## Table of Figures

Figure 1.1 – Complete wetting case.....	2
Figure 1.2 – Nonwetting case.....	2
Figure 1.3 – Partial wetting case.....	2
Figure 1.4 – The three-phase contact line .....	3
Figure 1.5 – Apparent pinning of a contact line on a defect edge.....	4
Figure 1.6 – Pressures on a fluid in a capillary.....	5
Figure 1.7 – Viscous dissipation .....	7
Figure 1.8 – Parabolic velocity profile of meniscus .....	8
Figure 1.9 – Height of the meniscus (in millimetres) as a function of time (in milliseconds), for a vertical glass tube of radius $r = 689$ mm put into contact at $t = 0$ with an infinite bath of ethanol .....	13
Figure 1.10 – Capillary rise dynamics observed for $C_{14}E_6$ surfactant solutions (hydrophobic capillary, radius 0.1 mm .....	16
Figure 1.11 – (A) Flow profile in hydrophobic capillary in the moving frame of reference. (B) Flow profile in an overflowing cylinder in the stationary frame.....	17
Figure 1.12 – Wedge model.....	20
Figure 1.13 – Close up of wedge.....	20
Figure 1.14 – Velocity profile at meniscus .....	21
Figure 1.15 – (1) Adsorption isotherms of SDS at the air/water interface .....	25
Figure 1.16 – Surface excess against CTAB concentration for a silica-water interface .....	26
Figure 2.1 – The capillary mount.....	33
Figure 2.2 – Experimental setup .....	34
Figure 2.3 – Before background subtraction.....	38
Figure 2.4 – Video frame after background subtraction .....	38
Figure 2.5 – An example of the raw data output from the MATLAB program after zero finding .....	39
Figure 2.6 – Ruler calibration image.....	40
Figure 2.7 – Water meniscus (circled) moving along a $3\mu\text{l}$ capillary.....	40
Figure 2.8 – The difference before (A) and after (B) contact of the capillary with the meniscus.....	41
Figure 2.9 – MATLAB image analysis .....	41
Figure 3.1 – Distance-time graph for $3\mu\text{l}$ capillaries and water.....	45
Figure 3.2 – Distance – square-root time plot for $3\mu\text{l}$ capillaries and water .....	46
Figure 3.3 – Distance-time plot for all sizes.....	47

Figure 3.4 – Slope vs. square-root radius and Lucas-Washburn (L-W) prediction for $\theta=0^\circ$ .....	48
Figure 3.5 – Distance vs. time curves at normal and high humidity for pure water in 1 $\mu\text{l}$ capillaries.....	51
Figure 3.6 – Distance square-root time plot for high humidity for 1 $\mu\text{l}$ capillaries.....	51
Figure 3.7 – Slope vs. [NaCl] for 1-3 $\mu\text{l}$ capillaries.....	52
Figure 3.8 – Distance vs. time plots with and without SDS present for 1 $\mu\text{l}$ capillaries .....	54
Figure 3.9 – Comparison of slopes with and without the presence of SDS for 1 $\mu\text{l}$ capillaries (conc. 0.0164 mol dm <sup>-3</sup> ). Three independent runs for each case are shown.....	54
Figure 3.10 – Plot of slope vs. [SDS] with Lucas-Washburn prediction for 1 $\mu\text{l}$ capillaries.	55
Figure 3.11 – Ln [SDS] vs. surface tension <sup>3</sup> .....	56
Figure 3.12 – Slope vs. [SDS] (log scale) with Lucas-Washburn prediction for 1 $\mu\text{l}$ capillaries .....	57
Figure 3.13 - Schematics of kinematically consistent flow patterns. A is the displaced phase, B is the displacing phase.....	58
Figure 3.14 – Illustration of shear stresses at the meniscus .....	59
Figure 3.15 – Slope vs. [CTAB] for different size capillaries.....	60
Figure 3.16 – Log concentration plots for C <sub>14</sub> E <sub>6</sub> and C <sub>12</sub> E <sub>6</sub> .....	61
Figure 3.17 – “Short time” dynamics of capillary rise observed for C <sub>14</sub> E <sub>6</sub> surfactant solutions with varying bulk concentration (hydrophobic capillary radius 0.1 mm). 63	63
Figure 3.18 – Distance vs. time plot for SDS into 1 $\mu\text{l}$ hydrophobic capillaries at the cmc (0.00814 mol dm <sup>-3</sup> ).....	64
Figure 3.19 – Distance vs. square-root time plot for SDS into 1 $\mu\text{l}$ hydrophobic capillaries at the cmc (0.0081 mol dm <sup>-3</sup> ) .....	64
Figure 3.20 – Distance-time plot for SDS penetrating hydrophobic capillaries ([SDS]= 0.0001628 mol dm <sup>-3</sup> ).....	65
Figure 3.21 – Water with “overflowing cylinder” (split ejection) model .....	66
Figure 3.22 – Split injection model.....	66
Figure 3.23 – Distance- time plot for water entering decane filled 1 $\mu\text{l}$ capillaries .....	67
Figure 3.24 – 0.00065 mol dm <sup>-3</sup> SDS penetrating oil filled 1 $\mu\text{l}$ capillaries; two different flow rates are sometimes seen .....	68

## Chapter 1 Introduction and Theory

### 1.1 Aims of the Project

This project aims to investigate the processes by which surfactant solutions penetrate macroscopic horizontal glass capillaries, which are either hydrophilic or have been made hydrophobic by exposing them to silane vapour. A high-speed camera was used to allow accurate tracking of the meniscus along the capillaries. An investigation on the effect of the presence and type of surfactant aimed to reveal the processes by which penetration occurs. The mechanisms for energy loss to account for deviations to Lucas-Washburn behaviour was also investigated. The flow in the capillary was compared to flow in an overflowing cylinder. Penetration of surfactant solutions into capillaries filled with oil was investigated, as by matching the viscosity of the two liquids, viscous dissipation can be neglected.

Two ways of looking at the imbibition (the displacement of one fluid by another immiscible fluid) of liquids into capillaries, at low Reynolds number (the ratio of inertial forces to viscous forces), when inertia and acceleration can be neglected, are from a Laplace pressure perspective and interfacial tension perspective. The interfacial (or surface) tension is the tension of the surface film caused by the attraction of the particles in the surface. The Laplace pressure perspective was used by Lucas<sup>1</sup> and Washburn<sup>2</sup> to derive the Lucas-Washburn equation (explained below), where the rate of penetration depends on  $\gamma_{lv}$ , the liquid vapour interfacial tension. An alternative view is to look at the penetration from an interfacial tension perspective, where the rate of penetration depends on  $\gamma_{sv} - \gamma_{sl}$ , the difference between interfacial tensions of the solid-vapour and solid liquid interfaces. If Young's equation (1.1) is obeyed then both give the same result. However, if the equilibrium contact angle is  $0^\circ$  – which is the expected result for pure water on a glass slide, or surfactants, which lower the interfacial tension, are present – then the two methods do not agree. This project aims to understand the dissipation mechanisms involved to try to remove this contradiction.

The dissipation mechanism will be looked at using a wedge approximation, assuming that most of the viscous dissipation occurs at or near the contact line and treating this area as a triangular wedge.

### 1.2 Background

The penetration of surfactants into solids has many applications including printing, painting, coating, glue and detergents.<sup>3</sup> Biscuit dunking is a common example of capillary action causing the liquid to wick into the small pores of the biscuit. Capillary action into gas-filled cavities has other practical uses, including allowing solder to wick under

integrated circuit chips and controlling flows in micro-fluidic devices.<sup>4</sup> Micro-fluidic devices often contain many capillaries on a substrate to control flow. Capillary action, in capillary channels, is also used in space to transport liquid propellants and to manage a satellite's temperature.<sup>5</sup>

By measuring the rate of penetration into capillaries or bundles of capillaries, one can model the wetting of porous materials in applications such as printing, use of detergents, building conservation, oil recovery from rocks and photographic film manufacture.

### 1.2.1 Wetting, Spreading and Young's Equation

Drops of different liquids deposited on a surface can behave differently.

The complete wetting case is shown in Figure 1.1, where the droplet spreads out and wets the surface completely over time to form a liquid layer of uniform thickness. Hence, only a dynamic contact angle<sup>5</sup> can be measured. The contact angle tends to zero over time and is between  $0^\circ$  and  $180^\circ$ . An example of complete wetting is the spontaneous spreading of water or decane on clean glass.



Figure 1.1 – Complete wetting case

The nonwetting case, shown in Figure 1.2, shows the contact angle to be  $180^\circ$ . No spreading occurs and the radius at the point of contact is zero. This case is never observed for liquids on flat solid surfaces in air, but can be seen, for example, with bubbles in water on clean glass.

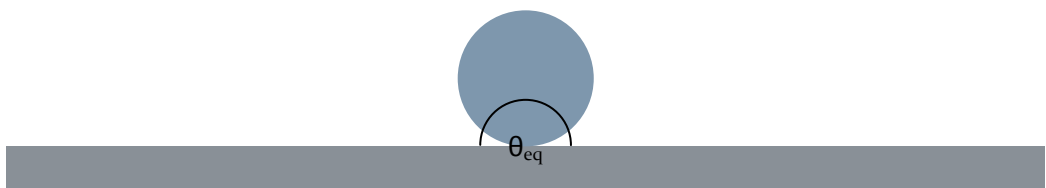


Figure 1.2 – Nonwetting case

The partial wetting case, shown in Figure 1.3, shows the contact angle to be between  $0$  and  $180^\circ$ . Spreading is non-spontaneous and the liquid remains as a droplet, with a finite radius at the point of contact.



Figure 1.3 – Partial wetting case

The nature of wetting depends not only on the choice of liquid, but also on the nature of the surface. For example, water spreads on a clean glass surface but beads up on a glass sheet coated with a monolayer of dimethyloctylchlorosilane (generating a hydrophobic surface). Spreading also depends on the nature of the surrounding immiscible fluid; for example, oil droplets on a surface under water have a different contact angle than an oil drop in air.

The degree of spreading of a liquid drop depends on the balance of the forces at the interfaces between the three phases; air, liquid and solid substrate, known as the three-phase contact (tpc) line. Figure 1.4 shows the tpc; balancing the tangential force here generates Young's Equation, (1.1), where  $\gamma_{sv}$ ,  $\gamma_{sl}$  and  $\gamma_{lv}$  are the solid-vapour, solid-liquid and liquid-vapour interfacial tensions respectively.  $\theta_{eq}$  is the equilibrium contact angle.



Figure 1.4 – The three-phase contact line

$$\cos \theta_{eq} = \frac{\gamma_{sv} - \gamma_{sl}}{\gamma_{lv}} \quad (1.1)$$

From equation (1.1), if  $\gamma_{sv} > \gamma_{sl} + \gamma_{lv}$  then the liquid will completely wet. Similarly, partial wetting occurs when  $-1 < \cos \theta < 1$  and nonwetting when  $\gamma_{sl} > \gamma_{sv} + \gamma_{lv}$ .

The above explanation, however, is incomplete: other factors affect the wetting of surfaces such as roughness discussed below.

### 1.2.2 Roughness and Contact Angle Hysteresis

Most surfaces are rough, that is, they are not perfectly molecularly flat, including the insides of capillaries. Roughness occurs when there is a change in topography of a surface with a consistent molecular structure. Molecularly flat surfaces can be created, for example by solidifying a floating liquid, e.g. molten glass on molten tin. However, even these molecularly flat surfaces may still have defects, known as chemical heterogeneity. Creating surfaces in this way creates variations similar to that of the thermal roughness of a liquid – around a few angstroms.<sup>6</sup> Surface roughness can pin a contact line and can keep a small droplet suspended against gravity on an inclined surface. The force created by the angle difference between the advancing and receding contact angles generates a Laplace pressure difference that can oppose gravity.

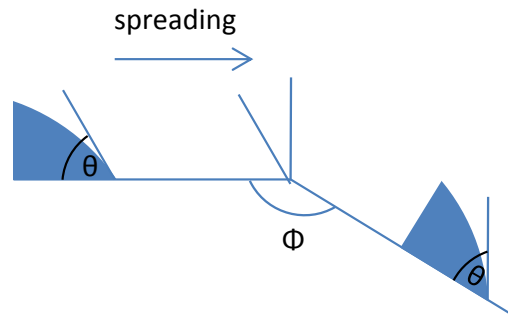


Figure 1.5 – Apparent pinning of a contact line on a defect edge

Wenzel's <sup>7</sup> model, equation (1.2), relates a roughness factor,  $r$ , to the actual surface area divided by the geometric surface area created by the surface roughness. He used a tilting plate method, first described by Huntington <sup>8</sup> in which a hydrophobic flat plate is dipped into a liquid and rotated until curvature of the water surface is no longer observable and beyond which the curvature reverses direction. This angle is then recorded.

$$\cos \theta_{\text{apparent}} = r \cos \theta_{eq} \quad (1.2)$$

Chemical heterogeneity is related by the Cassie-Baxter equation (1.3), where  $f_a$  is the area fraction of solid surface wet by the liquid,  $\theta_{eq}$  and  $\theta_b$  are the equilibrium contact angles on the surfaces  $a$  and  $b$ .<sup>9</sup> This equation can also be applied to surfaces that trap air, such as leaves and feathers, where  $b$  is air ( $\cos \theta_b = -1$ ).

$$\cos \theta = f_a \cos \theta_a + (1 - f_a) \cos \theta_b \quad (1.3)$$

When measuring contact angles, either equilibrium or dynamic, it is important to recognise the importance of roughness in changing the apparent contact angle. Figure 1.5 shows the flexibility of the contact angle at a defect, giving a contact angle between  $\theta$  and  $\pi - \phi + \theta$ . A fall in the surface can stop a spreading liquid (known as pinning). Similarly, a rise in the surface can lower the contact angle enough for spreading to occur. These are known as non-wetting and wetting defects respectively. A difference in advancing and receding contact angles for a moving drop is known as contact angle hysteresis. Similarly, hydrophobic patches on a chemically heterogeneous surface pin the advancing contact angle and hydrophilic patches pin the receding contact angle.

A defect or dirt on a surface can stop or slow down a spreading liquid and defects on the surfaces inside a capillary will affect the speed of penetration, hence care needs to be taken to minimise surface roughness and clean the capillaries well.

The wetting of materials is of particular practical interest, because surfaces that do not wet, dry quickly (repel water), as the liquid will fall off the surface under gravity when the

surface is angled. PTFE (polytetrafluoroethylene) is one such example of a surface. Cottin-Bizonne *et al.*<sup>10</sup> showed that surface roughness that is large on the scale of the fluid molecules affects the degree of boundary slip in a complete wetting system and hence results in a reduction in hydrodynamic forces.

### 1.2.3 Capillary Action

Capillarity, capillary action or wicking is the tendency by which liquids can flow into thin tubes or porous materials. Capillary action is a consequence of surface tension. For liquids such as water, on surfaces such as glass, the liquid spreads across the surface because the free energy at the surface, generated by the surface tension, is lowest when the glass is wet. The advancing film creates a curved surface, which lowers the pressure of the liquid as described by the Laplace equation (1.4), where  $r$  is the radius of curvature.<sup>11</sup>

$$p_{in} = p_{out} + \frac{2\gamma_{lv}}{r} \quad (1.4)$$

The pressure difference at equilibrium between the sides of a curved interface is due to the surface tension of the liquid generating a force to decrease its surface area being balanced by a rise in pressure on the concave side of the interface.

For a finite contact angle,  $r = R / \cos \theta$ , where  $R$  is the capillary radius. Therefore, the curved surface of the liquid in the capillary lowers the pressure to below that of atmospheric pressure by  $2\gamma \cos \theta / R$ . The increased pressure outside the tube causes the liquid to be forced into the capillary. For a vertical capillary, the liquid continues to rise until the pressures are equal (hydrostatic equilibrium), as gravity is working against the rise. Figure 1.6 details this pressure difference.

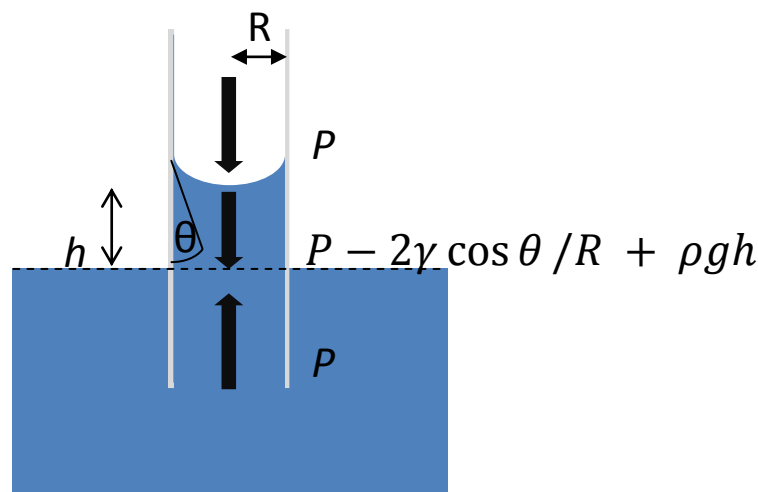


Figure 1.6 – Pressures on a fluid in a capillary

Adapted from Atkins<sup>11</sup>

For vertical capillaries, of radius  $R$ , with a contact angle of  $\theta^p$ , the height to which the liquid will rise can be found from calculating the pressure created by a column of liquid, equation (1.5).

$$p = \rho gh \quad (1.5)$$

This can also be expressed as the capillary force (1.6)

$$F_c = 2\pi R\gamma_{lv} \cos \theta \quad (1.6)$$

At equilibrium, these pressures are equal (1.7):

$$\frac{2\gamma_{lv}}{R} = \rho gh \quad (1.7)$$

This process can also work in reverse for liquids that do not wet the walls of capillaries, for example mercury, where the liquid is pushed out of the tube due to the reverse curvature of the meniscus increasing the pressure at the interface and pushing the liquid out. This is known as capillary depression.

#### 1.2.4 Lucas-Washburn Equation

The penetration of surfactant solutions into hydrophobic and hydrophilic capillaries has been studied since the early twentieth century. Hagen, Poiseuille, Lucas<sup>1</sup> and Washburn<sup>2</sup> were among the first to develop theories for describing the effect. Lucas in 1918 and Washburn in 1921 derived an equation, (1.8), for describing the distance,  $l$ , of penetration of a liquid in time,  $t$ , into porous materials, such as a capillary, under laminar flow.

$$l^2 = \left( \frac{\gamma_{lv} \cos \theta_{eq}}{\eta} \right) \frac{Rt}{2} \quad (1.8)$$

Where  $\gamma_{lv}$  is the liquid-vapour surface tension,  $\eta$  is the dynamic viscosity,  $\theta_{eq}$  is the dynamic contact angle and  $R$  is the radius.

This equation balances the Laplace pressure generated by the curved interface of the advancing meniscus, with equilibrium contact angle  $\theta_{eq}$ , against the viscous dissipation of the movement, distance  $l$ , of a cylinder of fluid, with surface tension  $\gamma_{lv}$  and viscosity  $\eta$  in a tube, radius  $R$  under Poiseuille flow in time,  $t$ .

Differentiating (1.8) with respect to time gives an equation for the rate of penetration (1.9):

$$\frac{dl}{dt} = \frac{R\gamma_{lv}}{\eta 4l} \cos \theta_{eq} \quad (1.9)$$

Equation (1.8) can also be written in linear form as (1.10):

$$l = \left( \frac{\gamma_{lv} \cos \theta_{eq} R}{2\eta} \right)^{\frac{1}{2}} t^{\frac{1}{2}} \quad (1.10)$$

Therefore, a plot of  $l$  against  $t^{\frac{1}{2}}$  should be a straight line with slope  $(\gamma_{lv} \cos \theta_{eq} R / 2\pi)^{\frac{1}{2}}$ .

Hilpert<sup>12</sup> derived different equations for determining interface velocity:

$$4\tau(\zeta) = \left[ \frac{P + \cos \theta_{eq} - A_0}{2} \zeta^{-2} - A_2 \ln \zeta + \sum_{n=3}^N A_n \frac{(1-n)}{n-2} \zeta^{n-2} \right]_{\zeta_0}^{\zeta}$$

Studies have also been made in the nanoscale using nanopores, and have found that the Lucas-Washburn equation can be applicable at these small radii.<sup>13</sup>

### Derivation of the Lucas-Washburn Equation

The Lucas-Washburn equation can be derived as follows:

Sliding a flat sheet of area  $A$ , at mean speed  $v_0$ , over another, stationary, flat sheet, separated by a liquid, thickness  $h$ , requires force  $F$ . (Figure 1.7).

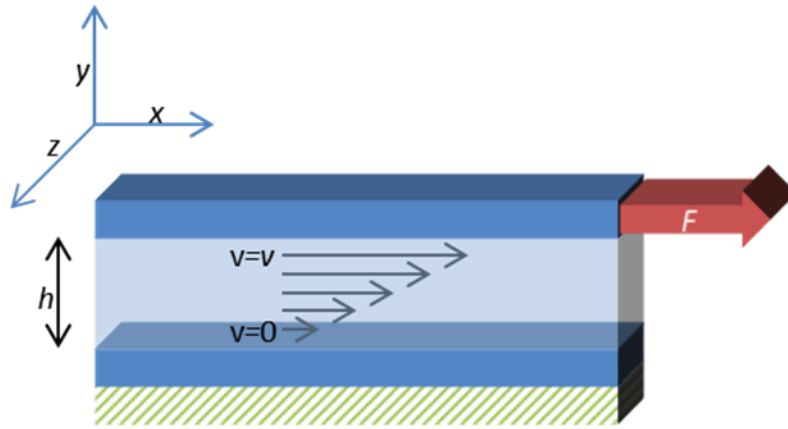


Figure 1.7 – Viscous dissipation

The strain ( $\epsilon$ ) and strain rate ( $\dot{\gamma}$ ) are defined by:

$$\epsilon = \frac{x}{h} \quad \dot{\gamma} = \frac{d}{dt} \left( \frac{x}{h} \right) = \frac{1}{h} \frac{dx}{dt} = \frac{v}{h} \quad (1.11)$$

The viscosity ( $\eta$ ) is defined by:

$$\frac{F}{A} = \eta \dot{\gamma} = \eta \frac{v}{h} \quad (1.12)$$

The power dissipated is the work done ( $W$ ) in time  $t$ :

$$P = \frac{W}{t} = \frac{Fx}{t} = Fv \quad (1.13)$$

the power dissipated per unit area is:

$$\frac{P}{A} = \eta \frac{v^2}{h} \quad (1.14)$$

and per unit volume of liquid:

$$\frac{P}{V} = \frac{P}{A \times h} = \eta \left(\frac{v}{h}\right)^2 = \eta \dot{\gamma}^2 \quad (1.15)$$

This is the general relationship for viscous dissipation and strain rate in laminar flow.

Hence, the power dissipated in a volume of flowing liquid is:

$$P = \int \eta \dot{\gamma}^2 dV \quad (1.16)$$

A parabolic flow has the form, as in Figure 1.8, in a cylindrical capillary of:

$$v = 2v_0 \left(1 - \left(\frac{r}{R}\right)^2\right) \quad (1.17)$$

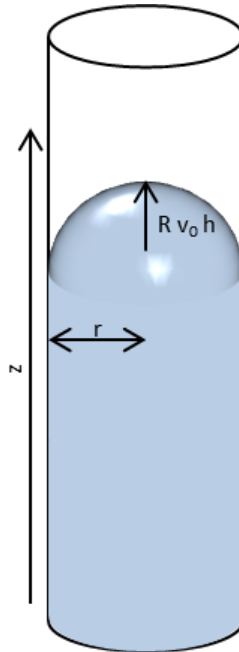


Figure 1.8 – Parabolic velocity profile of meniscus

Where  $v_0$  is the mean velocity. Thus the strain rate is:

$$\dot{\gamma} = \frac{dv}{dr} = -\frac{4v_0}{R^2} r \quad (1.18)$$

Therefore, power dissipated over the volume of this profile in a tube of length  $l$  and radius  $R$  is:

$$\begin{aligned} P &= \eta \int_0^l dz \int_0^R \dot{\gamma} 2\pi r dr \\ &= \eta l \frac{16v_0^2}{R^4} 2\pi \int_0^R r^3 dr \\ &= 8\pi v_0^2 \eta l \end{aligned} \quad (1.19)$$

Therefore rate of work done by capillary forces is, where  $l_c$  is the length of the contact line:

$$\begin{aligned} P &= (\gamma_{sv} - \gamma_{sl}) \times l_c \times v \\ &= 2\pi R (\gamma_{sv} - \gamma_{sl}) v_0 \end{aligned} \quad (1.20)$$

If inertia is neglected then the work done by capillary action exactly balances the viscous dissipation:

$$\begin{aligned} P &= 8\pi v_0^2 \eta l = 2\pi R (\gamma_{sv} - \gamma_{sl}) v_0 \\ \therefore v_0 &= \frac{dl}{dt} = \frac{(\gamma_{sv} - \gamma_{sl}) R}{4\eta l} \end{aligned} \quad (1.21)$$

Now, if Young's equation is obeyed, the result is the same as the Lucas-Washburn equation (1.8).

### 1.2.5 Dynamic Contact Angle

Contact angle is a dynamic quantity, which depends on the velocity.<sup>14</sup> There are few analytical solutions for capillary flow that account for the dynamic contact angle,  $\theta_d$ . One such analytical approach to accounting for the dynamic contact angle was performed by Hamraoui and Nylander<sup>15</sup> where they used a retardation constant to account for all other sources of dissipation, other than that in the bulk. They found that their dynamic contact angle was related to their friction coefficient by:

$$\begin{aligned} \gamma_{eq} \cos[\theta(t)] &= \gamma_{eq} \cos \theta_0 - \beta_0 \frac{\partial h(t)}{\partial t} \\ \text{where: } \beta_0 &= \frac{k_B T v}{\lambda^3 \kappa_0^s h} \end{aligned} \quad (1.22)$$

$\lambda$  and  $\kappa_0^s$  are two parameters that appear in the molecular kinetic theory of Blake and Haynes.<sup>16</sup>  $\lambda$  is the distance between adsorption sites on the solid,  $\kappa_0^s$  is the surface rate constant for molecular displacements,  $v$  is the molecular volume of the liquid, and  $k_B$  and  $h$  are the Boltzmann and Planck constants respectively.  $T$  is the temperature.

Dussan reviewed the methods of measurement of dynamic contact angles.<sup>17</sup> Some methods – other than high magnification – for observing the dynamic contact angle are: a

droplet spreading on a surface, submerging a cylinder or tape into a liquid bath, rotation of a partially submerged cylinder and the spreading of liquid between two parallel plates.

Blake<sup>18</sup> did attempt to draw conclusions for the origins of dynamic contact angle, however he found that contact angle hysteresis produced ambiguities in his measurements, making it difficult to draw firm conclusions. He also suggests performing experiments on two liquid systems to investigate the effects of competitive wetting and viscosity ratio.

Chebby<sup>19</sup> did consider solutions to the effects of dynamic contact angle when the inertia was small (small Weber number), but only for short and large times. His solutions are however, the same as the Lucas-Washburn equation, and are found to hold for most of the time for horizontal capillaries or when the effect of gravity was small.

He used the correlation by Jiang *et al.* based on Hoffmann's data:<sup>20</sup>

$$\frac{\cos \theta_{eq} - \cos \theta_d}{\cos \theta_{eq} + 1} = \tanh (\alpha Ca^m) \quad (1.23)$$

Where  $a=4.96$ ,  $m=0.702$  and  $Ca$  is the capillary number (ratio of viscos stresses against interfacial tension stress, see Appendix B).

For large times he derived:

$$X = \sqrt{\cos \frac{\theta_{eq}}{2} T^{\frac{1}{2}} - \Omega T^{\frac{1-m}{2}}} \quad (1.24)$$

$$\text{Where } \Omega = \frac{a}{2^{\frac{3(1+m)}{2}} (\cos \theta_{eq})^{\frac{1-m}{2}}} \times \frac{1+\cos \theta_{eq}}{1-\frac{m}{2}}, X = l/R, T = \gamma t/\eta R$$

This gave a dynamic contact angle of:

$$\theta_d = \arccos \left[ 4 \left( \sqrt{\frac{\cos \theta_{eq}}{2} T^{\frac{1}{2}} - \Omega T^{\frac{1-m}{2}}} \right) \times \left( \frac{1}{2} \sqrt{\frac{\cos \theta_{eq}}{2} T^{-\frac{1}{2}} - \Omega \frac{(1-m)}{2} T^{-\frac{(1+m)}{2}}} \right) \right] \quad (1.25)$$

For  $\theta_{eq} = 0$  and  $\theta_{eq} \neq 0$

The first term in (1.24) is a dimensionless form of the Lucas-Washburn equation and the second is the correction term for the dynamic contact angle.

### 1.2.6 Limitations of Lucas-Washburn Theory

The Lucas-Washburn theory neglects several factors. As the liquid is assumed to follow Poiseuille flow, the roles of nonlinear dissipation and flow pattern effects at both the meniscus and the capillary entrance are ignored.<sup>21</sup> A particular issue discussed later is the neglect of dissipation in the wedge at the tpc. The Lucas-Washburn model also does not account for inertia at the early stages of flow, as the model predicts incorrectly an infinite velocity at  $t=0$ . The presence of the corners of the capillary and the shape of its end may all have an effect on rate of imbibition. It is also worth noting that diffusion controlled mechanisms can also give  $t^{1/2}$  behaviour, therefore a distance vs.  $t^{1/2}$  plot does not always imply that the Lucas-Washburn equation applies.<sup>21</sup>

The Lucas-Washburn theory also neglects surface roughness except in as much as roughness affects the contact angle.

The theory also neglects the presence of liquid films ahead of the meniscus and so cannot account for changes in relative humidity.

Surfactants are accounted for indirectly, through their influence on  $\gamma_{lv}$  and  $\cos \theta_d$ ; the Lucas-Washburn equation provides no framework for the determining of the dynamic contact angle or dynamic surface tension (DST) in surfactant solutions.

Various attempts have been made to extend the Lucas-Washburn theory to overcome some of these limitations.

Hilpert<sup>22</sup> showed that Lucas-Washburn theory could be generalised to account for a dynamic contact angle that assumes the non-equilibrium Young force to depend on the velocity of the advancing liquid-vapour interface. He used the Lambert W function, a set of functions of the inverse form of  $f(w) = w \exp w$  where  $w$  is complex, to derive solutions for the interface position, velocity and acceleration as a function of time.

An ordinary differential equation (ODE) of the form:<sup>22</sup>

$$\frac{p_{l,0} - p_v}{l} + \frac{2\gamma}{Rl} \cos \theta = \frac{8\eta}{R^2} \dot{l} + \rho g \sin \psi \quad (1.26)$$

Where  $p_{l,0}$  is the pressure at the tube inlet,  $p_v$  is the constant gas pressure;  $l$  is the distance between the tube inlet and the meniscus. The contact angle  $\theta$  depends on the interface velocity  $\dot{l}$ .

Fries and Dreyer<sup>23</sup> developed a solution (1.35) to the momentum balance, which allows for the calculation of liquid rise behaviour for longer times than the Lucas-Washburn equation can predict. They did this using Lambert W functions ( $x = W(x)e^{W(x)}$ ) which we used to

solve their equation to avoid the problem of divergence near the equilibrium height. Where  $a$  and  $b$  are constants,  $h$  is the height at time  $t$ .

$$h(t) = \frac{a}{b} \left[ 1 + W \left( -e^{-1 - \frac{b^2 t}{a}} \right) \right] \quad (1.27)$$

### 1.3 Assumptions

The following assumptions are made in the Lucas-Washburn model:

#### Gravity

For vertical capillaries, the effect of gravity decreases the contact angle at the advancing liquid front, as the capillary pressure has to balance the hydrostatic pressure of the column of liquid.<sup>24</sup> The lower contact angle implies an increased solid-liquid surface excess, resulting in lower strain rate and lower velocity. Bain states that gravity may be neglected when the penetration depth is much less than  $2\sigma l v / \rho g R$ . Beyond this, gravity slows down the rate of penetration in addition to other forces.<sup>24</sup>

#### Inertia

The Weber number (1.28) gives the importance of inertial forces; the work done in time  $\Delta t$  by the meniscus is  $2\pi a \gamma l v \cos \theta V \Delta t$  and the work accelerating an element of fluid from rest to speed  $V$  is  $\pi a 2\rho V 3\Delta t / 2$ .<sup>24</sup> This gives  $\cos \theta = We / 4$ . Therefore, the effect of inertia on contact angle is negligible.

$$We = \rho V^2 R / \gamma_{lv} \quad (1.28)$$

Inertia may be neglected to affect the speed of penetration provided the following conditions are met:

- Inertia term:

$$\frac{1}{2}\pi R^2 V_0 \rho V_0^2 = \frac{1}{2}\pi R^2 V_0^3 \rho \quad (\text{From } E_K = \frac{1}{2}mv^2) \quad (1.29)$$

$$\frac{\text{inertia}}{\text{drag}} \approx \frac{3}{16} \frac{R V_0 \rho}{\eta} \left( \frac{R}{L} \right) \quad (1.30)$$

$$\approx \frac{3}{16} Re \left( \frac{R}{L} \right) \approx 1 \quad (1.31)$$

$$\therefore \text{Need } \frac{R}{L} \ll 1$$

- Therefore initial velocity:

$$V_0 = \frac{3}{4} \frac{R(\gamma_{sv} - \gamma_{sl})}{\eta L} \quad (1.32)$$

Therefore, inertia can be ignored in the first part of the capillary, where  $l$  is smaller than several multiples of the radii.

Quéré found that initially capillary rise position follows a linear relationship with time.<sup>25</sup> This relationship was found for capillaries with a radius of 689  $\mu\text{m}$  using ethanol, shown in Figure 1.9. For viscous liquids like silicone oil, the  $\sqrt{t}$  relationship holds. However, close to the moment when the tube touches the liquid, the Lucas-Washburn equation predicts an infinite velocity as according to Quéré, was first noticed by Bosaquet. Ignoring viscosity, he found that at early stages, the velocity was linear with time, (1.33)<sup>25</sup> however, the results did not qualitatively agree with this.

$$c = \sqrt{\frac{2\gamma}{\rho R}} \quad (1.33)$$

where  $c$  is the constant velocity and  $\rho$  is the density.

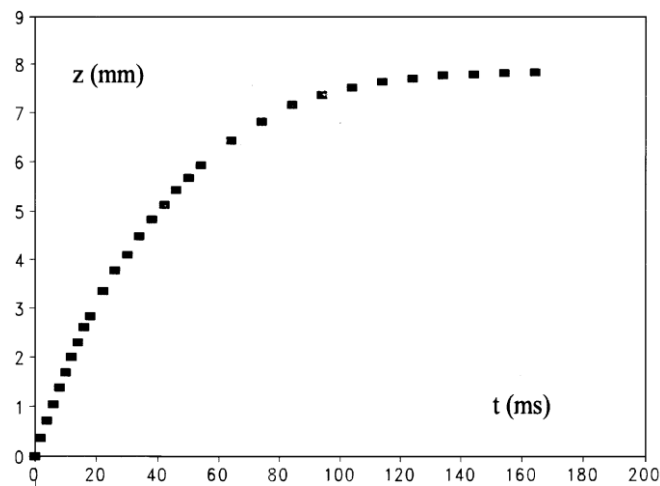


Figure 1.9 – Height of the meniscus (in millimetres) as a function of time (in milliseconds), for a vertical glass tube of radius  $r = 689 \mu\text{m}$  put into contact at  $t = 0$  with an infinite bath of ethanol

From Quéré *et al.*<sup>25</sup>

Quéré's argument for this disagreement was the existence of a dynamic contact angle. With the inclusion of the dynamic contact angle, the predicted value is much closer to the experimental result. He suggests that other causes of the discrepancy are the role of the reservoir, and the sharp edges of boundary between reservoir and tube generating vortices. By comparing the imbibition of liquid in a tube and a pipette, where the transition from reservoir and pipette is smooth, he found that there was an increase of velocity in the pipette of around 20%.

### Flow

Sufficiently far from the start of the capillary, flow is parabolic. Non-Poiseuille flow may be neglected after  $0.12 \times ReR$ ,<sup>24</sup> the lead-in length, where  $Re$  is the Reynolds number,  $Re = \rho VR/\eta$ . As  $Re$  is  $\approx 10$ , this length is around 0.1 mm.<sup>24</sup>

## Dissipation

Viscous dissipation only occurs in the bulk; additional dissipation in the meniscus is neglected (see 1.4).

### 1.3.2 Vertical Rise

Many measurements have been performed on capillaries mounted vertically. The capillary is put into contact with a trough of wetting liquid, of surface tension  $\gamma$ , density  $\rho$  and viscosity  $\eta$ . The liquid then rises up a set distance up the tube. The liquid stops advancing because the capillary force, Equation (1.34), balances with the weight of the liquid in the column, Equation (1.35).<sup>25</sup>

$$F_c = 2\pi r\gamma \quad (1.34)$$

$$F_g = \pi r^2 z_0 \rho g \quad (1.35)$$

where

$$z_0 = \frac{2\gamma}{\rho g r} \quad (1.36)$$

If the liquid does not completely wet the tube, the final height is multiplied by the cosine of the contact angle.

### 1.3.3 Horizontal Capillaries

Mounting of the capillaries in the horizontal rather than traditionally vertical position reduces the effect of gravity on the liquid mass. Gravity would still have some effect of changing the shape of the meniscus to make it non-spherical. However, for capillary diameters much less than the capillary number (1.37), the gravity effect is negligible.

$$Ca \stackrel{\text{def}}{=} \frac{\mu v}{\gamma} \quad (1.37)$$

### 1.3.4 Hydrophobized Capillaries

Tiberg *et al.*<sup>3</sup> developed a model for surfactant penetration into hydrophobic capillaries and discussed this in relation to surface tension relaxation and adsorption phenomena. At first, they assumed the capillary surface to be completely non-wettable with pure water, i.e. a contact angle of  $180^\circ$ . The surfactant adsorbs to the surface, reducing surface tension and increasing the wettability. They found that the link between the surface tension and the amount of surfactant adsorbed is established by the Gibbs equation; the simplest form being:

$$\gamma_{sl} = \gamma_{sl}^0 + [\gamma_{sl}^{180^\circ} - \gamma_{sl}^{0^\circ}] \exp\left(-\frac{k_{sl}^+}{h\Gamma_{sl}^m} \int \Gamma_{lv} dt\right) \quad (1.38)^3$$

where  $\Gamma_{ls}$  is the surfactant surface excess on the liquid-solid interface from the liquid-vapour interface near the tpc,  $\Gamma_{ls}^m$  is the monolayer capacity for the liquid-solid interface,  $b$

is the thickness of the adsorption layer and  $k_{ls}^+$  and  $k_{ls}^-$  are, respectively, the adsorption and desorption rate constants. Where  $m$  indicates the meniscus and  $+$  indicates the area immediately forward of the meniscus.

The capillary force can then be expressed as:

$$f(t) = \gamma_{lv}(t) \left[ 1 - 2 \exp \left( - \frac{k_{sl}^+}{h\Gamma_{sl}^m} \int_{t(z-\frac{h}{2})}^{t(z+\frac{h}{2})} \Gamma_{lv} dt \right) \right] \quad (1.39)^3$$

Hydrophobic capillaries do not undergo immediate imbibition. Starov describes an argument for this.<sup>26</sup> He states that the contact angle when the liquid first touches the capillary is greater than  $\pi/2$  this prevents imbibition. He assumed that the solid-liquid and liquid-vapour interfacial tensions do not vary with time because adsorption of surfactant to these surfaces is fast compared to adsorption onto the substrate-air interface. Starov assumed that the only interfacial tension that can vary is that between solid and air, hence (a sufficient amount of) surfactant must adsorb onto the bare hydrophobic surface in order for imbibition to occur. This was his reason why pure water and solutions with a surfactant concentration below some critical amount will not spontaneously penetrate a hydrophobic capillary. Due to the time required for the diffusion of surfactant to allow the capillary force to build up, the surfactant solution will not enter a hydrophobic capillary straight away. He suggests that the delay time can be calculated:

$$\tau = \frac{h\Gamma_{ls}^m \ln 2}{k_{sl}^+ \Gamma_{lv}^{eq}} \quad (1.40)^3$$

The meniscus of water immediately on entering the capillary will have a concentration equal to the equilibrium surfactant concentration, therefore depletion of surfactant does not immediately occur and this argument may not be the whole description of the cause of penetration delay.

The shape of the corner of the end of the capillary may be additionally inhibiting surfactant solution from entering the capillary because of the corner of the end of the capillary creating a Laplace barrier, where the meniscus has to flip, from forming a tpc with the end and then the insides of the capillary. The sharp corner can also act like a defect, as described in 1.2.2 Roughness and Contact Angle Hysteresis, above, pinning the contact line and preventing spontaneous imbibition.

The diffusion of surfactant ahead of the meniscus is however, likely to be slow as it is thermodynamically unfavourable, as  $\gamma_{sv}$  will have to increase. This increase is not recovered by the change in  $\gamma_{sl}$ . It is also unfavourable to remove a surfactant molecule from the

liquid/vapour interface where it interacts favourably with the water molecules and the surface. The actual process is likely to incorporate surfactant diffusion and a rolling carpet style mechanism, such as that seen by Cai.<sup>27</sup>

Tiberg *et al.* found that the initial rise of surfactant solution into a hydrophobic capillary was linear, rather than following the Lucas-Washburn  $t^{1/2}$  relationship.<sup>3</sup> The  $t^{1/2}$  relationship did return after some distance, and they related this change to the limiting of diffusion by depletion of surfactant from near the meniscus. The depletion occurs, as the surfactant will continually adsorb at the newly formed liquid-solid interface as the liquid enters the capillary, unless the loss of surfactant from the liquid front is replaced by diffusion from a deeper region. A region of surfactant-depleted solution therefore forms immediately behind the meniscus. This argument neglects convective transport of surfactant to the meniscus that occurs in Poiseuille flow. Data from Tiberg *et al.* shown in Figure 1.10 shows capillary rise occurring over tens of seconds and the transition between two regimes.

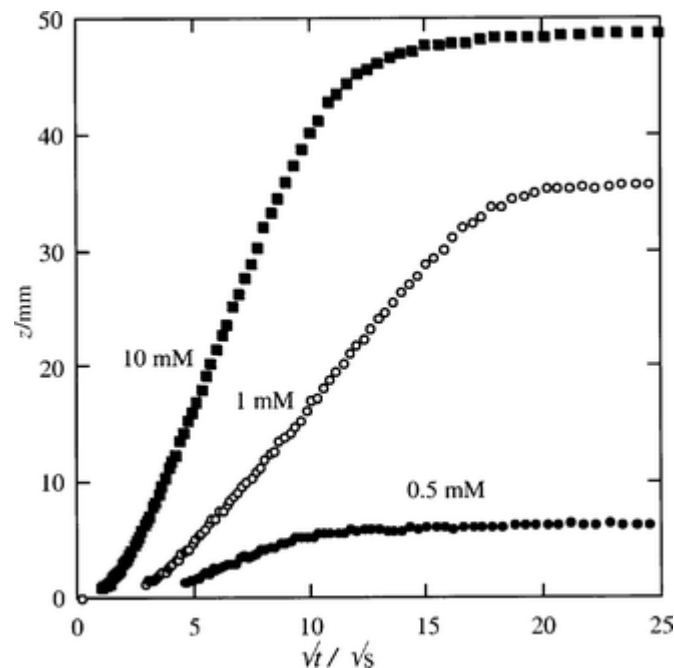


Figure 1.10 – Capillary rise dynamics observed for  $C_{14}E_6$  surfactant solutions (hydrophobic capillary, radius 0.1 mm)

From Tiberg *et al.*<sup>3</sup>

Bain<sup>24</sup> developed a steady-state solution for the penetration of surfactant solutions into hydrophobic capillaries by modelling it on the hydrodynamics of an overflowing cylinder. The model suggested that the velocity of penetration is determined by the adsorption kinetics at the air water interface.

He modelled the capillary, of radius  $R$ , as it plunged into a solution at the capillary rise velocity  $V$ . The fluid in contact with the walls, assuming the no-slip boundary condition,

has velocity  $-V$  and the radial velocity at the meniscus is  $v_r$ . The flow in the bulk of the capillary, a distance below the meniscus, was assumed to be parabolic, giving the velocity of the fluid in the centre  $+V$ . Due to the opposing flow directions, there is a stagnation cylinder, shown by the dashed lines in Figure 1.11A, at  $r = R/\sqrt{2}$ . Comparing this figure to Figure 1.11B, a model of an overflowing cylinder (OFC), which is an experimental platform with well-understood hydrodynamics, the flow profiles can be seen to be similar.

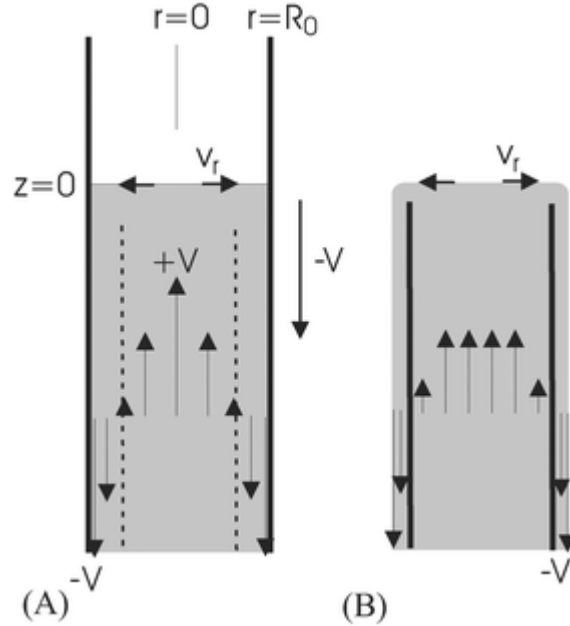


Figure 1.11 – (A) Flow profile in hydrophobic capillary in the moving frame of reference. (B) Flow profile in an overflowing cylinder in the stationary frame

The dashed lines show the stagnation cylinder where the flow velocity is zero. From Bain<sup>24</sup>

He obtained an expression for the capillary rise velocity in hydrophobic capillaries,<sup>24</sup> where  $c_b$  is the bulk concentration and  $c_s$  is the subsurface concentration,  $\kappa$  is a constant to be determined but is expected to be  $O(1)$

$$V = \frac{(c_b - c_s)^2 DR\kappa}{\pi\Gamma_{sl}^{\infty 2} \left( 1 - \exp\left(\frac{\gamma_{lv}^0 \cos \theta^0}{\Gamma_{sl}^{\infty} RT}\right) \right)^2} \quad (1.41)$$

Churaev *et al.*<sup>28</sup> developed theories to cover the transport mechanisms that take into account the micelle disintegration and solution concentration reduction near the meniscus as a result of adsorption, as well as the surface diffusion of surfactant molecules.

Churaev and Zorin<sup>29</sup> concluded that, for thin ( $5 \mu\text{m}$ - $15 \mu\text{m}$ ) capillaries, there were three mechanisms for the penetration of surfactant solutions into hydrophobized capillaries. The first mechanism occurs at concentrations above the cmc (critical micelle concentration), but is limited in length, which is dependent on bulk concentration, radius and the Henry constant (ratio of the surface excess to the bulk concentration in the limit of low

concentration<sup>30</sup>). In the second mechanism, found at concentrations below the cmc, the rate is controlled by the depleted concentration at the meniscus. The third mechanism is found at even lower concentrations where the rate is controlled by surface diffusion of surfactant in front of the meniscus. They assumed that the penetration took place slowly enough for diffusion to control the velocity.

### 1.3.5 Oil Filled Capillaries

The assumptions for viscous dissipation being negligible for air, cannot be made for an already oil filled capillary. However, viscous dissipation is independent of penetration distance if the viscosities are matched.

Hammond and Unsal<sup>31</sup> developed Tiberge's<sup>3</sup> model for the penetration of a surfactant solution into an oil wet capillary. The difference in capillary pressure across the meniscus drives the imbibition along the capillary. This pressure difference is linked to oil-water interfacial tension and the contact angle on the glass, which are linked to the surface energies of each liquid-solid interface by Young's equation (1.1). The adsorption of surfactant onto the glass and interfacial surfaces was assumed to be related by Langmuir isotherms similar to (1.42), to the concentrations in the adjacent fluid.<sup>31</sup>

$$\theta = \frac{K_p}{1 + K_p} \text{ where } K_p = \frac{k_a}{k_d} \quad (1.42)^{11}$$

Using the Poiseuille flow formulas, they determined the velocity of the meniscus,  $v$  at distance  $l$  along the capillary of length  $L$  to be (with an atmospheric pressure difference at each end):

$$v = \frac{R^2(p_L - p_-)}{8\eta_w l} = \frac{R^2(p_+ - p_R)}{8\eta_o(L - l)} \quad (1.43)^{31}$$

Where  $\eta_w$  and  $\eta_o$  are the viscosities of the surfactant solution and oil respectively,  $p_L$  and  $p_R$  are the pressures of the water and oil at the entrance and exit respectively,  $p_-$  is the pressure of the water at the meniscus  $p_+$  is the oil pressure at the meniscus. The contact angle was assumed to satisfy Young's equation.

The surface energies are related to the amount of surfactant adsorbed by the two liquids by the van Laar equation, (1.43)

$$\gamma_{ij}(\Gamma_{ij}) = \gamma_{ij}(0) + RT\Gamma_{ij}^m \log\left(1 - \frac{\Gamma_{ij}}{\Gamma_{ij}^m}\right) \quad (1.44)^{31}$$

Where  $\Gamma_{ij}^m$  is the monolayer capacity and  $T$  is the absolute temperature and  $R$  is the gas constant.  $i$  and  $j$  can be oil, water or solid (o, w or s).

They assumed that the speed of motion is slow enough that diffusion allows surfactant concentration to be uniform across the meniscus.<sup>31</sup> The surfactant is also assumed to transfer from the liquid to the liquid-oil interface to the liquid-solid and oil solid surface and therefore it can influence the capillary pressure on both sides of the meniscus.<sup>31</sup> Hammond and Unsal concentrated on the situations where the presence of surfactant on the oil-solid surface could be neglected. This model, however, neglects convective transport of surfactant.

In the presence of surfactant Hammond and Unsal showed that:<sup>31</sup>

$$\begin{aligned} \sigma_{ow}(\Gamma_{ow}) \cos \theta^0 - \sigma_{ow}(0) \cos \theta^0 \\ = \sigma_{ws}(0) - \sigma_{ws}(\Gamma_{ws}) - [\sigma_{os}(0) - \sigma_{os}(\Gamma_{os})] \end{aligned} \quad (1.45)$$

The final term disappears when the surfactant does not adsorb to the oil-solid interface.

By combining the two above equations, (1.44) and (1.45) they found that:

$$\begin{aligned} \sigma_{ow}(\Gamma_{ow}) \cos \theta &= \sigma_{ow}(0) \cos \theta^0 \\ &= -RT\Gamma_{ws}^m \log \left( 1 - \frac{\Gamma_{ws}}{\Gamma_{ws}^m} \right) \\ &\quad + RT\Gamma_{os}^m \log \left( 1 - \frac{\Gamma_{os}}{\Gamma_{os}^m} \right) \end{aligned} \quad (1.46)$$

Hence, the adsorption of surfactant changes the contact angle.

They then found that for low capillary numbers, – where the flow is slow and viscous stresses are low when compared to interfacial tension stresses – the pressure difference across the meniscus is:

$$\begin{aligned} \Delta P_c &= \frac{\sigma_{ow}(\Gamma_{ow}) \cos \theta}{R} \\ &= \frac{2}{R} [\sigma_{ow}(0) \cos \theta^0 - RT\Gamma_{ws}^m \log \left( 1 - \frac{\Gamma_{ws}}{\Gamma_{ws}^m} \right) \\ &\quad + RT\Gamma_{os}^m \log \left( 1 - \frac{\Gamma_{os}}{\Gamma_{os}^m} \right)] \end{aligned} \quad (1.47)$$

Where  $R/\cos \theta$  is the radius of curvature and  $P_c$  is the capillary pressure.

combining this with:

$$\begin{aligned} \Delta P_d + \Delta P_c &= \frac{8U}{a^2} [\eta_w X + \eta_o(L - X)] \\ \Delta P_d &= p_L - p_R \end{aligned} \quad (1.48)$$

allows the speed to be determined, provided the amount of surfactant adsorbed near the meniscus is known. They showed that at early times the rate of penetration is controlled by the dynamics of transfer of surfactant from the meniscus to the solid surface. At late times, the penetration rate is controlled by rate of diffusion of surfactant in the bulk.

The Péclet number (see Appendix B) characterises the ratio of convective to diffusive transport. In the model of Hammond and Unsal,  $Pe$  is small. However, the Péclet number for the capillaries used in this project ( $\sim 1 \mu\text{l}$ ) is not. Assuming a typical mass diffusion coefficient of  $10^{-10} \text{ m}^2 \text{ s}^{-1}$  and a typical velocity of  $6 \text{ mm s}^{-1}$ , the Péclet number along the axis of the capillary is  $O(10^6)$  and perpendicular to the axis is  $O(10^4)$ . Therefore, in this work, convection cannot be neglected.

#### 1.4 Dissipation in the Wedge

The Lucas-Washburn model assumes dissipative mechanisms are due only to viscous losses in the bulk, however, viscous losses also occur in the small wedge of liquid near the tpc. It is important to determine whether the dissipation in this wedge is significant compared to dissipation in the bulk and whether this dissipation can account for differences between the Lucas-Washburn model and experimental results presented later in this thesis.

By treating the advancing meniscus as a wedge as shown in Figure 1.12 and expanded in Figure 1.13, the viscous dissipation can be approximated. One can derive the velocity by balancing the driving and resistive forces. This model can be assumed to be an approximation for short, small capillaries, however as  $l$  increases, dissipation in the bulk becomes more important.

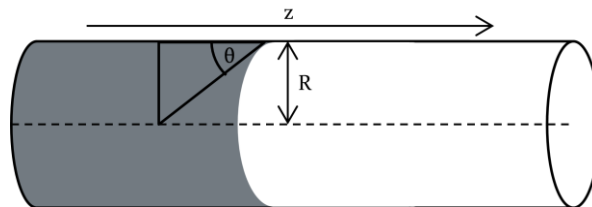


Figure 1.12 – Wedge model

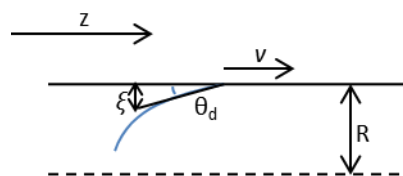


Figure 1.13 – Close up of wedge

We assume that the meniscus moves at speed  $v$  along the capillary, with a linear velocity profile, shown in Figure 1.14 and (1.49) we model the viscous dissipation in the meniscus, by treating the meniscus as an arc of a circle.  $\xi$  is the thickness of the meniscus,  $z = 0$ ,  $r = 0$  is the centre of the sphere defined by the meniscus. The precise value of the dissipation in the meniscus will depend on the details of the velocity profile, but the general form will be the same as calculated here. For the simple linear velocity profile the strain rate is independent of  $r$ .

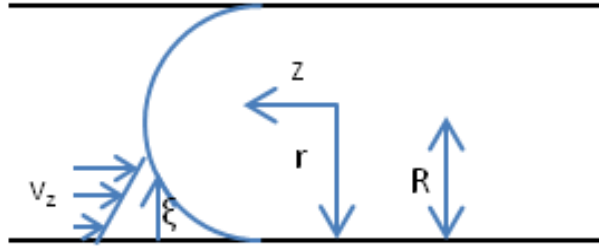


Figure 1.14 – Velocity profile at meniscus

$$\dot{\gamma} = \frac{dv_z}{dr} = \frac{V}{\xi} \quad (1.49)$$

The viscous dissipation per unit volume was shown earlier to be  $\eta\dot{\gamma}^2$ . The total dissipation in the meniscus is obtained by integrating over the volume of the meniscus:

Since  $\xi$  is in the limit of the integral, the integral needs to be over  $r$  first:

$$P = \int_0^R \frac{\eta v^2}{\xi^2} dz \int_{R-\xi}^R 2\pi r dr \quad (1.50)$$

Dissipation is dominated by the volume of fluid near the contact line, where  $\xi \ll R$  because  $\dot{\gamma} = V/\xi$  (where  $\dot{\gamma}$  is the strain rate) Therefore approximately:

$$\int_{R-\xi}^R 2\pi r dr \approx 2\pi R\xi \quad (1.51)$$

and the dissipation power is:

$$P = 2\pi R\eta V^2 \int_0^R \frac{dz}{\xi} \quad (1.52)$$

First considering the case of a zero advancing contact angle. The meniscus then obeys the equation:

$$r^2 + z^2 = R^2 \quad (1.53)$$

which can then be solved for the thickness  $\xi$  as a function of  $z$ :

$$\begin{aligned} r &= \sqrt{R^2 - z^2} \\ \xi &= R - r = R - \sqrt{R^2 - z^2} \\ \therefore \xi &= R \left[ 1 - \sqrt{1 - \frac{z^2}{R^2}} \right] \end{aligned} \quad (1.54)$$

Therefore the power dissipated is:

$$P = 2\pi\eta V^2 \int_0^R \frac{dz}{1 - \sqrt{1 - \frac{z^2}{R^2}}} \quad (1.55)$$

If the fact that most of the dissipation occurs where the meniscus is thin is used again, the expansion of the integral in the limit of  $z \ll R$  using  $\sqrt{1-x} \cong 1 - x/2$  gives:

$$\int_0^R \frac{dz}{1 - \sqrt{1 - \frac{z^2}{R^2}}} \cong \int_0^R \frac{dz}{1 - \left(1 - \frac{z^2}{2R^2}\right)} = \int_0^R \frac{2R^2}{z^2} dz \quad (1.56)$$

This integral diverges, implying that dissipation is infinite and the meniscus can never move. A molecular cut-off length,  $\delta$ , is used to avoid this unphysical result.  $\delta \cong 10^{-9}$  m, below which continuum fluid mechanics no longer apply.

Then:

$$\begin{aligned} P &= 4\pi\eta v^2 R^2 \int_{\delta}^R \frac{dz}{\eta^2} \\ &= 4\pi\eta v^2 R^2 \left[ \frac{1}{\delta} - \frac{1}{R} \right] \cong \frac{4\pi\eta v^2 R^2}{\delta} \end{aligned} \quad (1.57)$$

since  $\delta \ll R$ .

For typical values of  $v = 0.1$  m s<sup>-1</sup>,  $R = 10^{-4}$  m,  $\delta = 10^{-9}$  m,  $\eta = 10^{-7}$  Pa,  $P = 10^{-3}$  W.

The work done per unit time by the capillary:

$$2\pi R(\gamma_{sv} - \gamma_{sl})v = 4 \times 10^{-6} \text{ W} \quad (1.58)$$

When  $\gamma_{sv} - \gamma_{sl} \cong \gamma_{lv} \cos \theta = 0.072$  N m<sup>-1</sup>.

The power dissipated in the wedge far exceeds that available from the capillary penetration at the observed speeds. Therefore, the contact angle must be non-zero.

Now considering the case of a non-zero (finite) contact angle,  $\theta$ , and for simplicity changing  $z = 0$  to be at the tpc and approximating the curved meniscus as a wedge,  $\xi = z \tan \theta$ . This is a good approximation when  $\xi \ll R$ .

The power dissipated over the wedge shall be given by:

$$P = 2\pi R \xi \int_0^R \eta \frac{V^2}{\xi^2} dz \quad (1.59)$$

substituting  $\xi = z \tan \theta$  gives:

$$P = \frac{2\pi R\eta V^2}{\tan \theta} \int_0^R \frac{dz}{z} \quad (1.60)$$

Once again, this integral diverges, and a lower cut-off,  $\delta$ , needs to be introduced:

$$\begin{aligned} P &= 2\pi R\eta v^2 \int_{\delta}^R \frac{dz}{z} \\ &= \frac{2\pi R\eta V^2}{\tan \theta} \ln \frac{R}{\delta} \end{aligned} \quad (1.61)$$

Using the same values as above:

$$P = \frac{4 \times 10^{-8}}{\tan \theta} W \quad (1.62)$$

The fraction of the capillary energy dissipated in the wedge is thus:

$$\frac{P_{wedge}}{P_{capillary}} = \frac{\eta v \ln \frac{R}{\delta}}{(\gamma_{sv} - \gamma_{sl}) \tan \theta} = \frac{10^{-2}}{\tan \theta} \quad (1.63)$$

For  $\theta = 5^\circ$ ,  $\frac{P_{wedge}}{P_{capillary}} \approx 10\%$ .

Wedge dissipation in the meniscus therefore makes a small but significant contribution to the total dissipation and will give rise to deviations from Lucas-Washburn behaviour especially when  $v$  is large and  $\theta$  is small.

## 1.5 Surfactants

### 1.5.1 Introduction

Surfactants, or surface-active agents, are amphiphilic compounds, which, when added to a liquid (typically water) adsorb to the liquid surfaces. Their presence changes the surface tension of interfaces between phases, e.g. liquid and air. Most surfactants consist of two ends, one attracted to the solvent (lyophilic) and the other repelled by it (lyophobic). The lyophobic part is often lyophilic towards an immiscible liquid, and the reverse is often the case for the lyophilic part. This allows a favourable interaction between a solvent and an immiscible liquid, permitting it to become mobile in solution. This is the basis of emulsification and is how detergents clean oils from surfaces using water.

Surfactants can be classified according to the charge they possess: those, which do not have a charge, are called nonionic. Positively charged molecules are cationic and negatively charged surfactants are anionic, whilst those possessing both opposite charges are zwitterionic.

By lowering the surface tension of water and other liquids, surfactants can aid the wetting of a surface, by lowering the contact angle. Foaming in liquids can also be controlled by surfactants. Foaming can be prevented by choosing the right surfactant thereby preventing large volume increases during agitation of the liquid. Alternatively, it can be promoted by increasing the stability of liquid-air boundaries, for example to create a blanket of foam to put out fires.

Rapidly expanding or contracting surfaces, such as those on expanding bubbles when solutions are heated, undergo rapid diffusion of surfactant molecules. This rapid diffusion creates a surface tension gradient, causing shear stress at the surface. The change in surface stress must be balanced out by the change in shearing stress between the surface and the bulk fluid. This causes a change in speed of the surface as the surfactant adsorbs to the surface. This is known as the Marangoni effect.

The behaviour of surfactants under dynamic, non-equilibrium conditions is of interest as it is important for the understanding of foams, jets, emulsions and the spreading of liquids on surfaces. When added to printer ink, surfactants help stabilise the direction of ink as it is rapidly ejected from a fine nozzle; as the air-liquid interface surfaces are newly formed there is very little time for the surfactants to diffuse because of the speed of the drop and the short distance between the paper and the nozzle. The surfactant needs to diffuse rapidly to ensure that it has the desired effect before the ink hits the paper.

Above a certain concentration, specific to the surfactant used, the surfactant molecules aggregate and form micelles. The concentration at which these start to form is known as the critical micelle concentration (cmc). By forming micelles, the free energy of the system is lowered because although the orientations of the surfactant molecules are restricted, there is a favourable entropy change on removing the lyophobic parts of the surfactant molecules from the water.

The presence of salts or other dissolved species in the solution can affect the adsorption of ionic surfactants to the interfaces. Hence, the extent and rate of adsorption can be controlled by changing the salt concentration. This is important for detergents, where hard water, which has many ions dissolved, reduces their dirt cleaning effectiveness. Salt concentration can also affect the cmc of the surfactant.

### 1.5.2 Adsorption at the liquid/vapour interface

As the Lucas-Washburn model predicts that the velocity depends only on  $\gamma_{lv}$  (not the other surface tensions), the effect of the presence of surfactant is only accounted for by changes in  $\gamma_{sv}$ . However, as shown by Figure 1.15, the surface tension does not change significantly

until higher concentrations ( $\approx 1$  mM) and therefore the solution should behave as pure water until the surface tension decreases.

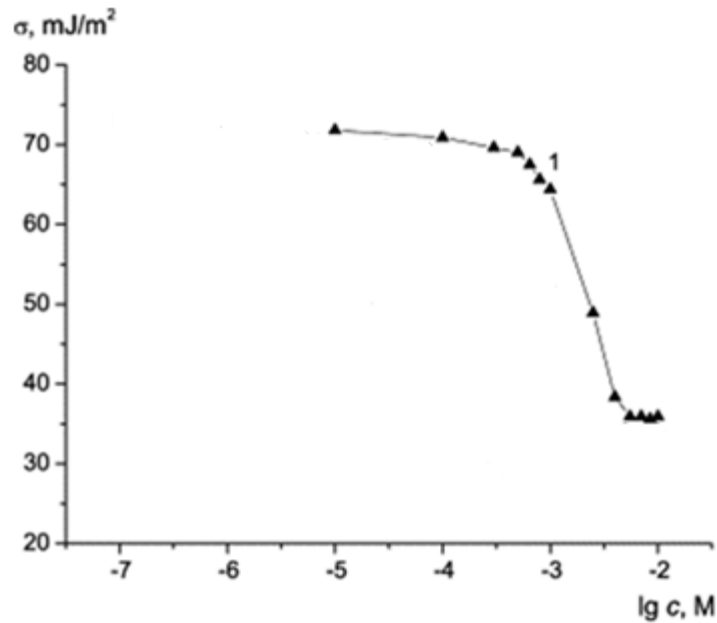


Figure 1.15 – (1) Adsorption isotherms of SDS at the air/water interface

Adapted from Sineva *et al.*<sup>40</sup>

### 1.5.3 Adsorption at the solid/liquid interface

Adsorption of surfactants at the solid-liquid interface depends on the nature of the solid: hydrophobic or hydrophilic – of like or opposite charge to the surfactant.

For example, Figure 1.16 shows how surface excess of the cationic surfactant changes with concentration on a hydrophilic, negatively charged surface. At concentrations well below the cmc, there is a plateau in surface excess associated with electrostatically bound  $CTA^+$  ions. Near the cmc, adsorption rises sharply as symmetric aggregates form at the interface. On a hydrophobic surface, the surface excess, for all the surfactants, changes more linearly with concentration and the adsorption stops at a monolayer. SDS does not adsorb at all on hydrophilic silica and non-ionic surfactants interact only weakly with this surface and show a step like isotherm near the cmc.

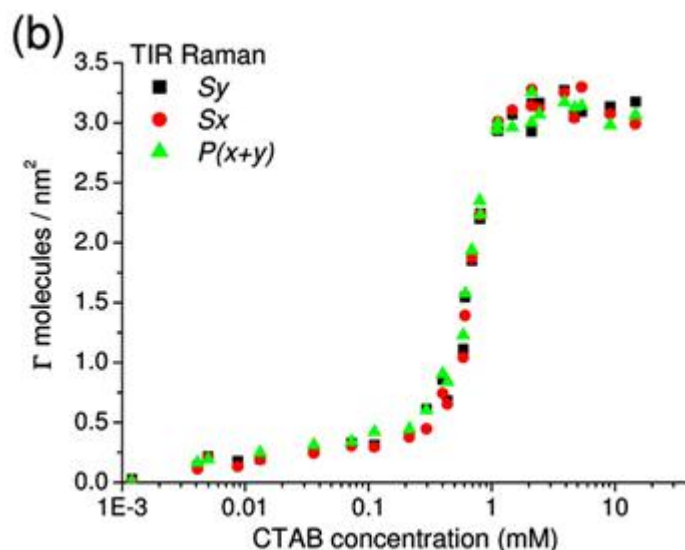


Figure 1.16 – Surface excess against CTAB concentration for a silica-water interface

Adapted from Tyrone *et al.*<sup>32</sup>

#### 1.5.4 Calculation of dynamic contact angle

In principle, one can calculate the dynamic contact angle of a liquid from the Lucas-Washburn equation, and measuring the distance of penetration against time of the liquid into the capillary. However, the value of  $\gamma_{lv}$  is assumed to be constant, and for low surfactant concentrations, or for surfactants which adsorb to the walls, this will not be the case. Hence it will not be possible to calculate the contact angle accurately, since  $\gamma_{sv}$  is not known and the assumptions made neglect other forms of dissipation, such as in the wedge.

#### 1.5.5 Surfactant Solutions in capillaries

With surfactant solutions in capillaries, the capillary force can change as the liquid penetrates the capillary. This is because the contact angle and hence the Laplace pressure changes with speed and speed depends on  $l$ , therefore deviations from the Lucas-Washburn distance square-root time behaviour should be expected.

Tiberg states that surfactants with a high cmc penetrate capillaries faster than those with a low cmc at the same concentration. This is due to slow diffusion in the micellar state because they diffuse slower and cannot adsorb directly to the surface.<sup>3</sup> The presence of micelles complicates the transport processes as they diffuse more slowly and cannot adsorb directly to surfaces. For the same total concentration of surfactant in solution, surfactants with long alkyl chains have a greater tendency to form micelles and their decay into monomers will be slower. Adsorption of surfactant to the glass creates a monomer depletion, which then generates a dynamic exchange of micelles and monomers.

## Bibliography

1. Lucas, R. *Kolloid Z.* **1918**, *23*, 15.
2. Washburn, E. W. The dynamics of capillary flow. *Physical Review* **1921**, *17* (3), 273-283.
3. Tibergh, F.; Zhmud, B.; Hallstenson, K.; von Bahr, M. Capillary rise of surfactant solutions. *Physical Chemical Chemical Physics* **2000**, *2*, 5189-5196.
4. Young, W.-B. Analysis of capillary flows in non-uniform cross-sectional capillaries. *Colloids and Surfaces A: Physicochemical and Engineering Aspects* **2004**, *234*, 123-128.
5. Haake, D.; Klatte, J.; Grah, A.; Dreyer, M. E. Flow Rate Limitation of Steady Convective Dominated Open Capillary Channel Flows Through a Groove. *Microgravity Science Technology* **2010**, No. 22, 129-138.
6. Quéré, D. Wetting and Roughness. *Annual Reviews of Materials Research* **2008**, No. 38, 71-99.
7. Wenzel, R. N. Resistance of Solid Surfaces to Wetting by Water. *Industrial & Engineering Chemistry* **1936**, *8* (28), 988-994.
8. Huntington, A. K. The concentration of metalliferous sulphides by flotation. *Transactions of the Faraday Society* **1906**, *1* (345), 345 - 355.
9. Cassie, A. B. D.; Baxter, S. Wettability of porous surfaces. *Transactions of the Faraday Society* **1944**, *40*, 546-551.
10. Cottin-Bizonne, C.; Cross, B.; Steinberger, A.; Charlaix, E. Boundary Slip on Smooth Hydrophobic Surfaces: Intrinsic Effects and Possible Artifacts. *Physical Review Letters* **2005**, *94*, 056102.
11. Atkins, P.; de Paula, J. *Atkins' Physical Chemistry*, 8th ed.; Oxford University Press: Oxford, 2006.
12. Hilpert, M. Effect of dynamic contact angle on liquid infiltration into inclined capillary tubes: (Semi)-analytical solution. *Journal of Colloid and Interface Science* **2009**, No. 337, 138-144.
13. Dimitrov, D. I.; Milchev, A.; Binder, K. Capillary Rise in Nanopores: Molecular Dynamics Evidence for the Lucas-Washburn Equation. *Physical Review Letters* **2007**, *99* (5), 054501.
14. de Gennes, P. G. Wetting: statistics and dynamics. *Reviews of Modern Physics Part 1* **1985**, *57* (3), 827-863.
15. Hamraoui, A.; Nylander, T. Analytical Approach for the Lucas-Washburn Equation. *Journal of Colloid and Interface Science* **2002**, *250*, 415-421.

16. Blake, T. D.; Haynes, J. M. Kinetics of liquid/liquid displacement. *Journal of Colloid and Interface Science* **1969**, *30* (3), 421-423.
17. Dussan V, E. B. On the spreading of liquids on solid surfaces: static and dynamic contact lines. *Annual Reviews of Fluid Mechanics* **1979**, *11*, 371-400.
18. Blake, T. D. The physics of moving wetting lines. *Journal of Colloid and Interface Science* **2006**, *299*, 1-13.
19. Chebbi, R. Dynamics of liquid penetration into capillary tubes. *Journal of Colloid and Interface Science* **2007**, No. 315, 255-260.
20. Hoffman, R. *Journal of Colloid and Interface Science* **1975**, No. 50, 228.
21. Zhmud, B. V.; Tiberg, F.; Hallstenson, K. Dynamics of Capillary Rise. *Journal of Colloid and Interface Science* **2000**, *228*, 263-269.
22. Hilpert, M. Explicit analytical solutions for liquid infiltration into capillary tubes: Dynamic and constant contact angle. *Journal of Colloid and Interface Science* **2010**, *344* (1), 198-208.
23. Fries, N.; Dreyer, M. An analytic solution of capillary rise restrained by gravity. *Journal of Colloid and Interface Science* **2008**, *320*, 259-263.
24. Bain, C. D. Penetration of surfactant solutions into hydrophobic capillaries. *Physical Chemistry Chemical Physics* **2005**, *7*, 3048-3051.
25. Quéré, D. Inertial capillarity. *Europhysics Letters* **1997**, *39* (5), 533-538.
26. Starov, V. M. Spontaneous rise of surfactant solutions into vertical hydrophobic capillaries. *Journal of Colloid and Interface Science* **2004**, *270*, 180-186.
27. Cai, Y. K. Phenomena of a liquid drop falling to a liquid surface. *Experiments in Fluids* **1989**, *7* (6), 388-394.
28. Churaev, N. V.; Martynov, G.; Starov, V. M.; Zorin, a. Z. M. Some features of capillary imbibition of surfactant solutions. *Colloid & Polymer Science* **1981**, *259* (7), 747-752.
29. Churaev, N. V.; Zorin, Z. M. Penetration of aqueous surfactant solutions into thin hydrophobized capillaries. *Colloids and Surfaces A: Physicochemical Engineering Aspects* **1995**, *100*, 131-138.
30. Do, D. D.; Do, H. D.; Wongkoblap, A.; Nicholson, D. Henry constant and isosteric heat at zero-loading for gas adsorption in carbon nanotubes. *Physical Chemistry Chemical Physics* **2008**, *10*, 7293-7303.
31. Hammond, P. S.; Unsal, E. Spontaneous and Forced Imbibition of Aqueous Wettability Altering Surfactant Solution into and Initially Oil-Wet Capillary. *Langmuir* **2009**, *25* (21),

12591-12603.

32. Tyrode, E.; Rutland, M. W.; Bain, C. D. Adsorption of CTAB on Hydrophilic Silica Studied by Linear and Nonlinear Optical Spectroscopy. *Journal of the American Chemical Society* **2008**, *130* (51), 17434-17445.
33. Starov, V. M.; Velarde, M. G.; Radke, C. J. *Wetting and spreading dynamics*; CRC Press - Taylor & Francis Group: Boca Raton, Florida, USA, 2007; Vol. 138, Surfactant science series.
34. CRC. CRC Handbook of Chemistry and Physics, 74th ed.; CRC Press, 1994.
35. Khoury, F. M. *Multistage separation processes*, 3rd ed.; CRC Press, 2005.
36. Hansen, R. J.; Toong, T. Y. Dynamic Contact Angle and Its Relationship to Forces of Hydrodynamic Origin. *Journal of Colloid and Interface Science* **1971**, *37* (1), 196-207.
37. Montgomerie, R. R. *Dynamics of Reactive Flow*; MSci Thesis; Worcester College, University of Oxford: Oxford, 1994.
38. Burnet-Hall, G. D. *Reactive Spreading of Drops on Surfaces*; MSci Thesis; Magdalen College, University of Oxford: Oxford, 1993.
39. Fries, N.; Dreyer, M. The transition from inertial to viscous flow in capillary rise. *Journal of Colloid and Interface Science* **2008**, No. 327, 125-128.
40. Sineva, A. V.; Parfenova, A. M.; Fedorova, A. A. Adsorption of micelle forming and non-micelle forming surfactants on the adsorbents of different nature. *Colloids and Surfaces A: Physicochemical and Engineering Aspects* **2007**, *306* (1-3), 68-74.
41. Savelski, M. J.; Shetty, S. A.; Klob, W. B.; Cerro, R. L. Flow Patterns Associated with the Steady Movement of a Solid/Liquid/Fluid Contact Line. *Journal of Colloid and Interface Science* **1995**, *176*, 117-127.

## Chapter 2 Experimental

### 2.1 Surfactants

Crystalline surfactants were stored in the freezer.

Sodium dodecyl sulfate (SDS) was recrystallized in ethanol twice from bulk purchased from Sigma-Aldrich and left to dry overnight under vacuum.

The twice-recrystallized SDS was purified further using a Soxhlet Apparatus overnight, as described by Miles and Shedlovsky<sup>1</sup> with diethyl ether as the solvent. The SDS could have been further purified by foam fractionation as described by Hines,<sup>2</sup> but it was decided that the small increase in purity would have had limited effect because the surface lifetimes were so short, therefore the impurities would not have had time to diffuse to the surface.

The CTAB, purchased from Sigma-Aldrich was recrystallized with ethanol and acetone.

The  $C_nE_6$  ( $n=12, 14$ ) (hexaethylene glycol monododecyl ether and hexaethylene glycol monotetradecyl ether respectively) compounds were used as provided, purchased from Sigma-Aldrich. Surfactants were weighed to an accuracy of  $\pm 0.0001$  g.

Surfactants were added to UHP water, produced by the Milipore Milli-Q A10 water purification unit. The water entering this purifier had first purified by a Milipore Elix system. The water used had a specific resistivity  $>18$  M $\Omega$  cm.

A stock solution was made up of the highest concentration required in a volumetric flask. From this, measured aliquots were transferred by volumetric pipette to another volumetric flask and diluted to the required concentration.

The concentrations used were chosen to span the cmc of that particular surfactant and which could be made up easily and accurately with the equipment (pipettes and volumetric flasks) available.

Sodium chloride from Sigma-Aldrich, 99.5% was used as received.

The decane from Sigma-Aldrich, 99+%, was further purified by passing through a column of activated neutral alumina to remove unsaturated impurities.

### 2.2 Capillary Setup

In initial experiments, a fibre optic halogen light source was used to illuminate the capillary from various angles. It was difficult to avoid reflections from the outside surface into the camera, which prevented the MATLAB program, discussed later, from distinguishing between these reflections and the meniscus. The best angle was found, by trial and

improvement, to be below  $45^\circ$  to the horizontal as this had the lowest reflection off the outside of the capillary. High contrast was still difficult to achieve and this made it difficult to track the meniscus automatically with a computer. It was also hard to obtain an image of uniform contrast along the length of the capillary, moving the light source back resulted in better uniformity, but dimmer images. Tests were performed using the light source to shine down the length of the capillary to see if there was any contrast improvement. These tests demonstrated that the meniscus was visible as a bright spot, which was much easier to locate automatically. However, even focusing the beam onto the end of the capillary did not produce enough scattered light for imaging at the required high shutter speeds. The brightness of the meniscus also rapidly decreased along the length of the capillary, due to light being progressively scattered by the walls.

The light source was swapped for a laser, as it was thought that a coherent beam would travel further along the capillary. The first laser was a 4 mW HeNe. While this did improve the images, the intensity of scattered light was still too low to use at the required shutter speed. This laser was then replaced with a 35 mW, 632 nm JDS uniphase 1144P HeNe laser and this produced much brighter images. Scatter from the walls was still a problem, and so a telescope was constructed using one +125 mm and one +60 mm lenses to reduce the width of the beam down to approximately 0.5 mm.

Curtains surrounded the laser table to prevent the beam or its reflections from escaping into the lab and a warning light was used to indicate when the laser was powered. A beam dump was positioned at the end of the laser beam's path and there was an additional black plastic wall beyond this. The operator wore green laser goggles at all times when the laser shutter was open and a tight iris was used to block reflections from the end of the capillary. Card was used to block reflections from the liquid drop on the end of the tube. During alignment, a neutral density filter was used.

The capillaries used for preliminary experiments were made by taking 0.9 mm internal, 1 cm external diameter glass pipe, heating it in a glassblower's burner and extruding quickly to make a thin tube of ca. 1 mm diameter. The diameter of the capillaries could be varied by adjusting the speed at which the ends of the glass tubing was pulled. While the internal diameter of these capillaries could have been determined, by weighing a volume of liquid, only an average could be taken, and the method of manufacture would have likely introduced variations along their length. So, for data gathering experiments, disposable Microcaps (Drummond Scientific) purchased from Sigma-Aldrich were used.

A syringe, controlled by a syringe pump, was connected to a horizontally mounted piece of 3.65 mm internal diameter PTFE (Polytetrafluoroethylene) tube. The syringe pump was started on its fastest setting to produce drops at the end of the tube, which fell into a funnel connected to a pipe for waste. The horizontal capillary was then dipped into the drop, allowing water to penetrate the capillary. This method was then refined by drilling a small hole in the wall of the pipe, and clamping off the end, so that the drops came out of a smaller hole to see if this was any different. The latter method however, did not produce large enough drops, and so they shrunk quite considerably when the capillary took up the liquid. This would result in a change in the Laplace Pressure, meaning that the pressure at the entrance to the capillary would vary.

The syringe was changed to a separating funnel connected to a pipe, so that a stream of water could then flow out of the end of the pipe, into which the end of the capillary could be inserted. The end of the tube was later fitted with a glass tube connected to a v-shaped trough or flat glass slide. This created a flat cascading solution and had the advantage of allowing the capillary to enter the bulk flow. These methods, however, required large volumes of surfactant solution, which would not have been suitable for expensive surfactants, such as the non-ionics. For surfactants like CTAB that strongly adsorb to glass, the large surface area of glass needed would have resulted in substantial surfactant losses and hence a lower surfactant concentration at the capillary.

In the final design, a PTFE tube was connected to a syringe with the other end clamped onto a laser post using a boss and clamp. The stand was made movable by mounting it on a micrometer stage, which could be moved freely by hand when the digital micrometer was wound all the way in. The syringe was rinsed thoroughly with surfactant solution before filling. The syringe was placed slightly higher than the tube outlet to help reduce the effect of a change in size of the liquid droplet on the end, and hence a change in Laplace pressure, affecting the rate of penetration. The droplet on the end was made as small as possible (virtually flat) to minimise the curvature. Additionally because the tube was approximately 10 times larger than the smallest capillary radius, the radius of curvature of the end drop was very large compared to that inside the capillary. For the largest capillaries, withdrawing 10  $\mu\text{l}$  of liquid from the drop would have changed the curvature the most, but as mentioned, the effect on change in pressure will be small compared to that inside the capillary.

The capillaries were placed in a v-groove machined in an aluminium support, which was painted black to reduce the amount of reflection from the surface, as the scatter of the light, particularly from the vertical surfaces resulted in the MATLAB program picking up

these edges instead of the meniscus. The support was later changed to plastic, as this was even less reflective. The final support is illustrated in Figure 2.1. Figure 2.2 illustrates the final setup.

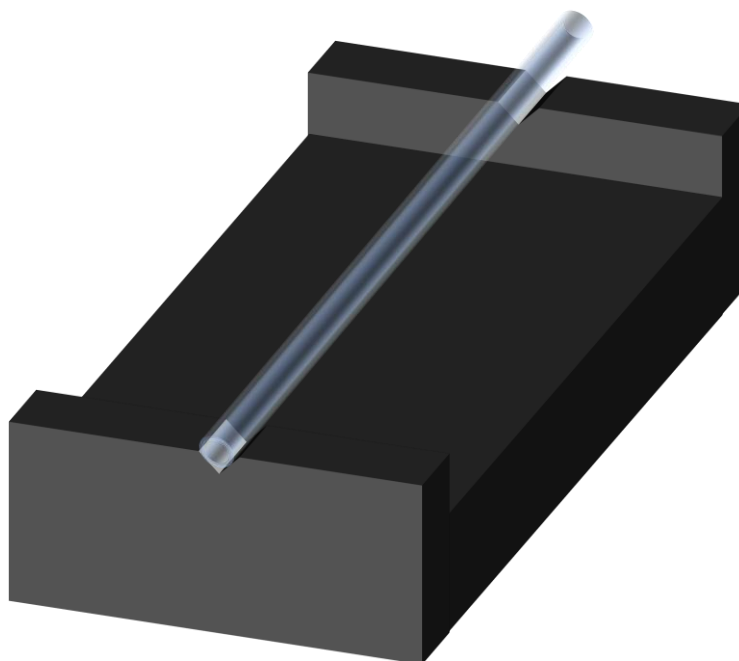


Figure 2.1 – The capillary mount

Some of the capillaries were made hydrophobic by exposing them to dimethyloctylchlorosilane (97%, Sigma Aldrich, used as received) vapour overnight, which reacts with the silanol groups present on the surface of the glass at room temperature as described in Tiberg *et al.*<sup>3</sup> The liquid silane was placed in a large petri dish with a lid, within which was a smaller petri dish containing the capillaries. These dishes were then placed in a large desiccator containing a silica-drying agent, and left overnight. The capillaries were then sonicated and rinsed after silation with tetrahydrofuran and absolute ethanol, and then dried in air, whilst covered, at around 100°C in an oven. Between washings, the solvents were blown out with compressed nitrogen gas.

A glass funnel was connected to a waste container via a 1 cm diameter plastic pipe to catch drips and purged fluid from the tube connected to the syringe.

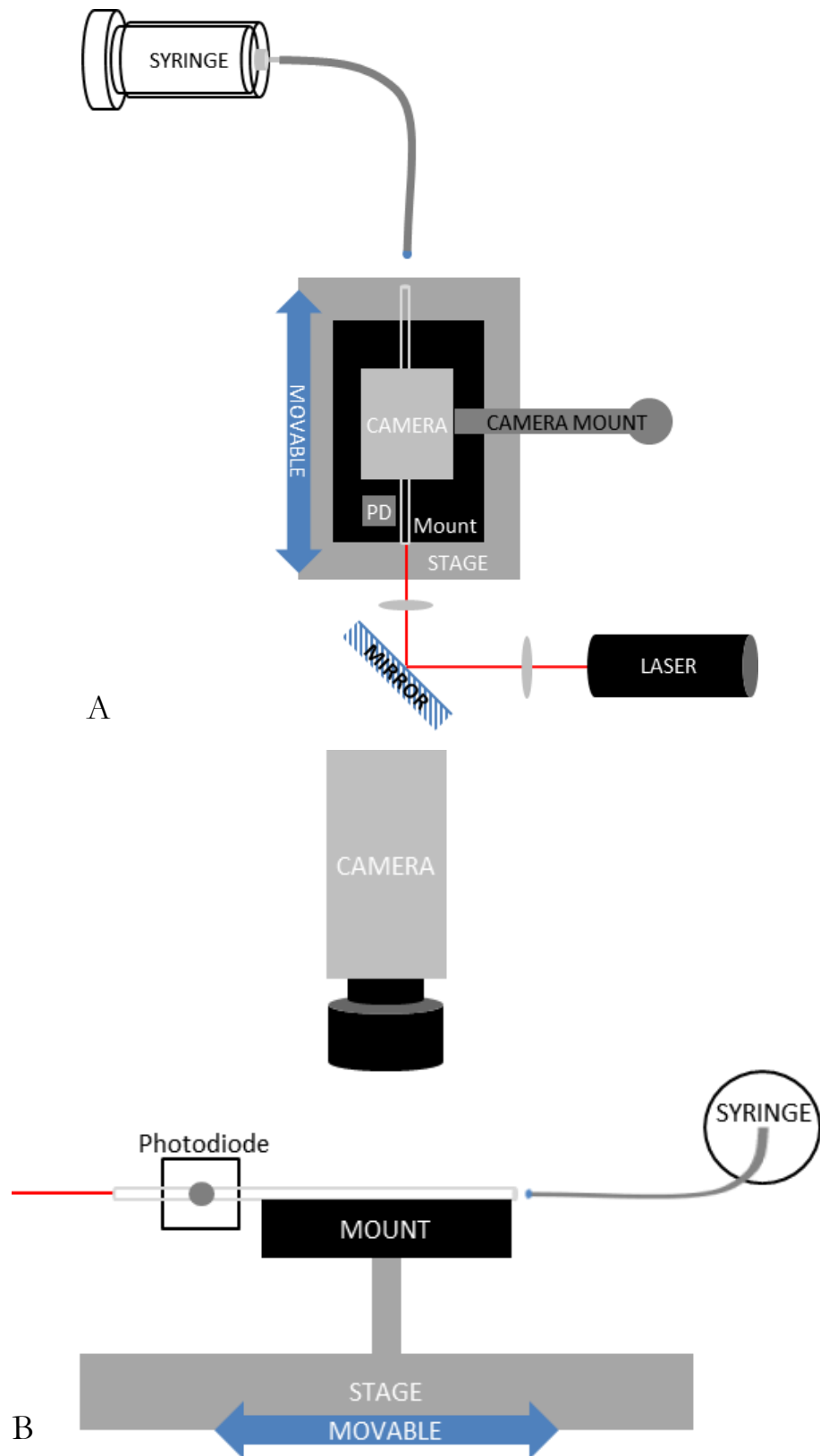


Figure 2.2 – Experimental setup

The diameters of capillaries, referred to in future by their capacity, are shown in Table 2.1.

Table 2.1 – Dimensions of capillaries used (accuracies are  $\pm 1\%$  volume)

<b>Drummond Microcaps Specifications</b>			
<b>Capacity (<math>\mu\text{L}</math>)</b>	<b>Length (mm)</b>	<b>O.D. (<math>\times 10^{-3}</math> m)</b>	<b>I.D. (<math>\times 10^{-3}</math> m)</b>
<b>0.5</b>	<b>32</b>	<b>0.5588</b>	<b>0.1422</b>
<b>1</b>	<b>32</b>	<b>0.6604</b>	<b>0.2007</b>
<b>3</b>	<b>32</b>	<b>0.8636</b>	<b>0.3454</b>
<b>10</b>	<b>41</b>	<b>0.8001</b>	<b>0.5563</b>

### 2.3 Glassware Preparation

Glassware for preparation and handling of solutions was sonicated with an alkaline detergent (Borer 15 PF) for at least 15 minutes at  $60^\circ\text{C}$ , and rinsed thoroughly several times with UHP water to ensure it was clean.

Capillaries were placed in an annealing oven at  $565 \pm 2^\circ\text{C}$  for 30 minutes and then allowed to cool overnight. The containers were then covered with Parafilm to protect the capillaries from dust and other contaminants. The capillaries were then transferred and left in chromosulphuric acid for 30 minutes and then rinsed thoroughly with UHP water. The capillaries were stored in sealed sample vials. They were only removed individually from these vials using plastic tweezers to prevent scratching, just before they were used. All glassware, optics and instruments were handled wearing gloves to prevent contamination.

The humidity was increased by leaving capillaries in a desiccator partially filled with hot water and then left overnight. The capillaries were removed individually when required. As the film of water present on the surface would start to evaporate as soon as the capillaries were removed from the desiccator, quick measurement was important. Therefore, practice in quickly moving the capillaries from the desiccator and running the experiment was required, to ensure time outside the humid environment was minimal. With practice it was found that this time was less than 15 seconds.

### 2.4 Camera Setup

Two types of video cameras were used to observe the penetration of solutions into the capillaries. These were levelled with a spirit level before use.

A high-speed CMOS (complementary metal–oxide–semiconductor) digital camera, the monochrome PixeLINK PL-B761U USB 2.0 VGA camera, was used to study the hydrophilic and oil wet capillaries. With a high-speed asynchronous electronic shutter to freeze motion, and a high frame rate of up to 2579 fps, the camera was the best already

available. The maximum resolution was 752x480 px although at a reduced frame rate. Problems were encountered running the camera at vertical resolutions higher than 752x135; although this restricted the frame rate to about 240 fps, it was still adequate to obtain videos that could be analysed to generate many data points as the meniscus moved along the capillary. This problem was probably related to the speed of the computer to which the camera was connected.

The exposure times varied between 0.2 and 0.4 ms depending on the contrast levels required for analysis. These varied because as the contact angle changed depending on the concentration of the surfactant used, the amount of light scattered into the camera also altered.

To study the slower penetration of solutions into hydrophobic capillaries, a JAI CV-M10 SX progressive scan monochrome analogue CCD (charge-coupled device) Camera with a shutter speed of 1/10000 s was used. This was connected to a DALSA PC2-Vision analogue PC frame grabber. The images taken were recorded at a resolution of 752x582 px, at 25 fps. A shutter speed of around 0.25 ms was used. The lower frame rate could be used for the hydrophobic case as the meniscus moved much more slowly. This had the advantage of improving contrast and, when used in combination with the lens iris, increased the depth of focus thus making the picture sharper. Additionally, the difference in sensitivity between the CMOS and CCD chips was noticed, with the CMOS sensor requiring slightly longer shutter times to obtain the same brightness for the same light source.

The camera record trigger consisted of a photodiode placed close to the capillary, connected to a Le Croy oscilloscope. It was found that when the water droplet touched the end of the capillary, the light scattered from the sides of the capillary dropped in intensity and that this drop could be detected by a photodiode. This drop was detected by the voltage dropping below a predefined threshold on the oscilloscope. When triggered an output voltage was generated on the CAL channel, which was connected to the capture card for the JAI camera or directly to the PixeLINK camera. This CAL signal was too low a voltage to trigger the camera, so a small amplifier, adapted from a TTL amplifier, was used to amplify the signal to above the 5 V threshold voltage, to 9 V, for the card/camera's trigger. A manually switched battery box later replaced the trigger as it was found more reliable to trigger the camera before water entered the capillary. The automatic trigger suffered from either not triggering or triggering spontaneously. With time this trigger could have been perfected, however manual triggering still worked well.

## 2.5 Analysis

An image-processing program was written in MATLAB to analyse the moving meniscus in videos and in a series of images. The code is available in Appendix C. Two input functions were needed as the PixelLINK camera recorded videos whereas the software controlling the JAi camera crashed when trying to record videos, so a series of images were recorded instead. Care had to be taken to ensure that using images and videos produced the same results, as the pixel indexing in MATLAB of each type was different. This included writing another program, which split up the frames from the video into separate image files, which were then run through the image-processing program.

The program underwent many revisions, and care was made to ensure data generated by later versions was identical to data processed earlier. The first version simply used an algorithm, which located the brightest part of the image along a line selected by the user. This worked well for when the illumination was perfect, but often selected the wrong points due to noise and light scatter off the surface of the capillary.

The second version of the program utilised a convolution with a Sobel operator to process the image for edge detection. Both combinations of horizontal, vertical and just horizontal, along with multiple passes of Sobel operators were used, but it was found that a single pass of a simple operator in the form of Equation (2.1) was best.

$$\begin{pmatrix} -1 & 0 & +1 \\ -2 & 0 & +2 \\ -1 & 0 & +1 \end{pmatrix} \quad (2.1)$$

The Sobel operator is a commonly used discrete differential operator edge detection algorithm. Its output when convoluted in two dimensions with the horizontal lines of pixels (5 lines from the middle of the capillary, chosen manually with the mouse) from the images is a gradient vector of the image's intensity. The maximum of this gradient, multiplied by the original image lines is then found and labelled as the point at which the meniscus lies. A simple counter works out the timescale from the frame rate whilst looping over all the frames.

Later an additional edge-finding algorithm was added. This performed a sum down each of the columns of pixels and then found the column with the highest sum, again using a Sobel operator; in most of the images, the meniscus was the brightest part. This algorithm worked alongside the former Sobel-only one and was sometimes capable of finding the meniscus when the first failed to locate it correctly. Hence, it could be used to reduce the number of data points needing to be deleted, details of which will be described later. Later still, refinements in laser alignment and minor tweaks with the first algorithm reduced the

need for the second algorithm, but it was left in the program as the added calculation time was negligible and it had no effect on the results.

A function that produced an average of all the images and then subtract this from each individual frame was added, and greatly improved results by reducing the number of static bright points. Captured frames typically had lots of background light, as shown in Figure 2.3. Attempts were made to reduce this by first painting black the aluminium support block and then replacing it with a black plastic design. The results of the background subtraction on Figure 2.3 are shown in Figure 2.4

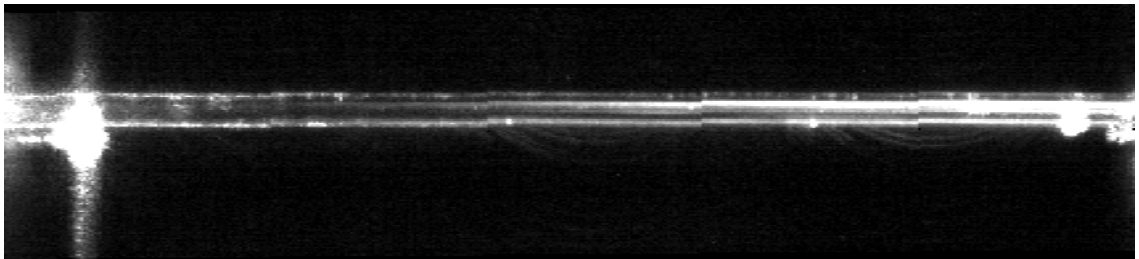


Figure 2.3 – Before background subtraction

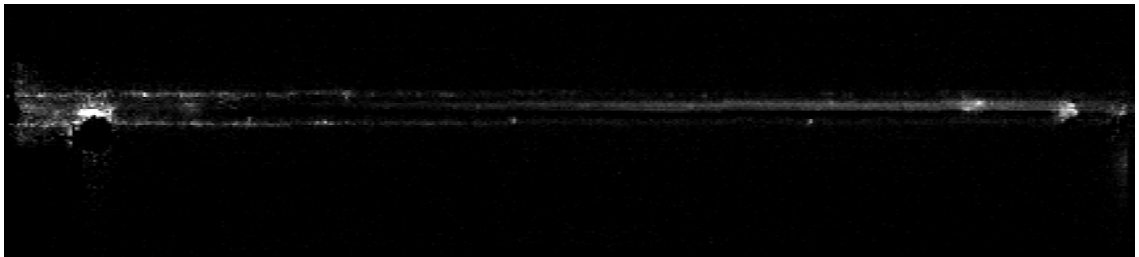


Figure 2.4 – Video frame after background subtraction

A low pass filter in the y-axis was also later added which further reduced misidentification by averaging over a few horizontal lines. This meant that for the program to “see” the meniscus, there had to be a gradient present on a few (five were selected) horizontal lines of the image. This addition almost completely eliminated misidentification and, as the filtering only occurred on the y-axis, there was no effect on the accuracy of position determination.

### 2.5.1 Data Removal

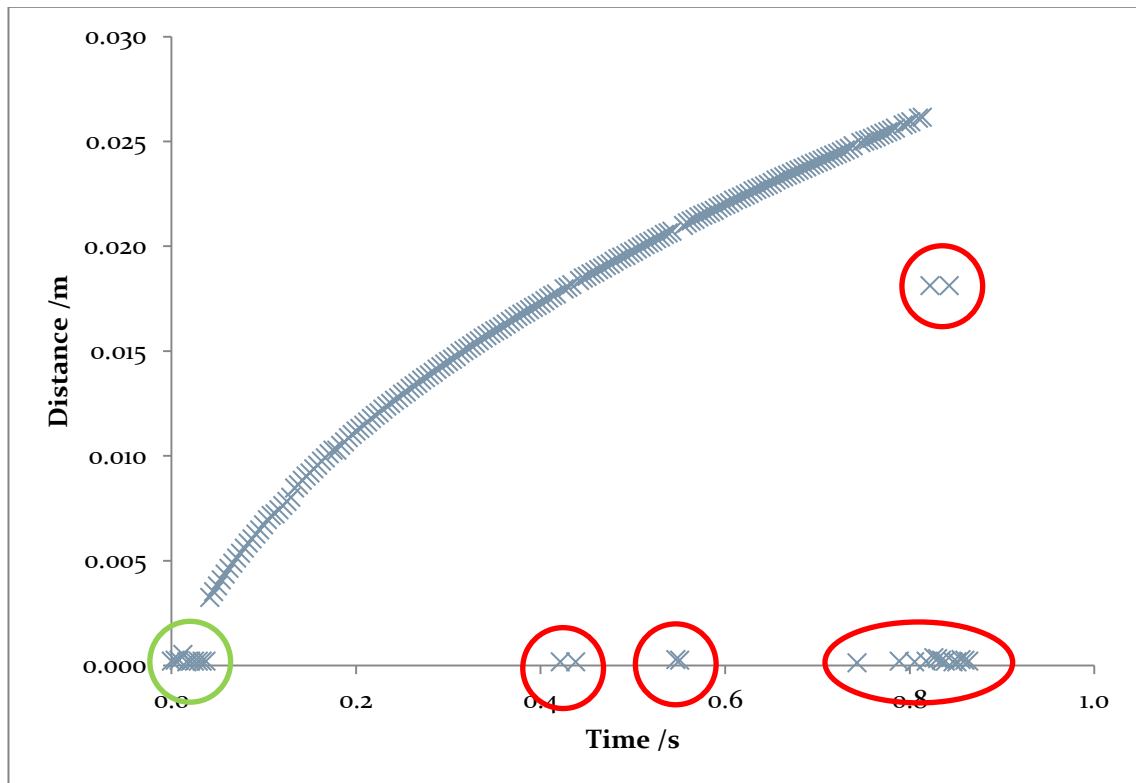


Figure 2.5 – An example of the raw data output from the MATLAB program after zero finding

Figure 2.5 shows the output directly from a sample analysis by the MATLAB program, with the low pass filter turned off for emphasis. Clearly, there are several points that do not follow the line (circled red), where the program incorrectly identified the meniscus position. Hence, these points are deleted and ignored. Some of the points at the start (circled green) could lie on the line; however, it is clear from watching the circles plotted on the images during processing (described later), in slow motion, by introducing a time pause between each image display, that they are not the meniscus and just random reflections or scatterings.

### 2.5.2 Pixel Size Calibration

To calibrate the pixel size and hence calculate the distance from the size of the pixels, a high contrast picture of a  $\frac{1}{2}$  mm scale ruler was taken, Figure 2.6, under illumination by an angle-poise lamp, with the camera after each experiment. The image was then run through another MATLAB program, which performed a Fourier transform on the image to calculate the number of  $\frac{1}{2}$  mm divisions per picture and then the size per pixel from the width and number of pixels in the image.

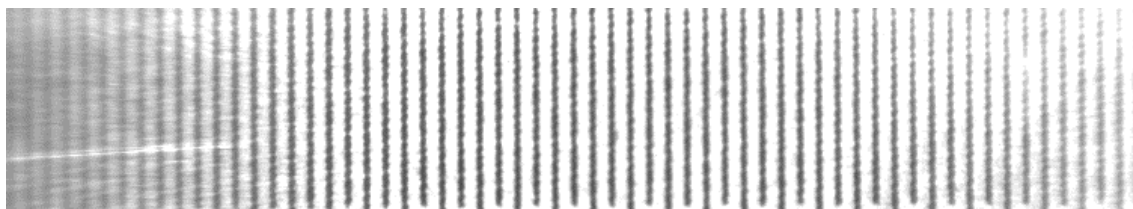


Figure 2.6 – Ruler calibration image

The frames were pre-processed before the meniscus finding algorithms were run. The images were first rotated by selecting two points in the image that should have been horizontal (the edge of the capillary) and then calculating the position of each pixel after the rotation. This process did leave a few step artefacts in the image, due to the need for the pixels to be placed back on the original grid, but as the images were typically only rotated a few degrees, the effects were small and would only have affected pixels on the y-axis.

## 2.6 Experimental Examples

Figure 2.7 shows the progress of the meniscus, illuminated by the laser, along the capillary as viewed by the camera after an average of all the frames has been subtracted and the image rotated to make the capillary horizontal.

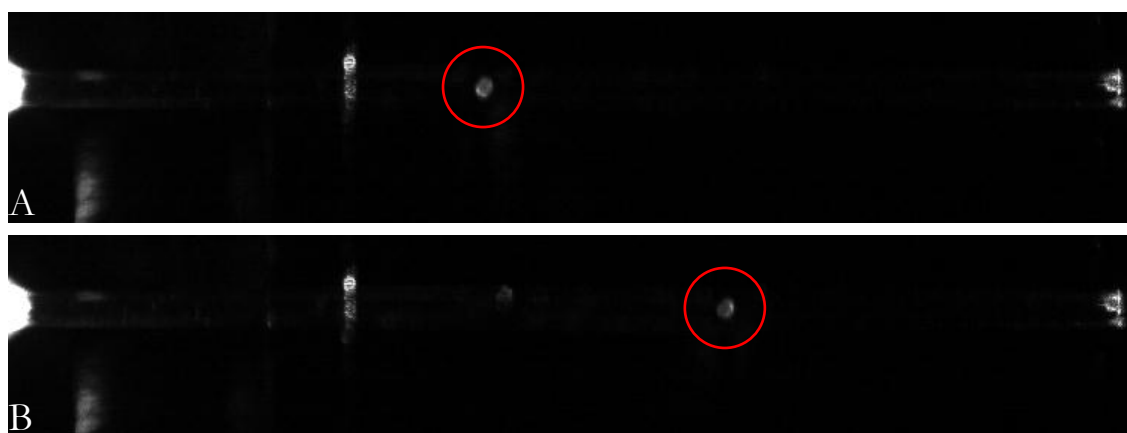


Figure 2.7 – Water meniscus (circled) moving along a 3 $\mu$ l capillary

A is ten frames before B at 239.6 frames per second

To plot the graphs, the time at which the meniscus entered the capillary was required. It was very difficult to image the meniscus moving right at the start, due to its speed and amount of light already scattered by the capillary walls. However, due to the inertial effects at the capillary entrance the speed in the first few millimetres was not expected to follow Lucas-Washburn behaviour, so these points are not required. At the point at which the meniscus of the water droplet was broken by the end of the capillary, the amount of light scattered by the end and out the sides of the capillary dropped. This was probably because the end of the capillary acted as a mirror when in air, reflecting the laser light back along the capillary. When the end was in water, the increase in refractive index, closer to that of

the glass resulted in the light not reflecting back down the capillary. Figure 2.8 shows the difference in brightness. A GUI (graphical user interface) was written to allow the manual stepping through of images to determine this contact time to an accuracy of one frame interval.

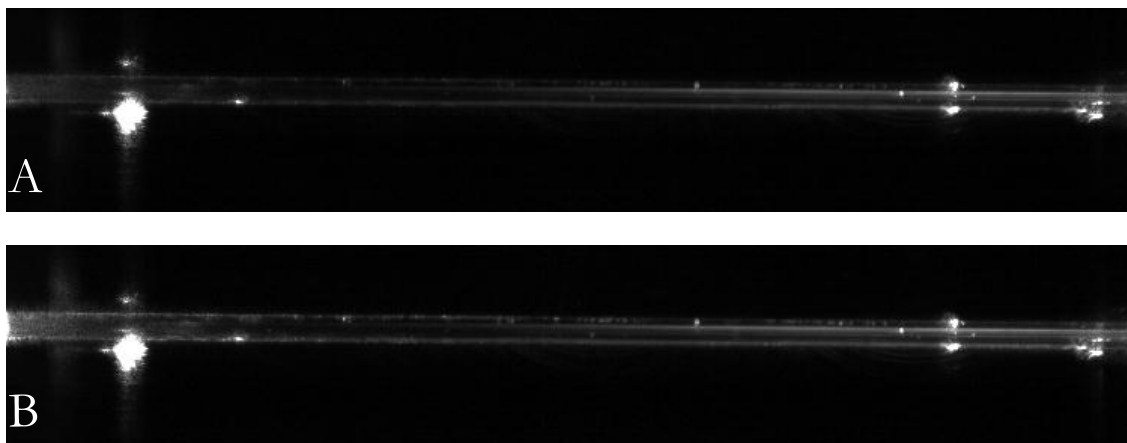


Figure 2.8 – The difference before (A) and after (B) contact of the capillary with the meniscus

While running through the frames, the MATLAB program displayed a green and blue circle at the point where the program detected the meniscus, as shown in Figure 2.9 this allowed the user to see how good the program was at detecting the meniscus.

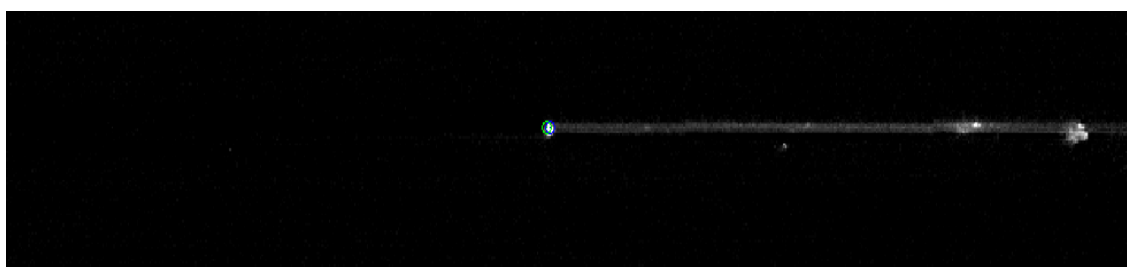


Figure 2.9 – MATLAB image analysis

The green and blue marks indicate where the algorithm has detected the meniscus

Attempts were also made to use the Sobel operator and a cross correlation of two consecutive images to analyse the images, which produced units of pixels moved per time difference in the two images, i.e. a speed. At 239 frames per second, the number of pixels moved by the meniscus in two consecutive images was too small to detect and so five images were selected, i.e. an image and the one five frames after it. However, improvements to the previous program meant that this cross correlation was not required.

## 2.7 Error Calculation

Table 2.2 shows the accuracies of the glassware used in the preparation of the surfactant solutions.

Table 2.2- Accuracies of glassware used

Capacity/ml	Item	Accuracy /ml
100	volumetric flask	0.15
50	volumetric flask	0.06
25	volumetric flask	0.08
10	volumetric flask	0.025
25	volumetric pipette	0.06
10	volumetric pipette	0.1
5	volumetric pipette	0.05
1	volumetric pipette	0.01
0.1	volumetric pipette	0.01

Propagation of these glassware accuracies and the accuracy of the mass balance (0.0001 g) through showed that all concentration accuracies were to  $10^{-5}$  mol dm<sup>-3</sup> or better, with the exception of the highest concentration of nonionic surfactants, where the accuracy was to  $10^{-4}$  mol dm<sup>-3</sup>. The concentration error bars are omitted from the graphs for clarity and because they did not exceed the diameter of the points on the graph.

When averaging data,  $\sigma_{\text{mean}}$  can be calculated as:

$$\sigma_{\text{mean}} = \frac{\sigma}{\sqrt{n-1}} \quad (2.2)$$

Where  $n$  is the number of data sets and  $\sigma$  is the standard error

### 2.7.1 Dynamic Contact Angle Determination

Attempts were made to determine the dynamic contact angle of the water penetrating the capillaries. The set up used a microscope and the JAI digital video camera. Several problems were encountered whilst trying to view the moving meniscus. Firstly, the small size of the meniscus meant that a high-powered objective was required. This greatly reduced the size of the viewable area to about half the width of the capillary. Additionally, due to the speed at which the meniscus moved, it was very hard to capture an image of the meniscus in the frame. Even switching later to the higher speed camera, results did not improve.

The distortion of the image due to the curved nature of the capillary walls acting like a lens also made it very hard to determine exactly what the contact angle was, as the location of the wall of the capillary had to be estimated.

Attempts were made to reduce the amount of distortion by using a water immersion lens, which had a working distance of 3.6 mm, as the refractive index of water is closer to that of glass than that of air. If an oil immersion lens had been available, this would have further reduced the distortion.

For the hydrophobic capillaries, using the water immersion lens produced further difficulties, as the outside of the capillaries was also hydrophobic, making it hard to keep the light capillary in the droplet of water under the lens. A glass slide was modified to produce a central groove to hold the capillary. However, this made it harder to get water to penetrate the capillary. Addition of surfactant to the droplet of water for immersion, to prevent the capillary from being pushed out of the drop, reduced the surface tension, which was required to hold the drop on the end of the water immersion lens.

Capillary rise experiments do allow for contact angles to be measured, however for the capillaries that were available, the capillary rise was higher than the length of the tube.

### 2.7.2 Oil wet capillaries

Clean hydrophilic capillaries were filled with decane, using capillary action. The oil was purified by passing through a column of activated neutral alumina in a fume cupboard. Due to the harmful effects of breathing in oil vapour during measurements, an approximately 1" diameter pipe was connected up to the fume extraction system to extract air from around the support area. Decane was chosen because of its availability in the lab, and its similar viscosity to water. The viscosities of decane and water are shown in Table 2.3.

Table 2.3 – Liquid viscosities <sup>4</sup>

Liquid	Viscosity/ mPa s	Temperature of Measurement/ °C
Decane	0.838	25
Water	0.1002	20

## Bibliography

1. Miles, G. D.; Shedlovsky, L. Minima in Surface Tension–Concentration Curves of Solutions of Sodium Alcohol Sulfates. *Journal of Physical Chemistry* **1944**, *48* (1), 57–62.
2. Hines, J. D. The Preparation of Surface Chemically Pure Sodium n-Dodecyl Sulfate by Foam Fractination. *Journal of Colloid and Interface Science* **1996**, *180*, 488-492.
3. Tiberg, F.; Zhmud, B.; Hallstenson, K.; von Bahr, M. Capillary rise of surfactant solutions. *Physical Chemistry Chemical Physics* **2000**, *2*, 5189-5196.
4. CRC. CRC Handbook of Chemistry and Physics, 74th ed.; CRC Press, 1994.

## Chapter 3 Results and Discussion

### 3.1 Experimental Procedures

It was important to ensure methods used were consistent as slight variations affect the results and so care needed to be taken to maintain conditions. All experiments from one data set were performed on the same day to prevent a change in ambient conditions in the lab from affecting results.

The room temperature of experiments was  $21 \pm 0.5^\circ\text{C}$ , unless stated otherwise. The solutions were equilibrated to room temperature by placing the flasks in a beaker of water already at room temperature.

Continual, repeated problems with the lab HVAC (heating, ventilation and air-conditioning) system caused many problems for all experiments conducted in the lab and while several complaints were made to maintenance, no solution was ever provided. On some days, the lab was so humid, water condensed on the ceiling and walls, and dripped down onto all the equipment. This prevented experiments, as the delicate cameras and computers had to be covered to prevent damage. At the start of the experiments, during the testing phase, there were minor problems; however, the humidity and temperature fluctuated widely during the later months of the project. The relative humidity is related to the thickness of the condensed film of water present on the walls of the capillaries. The effect of humidity on capillary penetration will be discussed later in 3.3. An enclosed, temperature-controlled environment around the apparatus could have been developed, but time constraints for this project would have made this difficult. Additionally, because the major variation occurred towards the end of the project, the apparatus had already been set up and results had been recorded and hence would have required starting setup from the beginning.

Determination of the zero point of time, when the water penetrated the capillaries is important, as it will affect the gradient of a graph of distance vs.  $t^{1/2}$ . As a first step, the time of the first frame in which the meniscus was detected was set to be zero. This frame will in fact be before the Lucas-Washburn zero time, due to the effects of inertia. There is an additional uncertainty, due to the frame rate of the camera. The true entry time could be out by up to one frame. Although at 239.6 frames per second this error is less than 0.004 s, at the high velocities generated at the beginning the contribution from this uncertainty may become significant.

The experimental and data processing techniques, after they had been refined, produced data which was had very low uncertainty (e.g. Figure 3.1), as shown by the scatter of the points, and very low systematic errors, as shown by the linearity. This demonstrates a fit to square-root time Lucas-Washburn behaviour, which assumes surface tension, viscosity and contact angle remain constant.

The Lucas-Washburn equation is reproduced below (3.1):

$$l = \sqrt{\frac{\gamma_{lv} R \cos \theta}{\eta} \frac{1}{2} t^2} \quad (3.1)$$

The gradient for this line can be found by linear regression.

Figure 3.1, a graph of distance against time, demonstrates the reproducibility of the data between data sets; four sets of data lie almost directly on top of each other. The results obtained are for pure water in a clean capillary and for these experiments, the reproducibility was generally excellent. This data also shows that later, when the experimental data showed less reproducibility, the errors were not due to the techniques, but the samples.

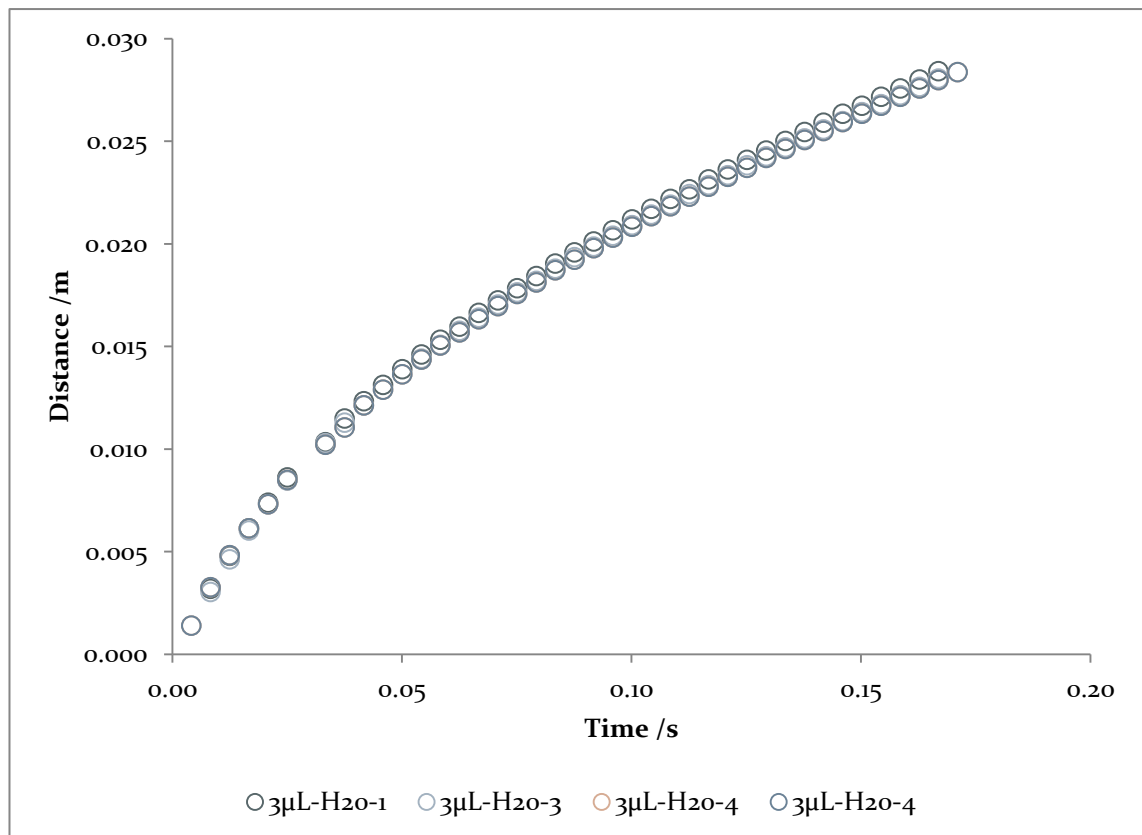


Figure 3.1 – Distance-time graph for 3µL capillaries and water

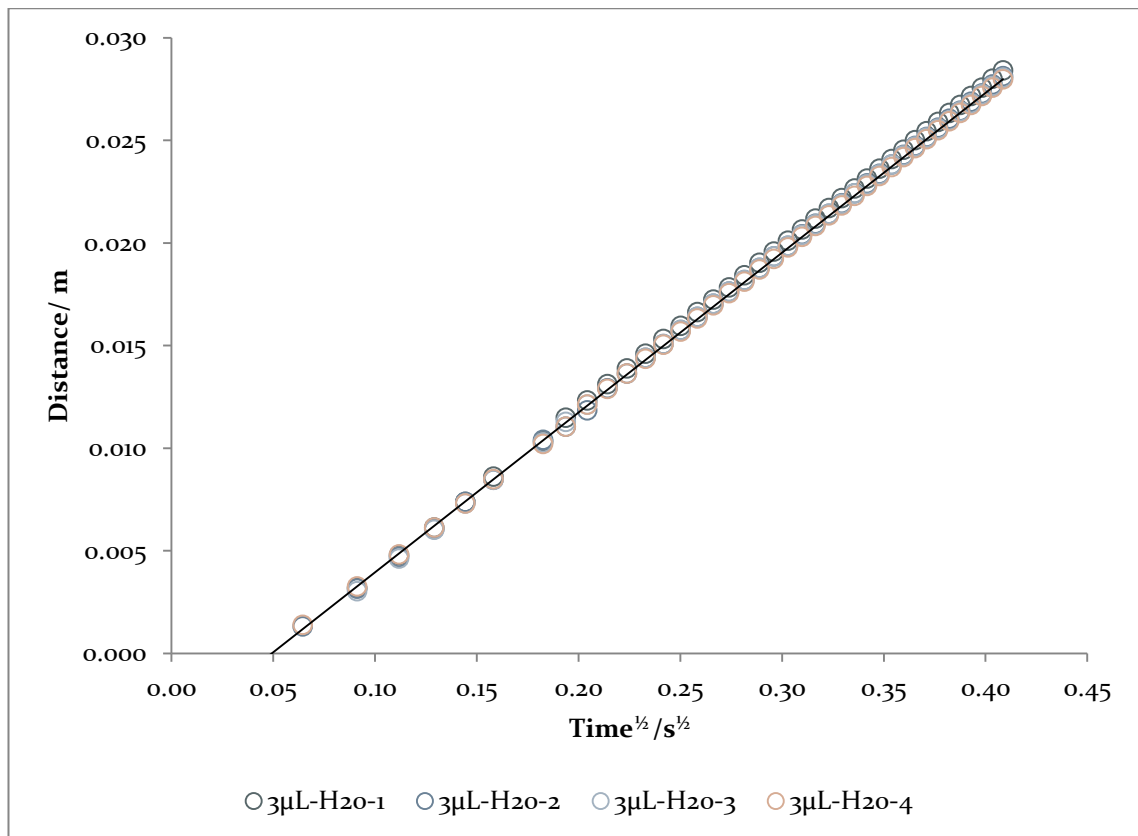


Figure 3.2 – Distance – square-root time plot for 3µl capillaries and water

Figure 3.2, a distance square-root time plot the same data as Figure 3.1, does not intercept at the origin, which demonstrates the deviation from the Lucas-Washburn behaviour that is due to the three aforementioned reasons: (I) frame rate error, discussed above, however this would result in a negative offset, (II) inertia of the fluid and (III) viscosity of the air.

The Lucas-Washburn theory assumes that the only dissipation mechanism is viscous losses in the bulk liquid.

Table 3.1 Slopes and errors for measurements

Run	Slope/ (m s <sup>-1/2</sup> )	Error
1	0.07939	0.00014
2	0.07860	0.00013
3	0.07865	0.00014
4	0.07787	0.00011
<b>Mean</b>	<b>0.0786</b>	<b>0.0006</b>

The random error on the line is very small, as shown in Table 3.1. The reproducibility of the slope is poorer than the standard error in individual slopes, showing the existence of some systematic variations. Nevertheless, the relative error in the slope is still only 1%, which represents a high degree of reproducibility. The problem occasionally encountered

was that, due to small variations in horizontal positioning of the capillary in the mount, the illumination of the meniscus was poor and prevented the program from being able to “see” the meniscus. Even though normally at least four repetitions were taken for each experiment, sometimes, the MATLAB program could not detect the meniscus for a sufficiently large number of images and the data had to be discarded.

Plates of the same borosilicate glass as the capillaries were not obtainable. This meant that any contact angle measurements and studies on macro surfaces were difficult. Only lime glass was available. Crude contact angle measurements on clean lime glass gave an approximately zero contact angle for pure water, meaning that the water spread. One can therefore also expect water to spread on borosilicate glass. Experiments to attempt to measure the contact angle inside the capillary by microscopy appeared to give an angle of roughly  $35^\circ$  for the static contact angle in the capillary. However, optical aberrations make this angle difficult to measure with certainty because the curved glass surface distorts the image and makes it hard to determine where the capillary wall is.

Another interesting observation is that the smallest  $0.5 \mu\text{l}$  capillaries were sometimes sucked into the PTFE tube. Due to their small weight of the capillary, the frictional forces between the capillary and mount were lower than the surface tension forces on the outside of the capillary.

### 3.2 Varying Radius

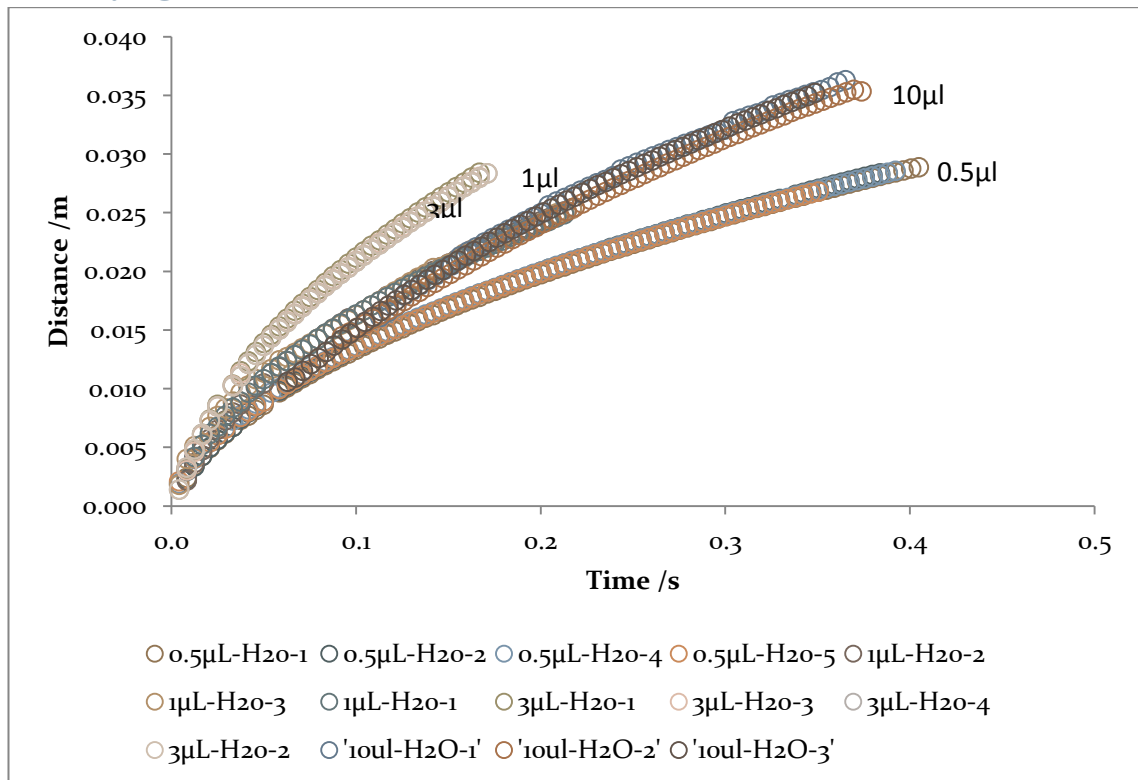


Figure 3.3 – Distance-time plot for all sizes

Figure 3.3 shows the distance-time data for all four sizes of capillary. Increasing the diameter of the capillary increases the speed of penetration, for sizes other than 10  $\mu\text{l}$ . Figure 3.4 shows the slope of the distance vs. time<sup>1/2</sup> graph against capillary radius<sup>1/2</sup>. The speed increase on increase in radius is due to the capillary force being proportional to the perimeter of the meniscus, as it is this that drives the penetration. The first three points lie on a straight line through the origin, demonstrating Lucas-Washburn type behaviour. The 10  $\mu\text{l}$  capillaries do not fit this line.

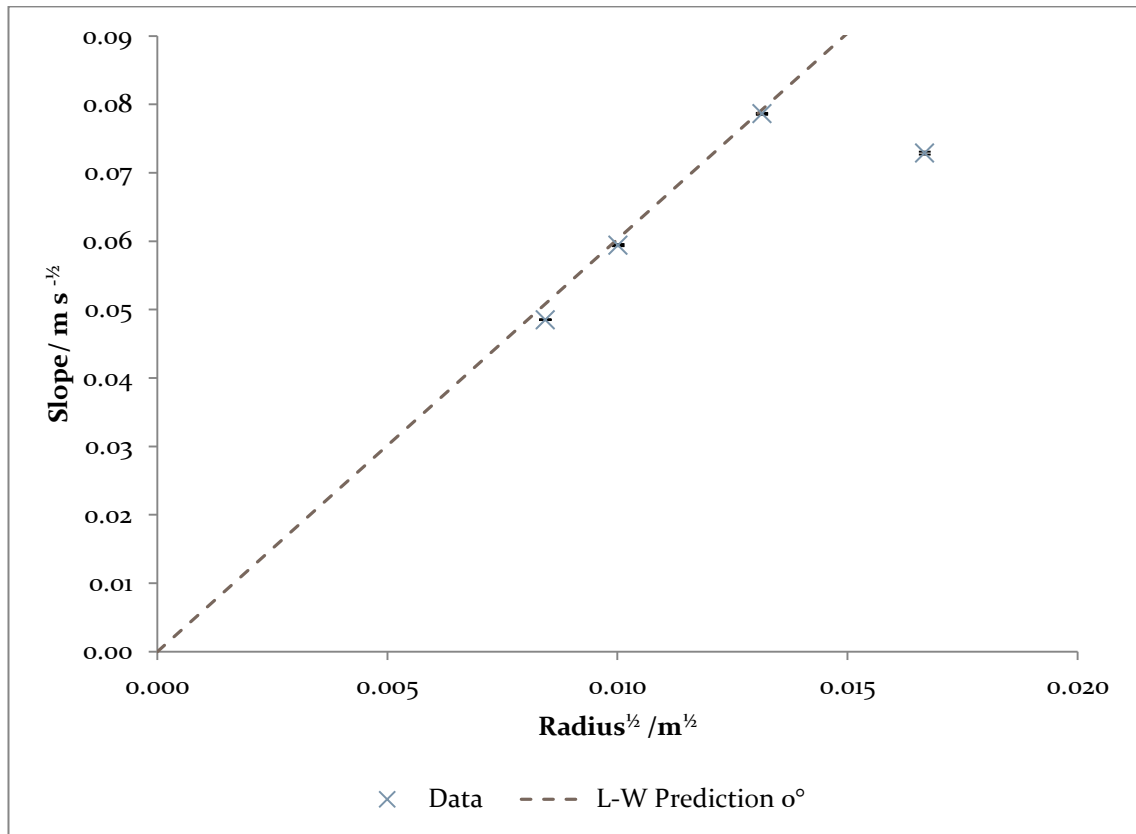


Figure 3.4 – Slope vs. square-root radius and Lucas-Washburn (L-W) prediction for  $\theta=0^\circ$

Figure 3.4 also shows the Lucas-Washburn prediction for  $\theta=0^\circ$  as a dashed line. The predicted and experimental slopes are not equal.

There are several possible reasons for the deviation in the slope from the Lucas-Washburn prediction. (I) Wedge dissipation: As shown, the dissipation in the wedge is approximately 10% of the work done and this partially accounts for this deviation. (II) The prediction assumes  $\theta=0^\circ$ . If  $\theta$  is allowed to vary, one can fit a line of best fit, using the Excel solver tool, through zero and the points, at a dynamic contact angle of about  $15^\circ$  for pure water. In addition, from the wedge approximation, the dynamic contact angle cannot be  $0^\circ$  because this gives an infinite answer for the dissipation; therefore, we can assume the dynamic contact angle is not zero. At a contact angle of  $15^\circ$ , the dissipation in the wedge is  $1.5 \times 10^{-7}$  W and therefore insignificant because the volume of liquid in the thickness

region of interest is small. (III) The viscosity of air, which is ignored in the Lucas-Washburn Equation. Due to the dynamic viscosity,  $\eta$  of the air and its compressibility, at early times, when the capillary is mostly full of air, the effect will be at its greatest. The dynamic viscosities of air and water are shown in Table 3.2. It can be seen that the viscosity of air is much less, around 2%, than that of water. However, at short times the capillaries are mostly filled with air, hence this will cause the imbibition to deviate from the Lucas-Washburn model and slow down the rate of penetration at the start. As the capillary fills with water, the deviation due to the viscosity of air will decrease and hence the deviation will decrease with distance. The viscosity of air should lead to curvature of the  $l$  vs.  $t^{1/2}$  plot, which is not found to be significant; this suggests that viscosity of air is not the cause of the discrepancy in the slope.

**Table 3.2 – Dynamic viscosities of air and water<sup>1</sup>**

Medium	Viscosity /cP (centipoise)
Air @ 18°C	0.0182
Water @ 20°C	0.9707

There are several possible reasons for the low slope of the 10  $\mu$ l capillaries: (I) Due to the faults with the ventilation system in the lab, the ambient temperature when studying the 10  $\mu$ l capillaries was 18.4°C compared with the other sizes, where the temperature was  $21 \pm 1^\circ\text{C}$ . As the temperature decreases the viscosity increases and hence there will be a decrease in velocity. However, the temperature difference does not account for all of this discrepancy as this temperature change results in a viscosity change of  $\sim 7\%$ , which corresponds to  $\sim 3\%$  change in the velocity. (II) The flow in the larger capillaries could be turbulent and this could account for some of the deviation, however, one would normally expect laminar flow for a Reynolds number of less than 2000. For the case of the 10  $\mu$ l capillaries  $Re \approx 90$ , so  $Re \ll 2000$  and the flow is predicted to be laminar. (IV) The humidity in the lab was uncontrolled, as attempts to construct a chamber to control it would have greatly complicated the setup. As we will see later, increased humidity slows down rate of penetration, and therefore this could have also contributed to the decrease in slope for the 10  $\mu$ l capillaries. (V) The 10  $\mu$ l were 9 mm longer than the other sizes. Although the total length of the capillary does not appear in the Lucas-Washburn equation, the longer capillary will increase the dissipation from viscosity in the air, but as discussed above, the effect of the viscosity of air is small.

### 3.3 Varying Humidity

Qualitative experiments were performed to see if changing the relative humidity of the air has any effect on the rate of penetration. If the solid-vapour surface tension is greater than

the sum of the solid-liquid and liquid-vapour surface tensions, i.e. the initial spreading coefficient  $> 0$  (3.2), then a film of water will precede the meniscus. This film of water will reduce the free energy change upon wetting by the meniscus from  $\gamma_{sv}^0$  to  $\gamma_{sl} + \gamma_{lv}$ .

$$S_i = \gamma_{sv}^0 - (\gamma_{sl} + \gamma_{lv}) > 0 \quad (3.2)$$

Table 3.3 – Effect of change in humidity

Relative Humidity (RH)	Average Slope	Error
Ambient (60% RH)	0.0594	0.0001
High (~100% RH)	0.0485	0.0002

Table 3.3 and Figure 3.5 show a decrease in slope with increase in humidity. The linearity of Figure 3.6 shows that the penetration still follows Lucas-Washburn type behaviour, but as we shall see below, the decrease in speed cannot be explained by this model. The thickness of the precursor film depends on the relative humidity; for 100% RH a thick film of water will condense on a glass surface and therefore  $\gamma_{sv} = \gamma_{sl} + \gamma_{lv} < \gamma_{sv}^0$ .

The Lucas-Washburn equation depends only on  $\gamma_{lv}$  and therefore predicts that there should be no change in velocity, as there is no change in this surface tension. However, the change in solid-vapour surface tension would result in a change in contact angle, but again the Lucas-Washburn model assumes this to be  $0^\circ$ .

In the surface free energy model, increased humidity causes  $\gamma_{sv}^0$  to become  $\gamma_{sl} + \gamma_{lv}$ . Consequently, the driving force  $\gamma_{sv} - \gamma_{sl}$  is reduced to  $\gamma_{lv}$ , therefore the velocity should be lower, which agrees with the experimental result.

The wedge approximation model predicts that, as the humidity increases, the minimum film thickness increases and the velocity should increase. It is important to note that the thickness of the water film present on the surface of the capillaries is dependent on the relative humidity, and hence any variations in ambient humidity will have an effect on the speed of penetration. This is an important note to make, due to the aforementioned variation of the humidity in the lab.

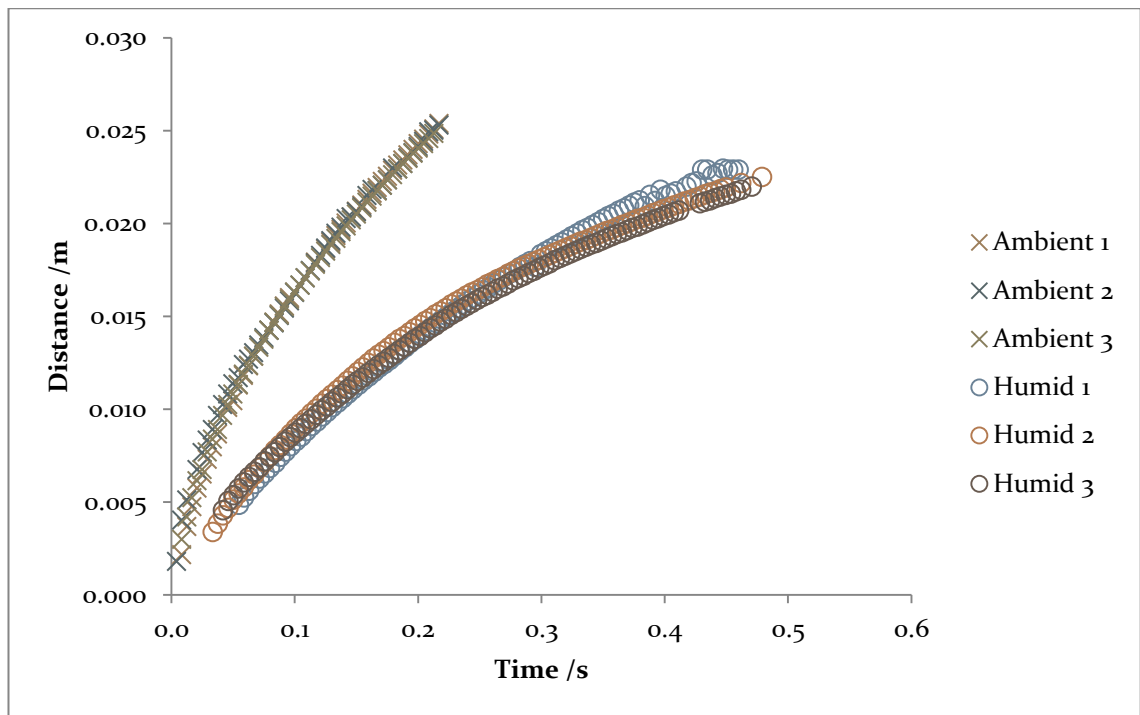


Figure 3.5 – Distance vs. time curves at normal and high humidity for pure water in 1  $\mu\text{l}$  capillaries

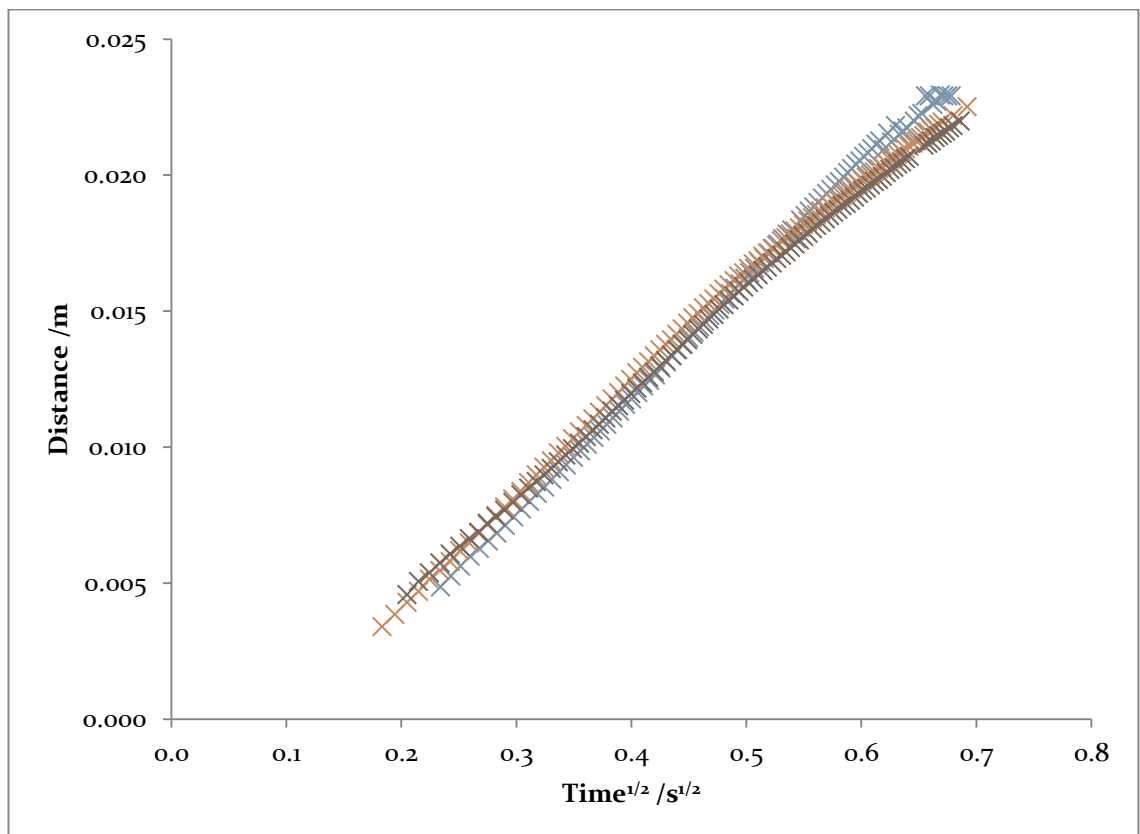


Figure 3.6 – Distance square-root time plot for high humidity for 1  $\mu\text{l}$  capillaries

The data in Figure 3.6 show less reproducibility than previous data. This was probably due to the experimental procedure being poor at controlling the relative humidity after the capillaries had been removed from the desiccator. The liquid film would have started to

evaporate before and during the data acquisition. However, as the experiments are only used qualitatively, the procedure was good enough.

### 3.4 Varying Salinity

These experiments were performed to determine whether salinity (from adding NaCl to water), and therefore ionic strength, would have an effect on rate of penetration. The experiment was a control to determine whether the ionic strength, which changes when adding ionic surfactants, influences the rate of penetration.

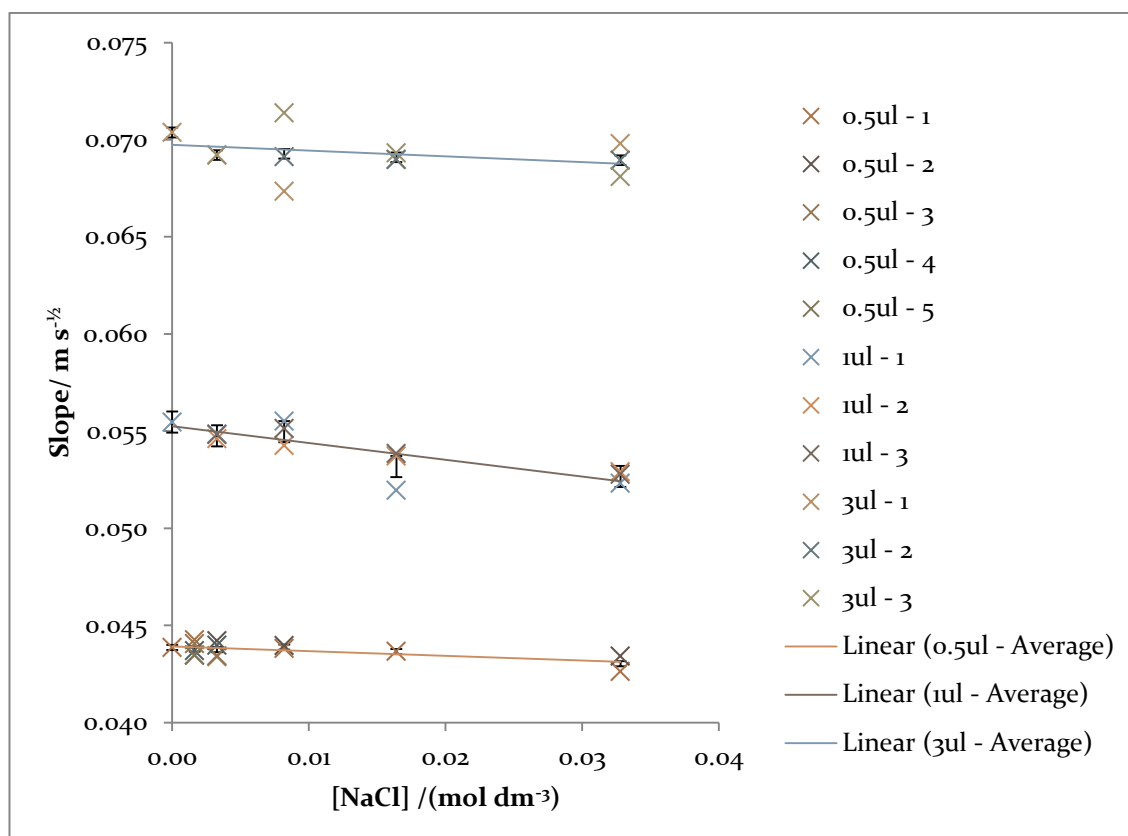


Figure 3.7 – Slope vs. [NaCl] for 1-3  $\mu\text{l}$  capillaries

It can be seen from Figure 3.7 and Table 3.4 that there is virtually no change with increase in concentration for two of three capillary sizes. There is a small decrease with increasing concentration; however, this was within the general experimental error. Only the 1  $\mu\text{l}$  capillaries show a statistically significant slope.

Table 3.4 – [NaCl] Data Confidence for 1-3  $\mu\text{l}$  capillaries

Size/ $\mu\text{l}$	Gradient/(m s <sup>-1/2</sup> dm <sup>3</sup> mol <sup>-1</sup> )	$\sigma$ (Standard Error)	$n\sigma$
0.5	-0.02348	0.008238	<3
1	-0.08316	0.01702	5
3	-0.02091	0.025819	<1

The scatter in the data for each set of measurements shows the good repeatability of the experiments.

The highest concentration of NaCl used was  $0.0656 \text{ mol dm}^{-3}$  whereas the highest concentration of SDS used was  $0.0164 \text{ mol dm}^{-3}$ . Therefore, the effect of increase in ionic strength on increase in SDS concentration can be assumed negligible. The effect on surface tension of these low concentrations of salt is also negligible.

Increasing salinity to 30 mM increases viscosity from  $1 \text{ mPa s}$  to  $1.01 \text{ mPa s}$  at  $20^\circ\text{C}$ ,<sup>1</sup> which is an increase of 1% and small in comparison to the effects due to temperature/humidity variation.

There is a small variation between the value of the slope for water measured during this experiment and that measured later in 3.5, which is probably due to humidity fluctuations, as separate experiments were performed on different days. Future developments of this experiment will need to control the humidity.

Up to now, control experiments have been performed to understand the case of pure water penetrating a clean hydrophilic glass capillary. Now the presence of surfactant in the water will be investigated.

### 3.5 Varying SDS Concentration

Concentration was varied to see what effect it might have. SDS does not adsorb to hydrophilic glass, therefore  $\gamma_{sl}$  does not change. Therefore, the surface free energy model, in which the velocity depends on  $\gamma_{sv}-\gamma_{sb}$ , predicts there to be no change in the velocity in the presence of surfactant.

Figure 3.8 shows that the presence of surfactant slows down the rate of penetration. Figure 3.9 shows the same data vs.  $t^{1/2}$ . The Gibbs equation is:<sup>2</sup>

$$\frac{d\sigma}{d \ln c} = -nRT\Gamma \quad (3.3)$$

Therefore, below the cmc, the surface tension decreases as the concentration of surfactant increases. Young's equation then shows that the contact angle decreases (until it reaches zero) with increasing surfactant concentration.

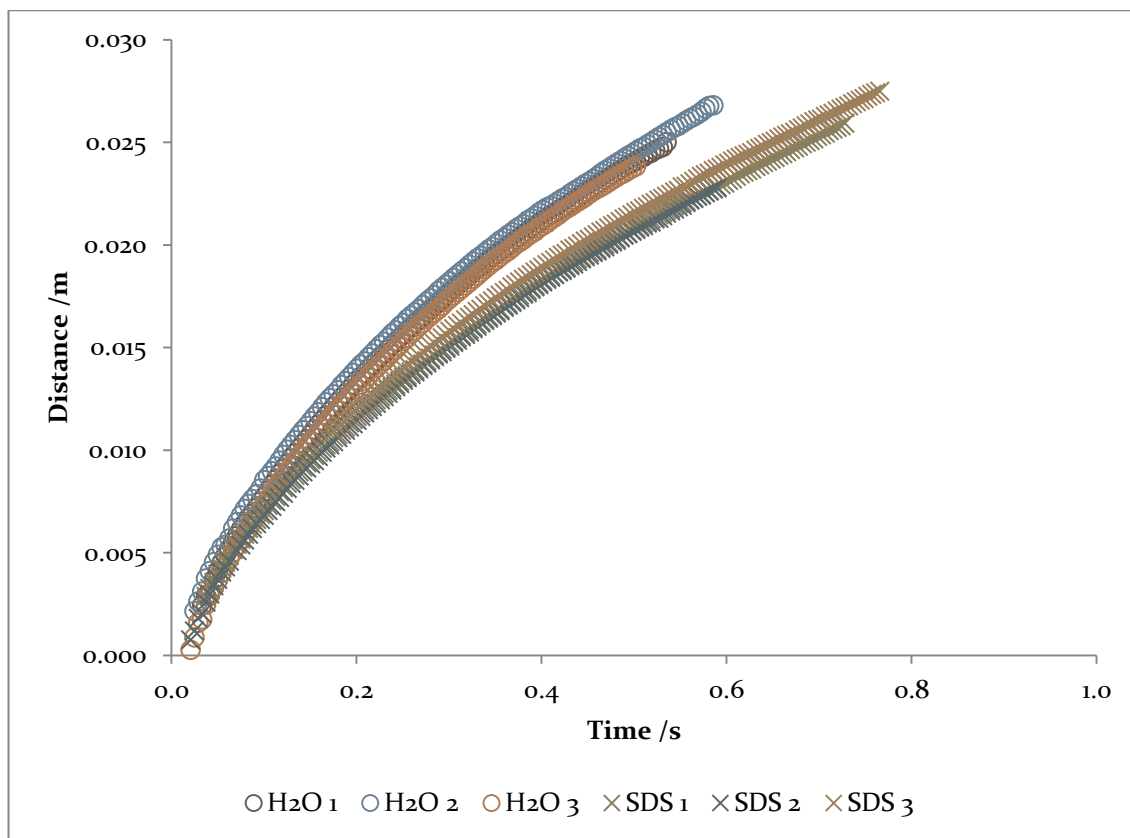


Figure 3.8 – Distance vs. time plots with and without SDS present for 1 µl capillaries

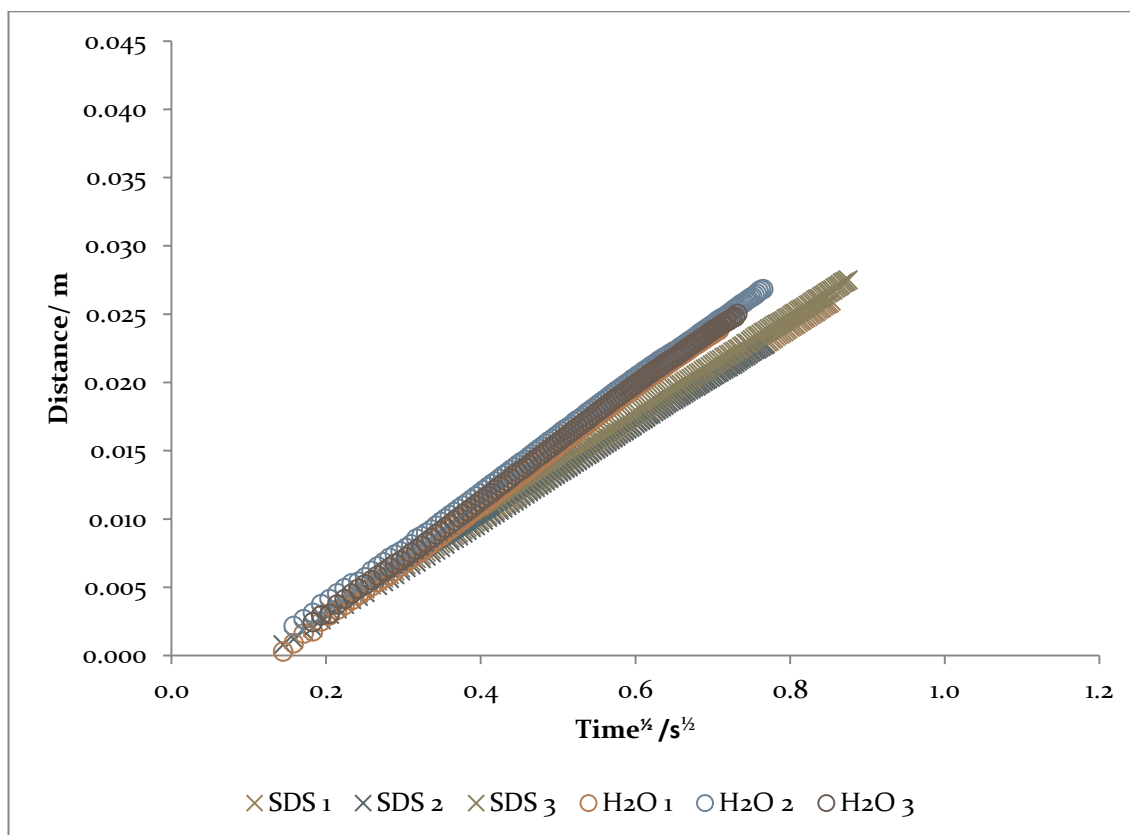


Figure 3.9 – Comparison of slopes with and without the presence of SDS for 1 µl capillaries (conc. 0.0164 mol dm<sup>-3</sup>). Three independent runs for each case are shown

The Lucas-Washburn behaviour predicts that the velocity will vary with  $\sqrt{\gamma_{lv}}$ , which depends on surfactant concentration at a static contact angle of  $0^\circ$ . Therefore, if the free energy of the water surface is assumed to be equilibrated, one can predict the velocity from a  $\gamma$  vs. surfactant concentration plot. Figure 3.10 shows the slope of the distance vs.  $t^{1/2}$  plot as a function of SDS concentration. The dash-dot line in Figure 3.10 is the slope calculated from the Lucas-Washburn equation, with the surface tension calculated from Figure 3.11 generated from data provided by Dr Lisong Yang in the Colin Bain laboratory group. The 2<sup>nd</sup> degree polynomial fits the data quite well over the region of interest giving approximately linear dependence of the slope on concentration below the cmc. Above the cmc, the prediction shows no change in penetration speed because there is negligible change in the surface tension above the cmc.

There does not appear to be any change in the velocity of penetration above the cmc for SDS (or for any of the other surfactants used later). This may be because the timescales involved with imbibition do not allow for micelle formation or breakdown and therefore their presence or absence has no effect on the effective bulk concentrations, which affect the penetration.

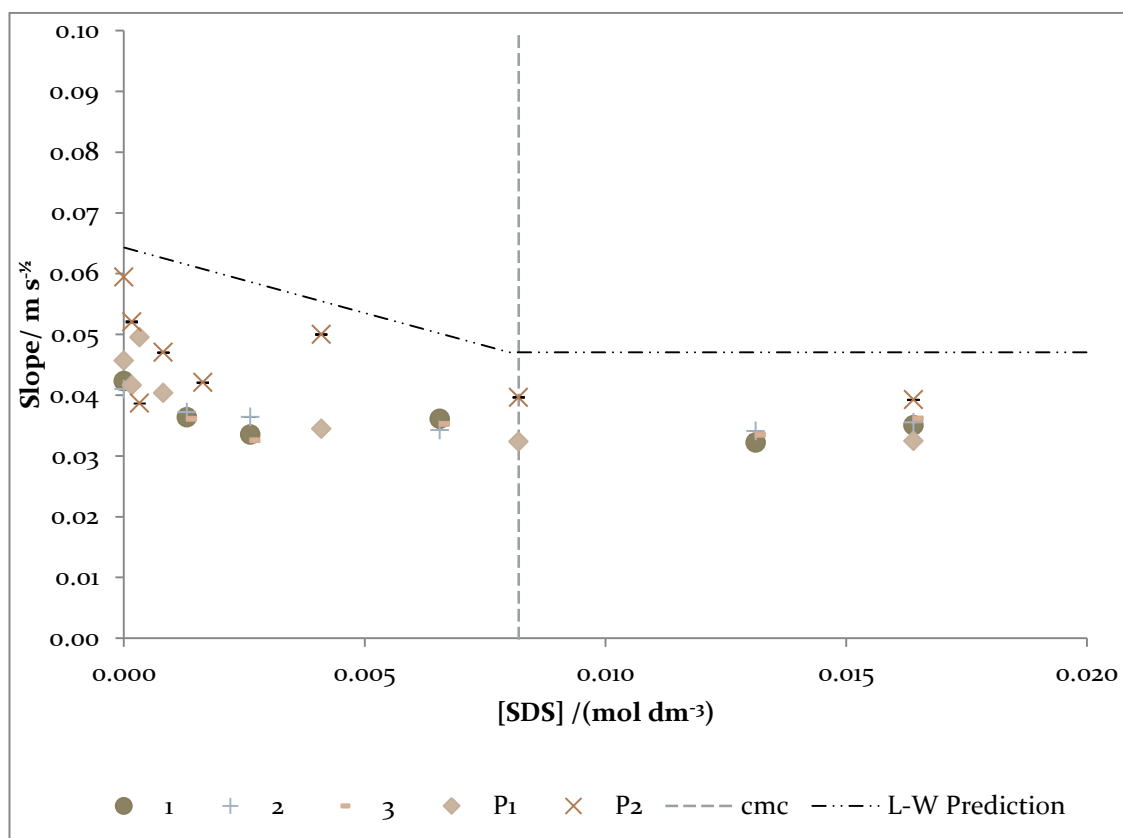


Figure 3.10 – Plot of slope vs. [SDS] with Lucas-Washburn prediction for 1 $\mu$ l capillaries

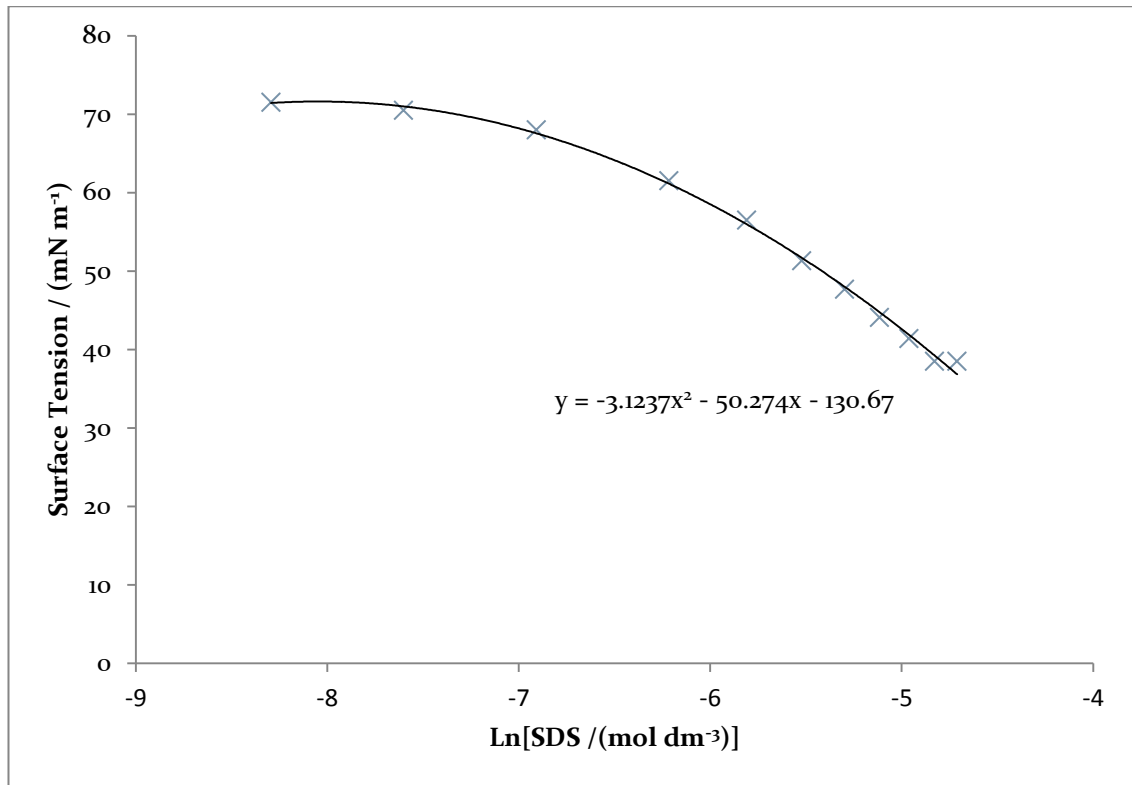


Figure 3.11 – Ln [SDS] vs. surface tension <sup>3</sup>

Figure 3.10 shows that the slope decreases at lower SDS concentration than the Lucas-Washburn model predicts. If the dynamic contact angle  $\theta_d$  were to decrease (as expected from Young's equation in the presence of surfactant) then the slope should increase. This is the opposite of what has been observed.

Figure 3.10 also shows that the Lucas-Washburn prediction is faster than experimental results, as was seen previously for pure water.

The results P1 and P2 were recorded early in the project and show poor consistency. Results 1, 2 and 3, later, give good agreement. The early results were poor because the setup and techniques had not been optimised.

In contrast, the overflowing cylinder model predicts that due to the very high expansion rates present, the surfactant will not have had time to adsorb to the surface. The surface excess of surfactant at a continuously expanding surface is given by (3.4):<sup>4</sup>

$$\Gamma = \sqrt{\frac{2D}{\pi S}} (c_b - c_s) \quad (3.4)$$

where  $S$  is the surface expansion rate,  $c_b$  is the bulk concentration,  $c_s$  is surface concentration and  $D$  is the diffusion coefficient.

If we assume that the radial velocity,  $v_r$ , of fluid where the meniscus meets the surface is the same as the advancing meniscus,  $v_a$ , i.e. of the order of  $0.1 \text{ m s}^{-1}$ , then:

$$v_r R = v_z \quad (3.5)$$

For the flow pattern in and OFC,  $v_r = aR$  and hence:

$$\begin{aligned} a &= \frac{v_z}{R} \approx \frac{0.1}{10^{-3}} = 10^3 \text{ s}^{-1} \\ S &= 2a \\ \therefore \text{Surface expansion rate: } S &\approx 2000 \text{ s}^{-1} \end{aligned} \quad (3.6)$$

If the free surface is far from equilibrium,  $c_b \gg c_s$  and we can neglect  $c_s$  in (3.4):

Considering for example,  $c_b = 0.0025 \text{ mol m}^{-3}$  and taking  $D_{\text{SDS}} \approx 5 \times 10^{-10} \text{ m}^2 \text{ s}^{-1}$  one can then calculate the dynamic surface excess:

$$\Gamma_{\text{dyn}} = \sqrt{\frac{10^{-9}}{\pi \times 2 \times 10^3}} \times 0.0025 = 4 \times 10^{-7} \text{ mol m}^{-2} \quad (3.7)$$

Dynamic surface excess represents only one tenth of a monolayer of SDS ( $\sim 4 \times 10^{-6} \text{ mol m}^{-2}$ )<sup>6</sup>, with a surface tension very close to that of pure water. The overflowing cylinder model therefore predicts that SDS, for concentrations near and below the cmc, will have no effect on velocity. If the overflowing cylinder model were to apply, the velocity would be expected to fall at a higher concentration, where experimentally there is no further drop in speed.

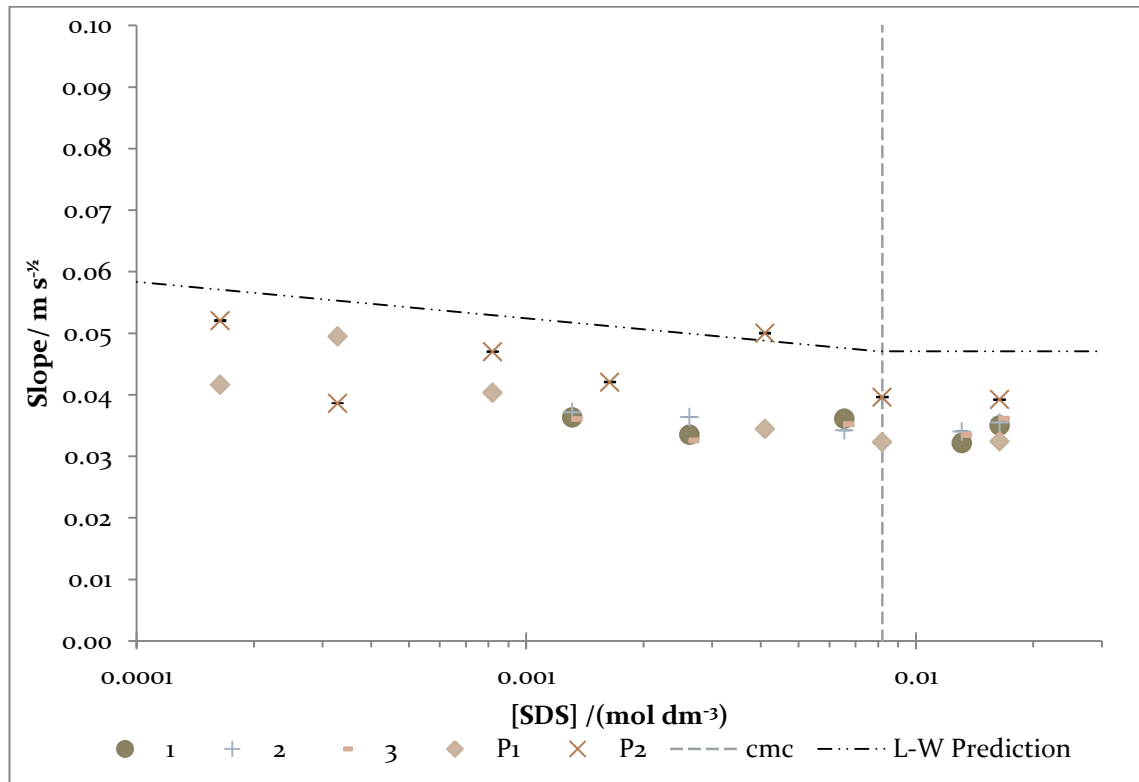


Figure 3.12 – Slope vs. [SDS] (log scale) with Lucas-Washburn prediction for 1 $\mu$ l capillaries

Figure 3.10 (and Figure 3.12 as a log scale) shows that at low concentrations, the presence of SDS does have an effect on the velocity. However, above approximately  $0.0025 \text{ mol dm}^{-3}$ , the presence of surfactant appears to have no effect on the slope. This may be due to the problem of surfactant molecules not adsorbing on the liquid-solid interface. If the meniscus is viewed as rolling onto the walls of the capillary, then the surfactant needs to desorb from the interface. As SDS does not adsorb to the liquid-solid interface, there may be a thermodynamic penalty to pay when the surfactant molecules diffuse back into solution.

It is helpful to consider what the flow pattern might be inside the capillary between the two immiscible fluids.

Cerro and collaborators<sup>7,8</sup> have studied flow patterns near a moving tpc line using a flat plate plunging into a tank, with neutral buoyancy particles and video-imaging techniques. They found that the flow patterns depend on the apparent  $\theta_d$  and the viscosity ratio of the two fluids. These were found to differ from theoretical results. Figure 3.13 shows their kinematically consistent flow patterns. A is discussed as a possible flow pattern in oil filled capillaries. In these schematics, if A is air and B is water, then (c) is equivalent to the overflowing cylinder model. (b) has a stationary meniscus, which should have an equilibrium surface tension. SDS experimental data shows that neither of these two models apply. (a), the split injection flow pattern is redrawn in Figure 3.14 for a capillary geometry.

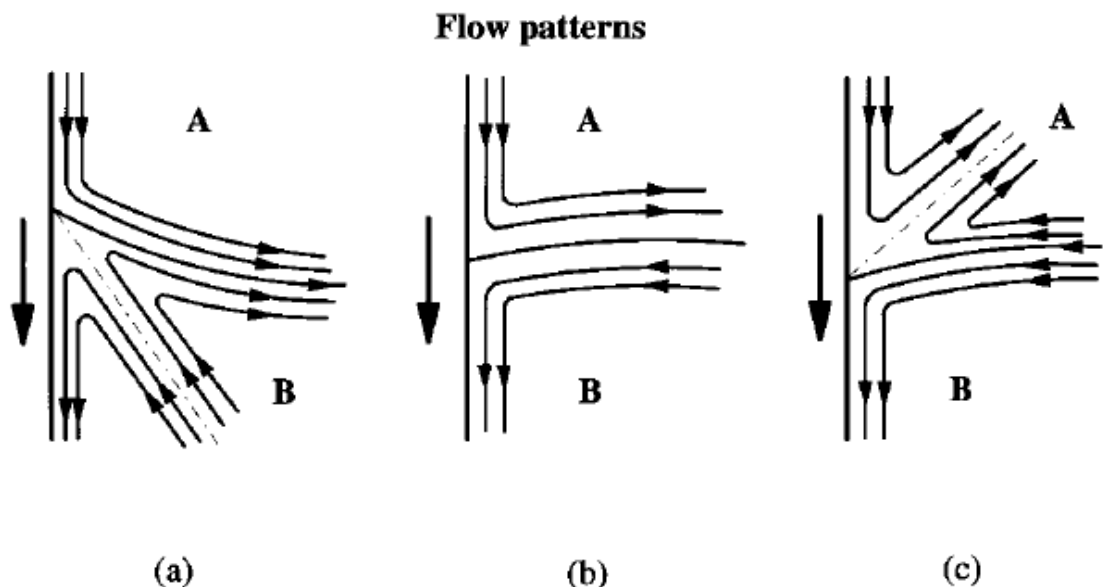


Figure 3.13 - Schematics of kinematically consistent flow patterns. A is the displaced phase, B is the displacing phase

(a) Split injection in phase B, contradiction between the no-slip boundary condition and rolling ejection in phase A, (b) motionless interface pattern with rolling the need for one fluid to completely displace the other over injection in phase B and rolling ejection in phase A, and (c) rolling injection over the solid surface From Savelski *et al.*<sup>7</sup>

At the meniscus, there are large Marangoni stresses, due to the rapid destruction and creation of surface, likely to be demonstrated in Figure 3.14. For example, at the capillary wall, surface is rapidly created resulting in a low surface excess and hence a high surface tension. The opposite is true at the centre where surface is rapidly destroyed. This large surface tension gradient would generate large Marangoni stresses, which oppose the fluid convection. The result of this stress makes the theory rather more complex, which is beyond the scope of this MSc. Understanding the behaviour of the fluid at the meniscus is crucial before any firm conclusions can be drawn. Holographic particle image velocimetry (PIV) is one such technique currently been investigated in the group.

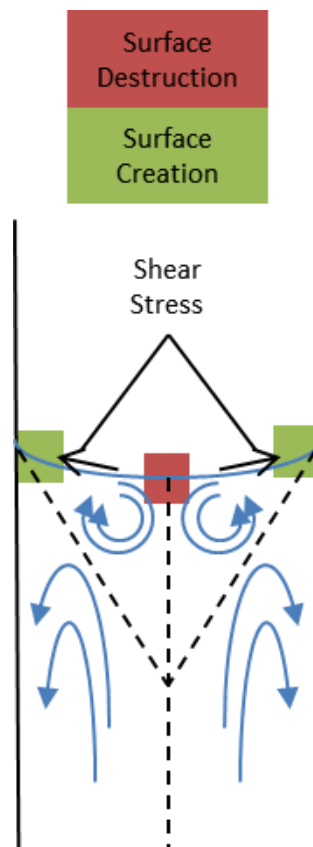


Figure 3.14 – Illustration of shear stresses at the meniscus

## 3.6 Varying type of surfactant

### 3.6.1 CTAB

Different surfactants were used to investigate different effects. CTAB was used because it reduces  $\gamma_{sl}$  as it adsorbs to the surface (SDS does not). This adsorption generates a larger driving force than for SDS and therefore this should result in a higher velocity. However, as CTAB only adsorbs to a large extent near the cmc, low concentrations should not affect  $\gamma_{sl}$ . This behaviour is not displayed in the results (Figure 3.15) as a rise in rate below the cmc would be expected. In fact, the velocity drops sharply at concentrations below the cmc

( $\sim 0.001 \text{ mol dm}^{-3}$ ) and is constant above it. The fact that an increase in the capillary force ( $\gamma_{sv} - \gamma_{sl}$ ) results in a lower velocity shows that additional dissipative mechanisms must be present.

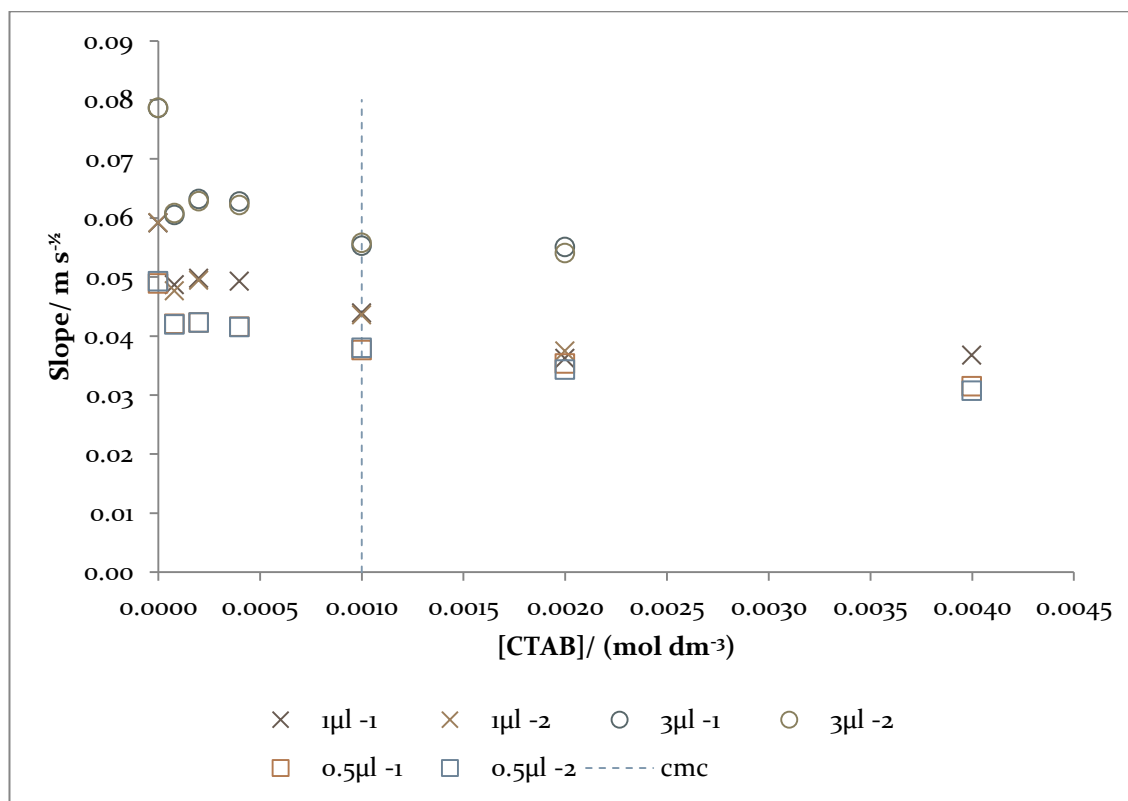


Figure 3.15 – Slope vs. [CTAB] for different size capillaries

The results also show an increase in concentration of CTAB results in a slower rate of penetration. The presence of CTAB also results in a reduction in rate when compared to pure water. One may predict an increase in rate on increase in concentration because CTAB adsorbs to glass. However, the reduction in Gibbs free energy from the work done by adsorption to the glass only changes the surface tension. This increases the contact angle and hence the capillary force. This is because the thermodynamic advantage of CTAB adsorbing to the glass surface decreases.

Figure 1.16 (page 2) shows the change in surface excess on increase of CTAB concentration and no change would be expected until the sharp rise. Therefore, we have shown that the overflowing cylinder model cannot apply in this case. It is also worth noting that surface tension is linked to the surface excess, by an equation of state. Therefore, if  $\Gamma$  is very small,  $\gamma \approx \gamma_0$  so the speed should not have dropped.

Comparing CTAB,  $C_{12}E_6$  and SDS in Table 3.5, at approximately the same concentration, the slopes all show that pure water penetrates faster than when surfactant is present. The

decrease when comparing the surfactants may be related to the molecular weight of the surfactant molecules affecting the rate of diffusion.

Table 3.5 – Slopes for different surfactants in 1  $\mu\text{l}$  capillaries

Surfactant	Concentration/ ( $\text{mol dm}^{-3}$ )	Gradient/ ( $\text{m s}^{-1/2}$ )	$\sigma$ (Standard Error)	Molecular Weight/ ( $\text{g mol}^{-1}$ )
(None)	N/A	0.05921	0.00009	N/A
SDS	0.00082	0.04701	0.00005	288.38
CTAB	0.001	0.04356	0.00004	364.45
$\text{C}_{12}\text{E}_6$	0.00094	0.0386	0.0001	450.65

### 3.6.2 Non-ionic Surfactants

$\text{C}_{12}\text{E}_6$  and  $\text{C}_{14}\text{E}_6$  were chosen because of their very low cmc values<sup>9</sup> of  $8.9 \times 10^{-5}$  and  $6 \times 10^{-6}$   $\text{mol dm}^{-3}$  respectively and to investigate the effect of chain length on imbibition. For all concentrations above the cmc, the rate should be the same.

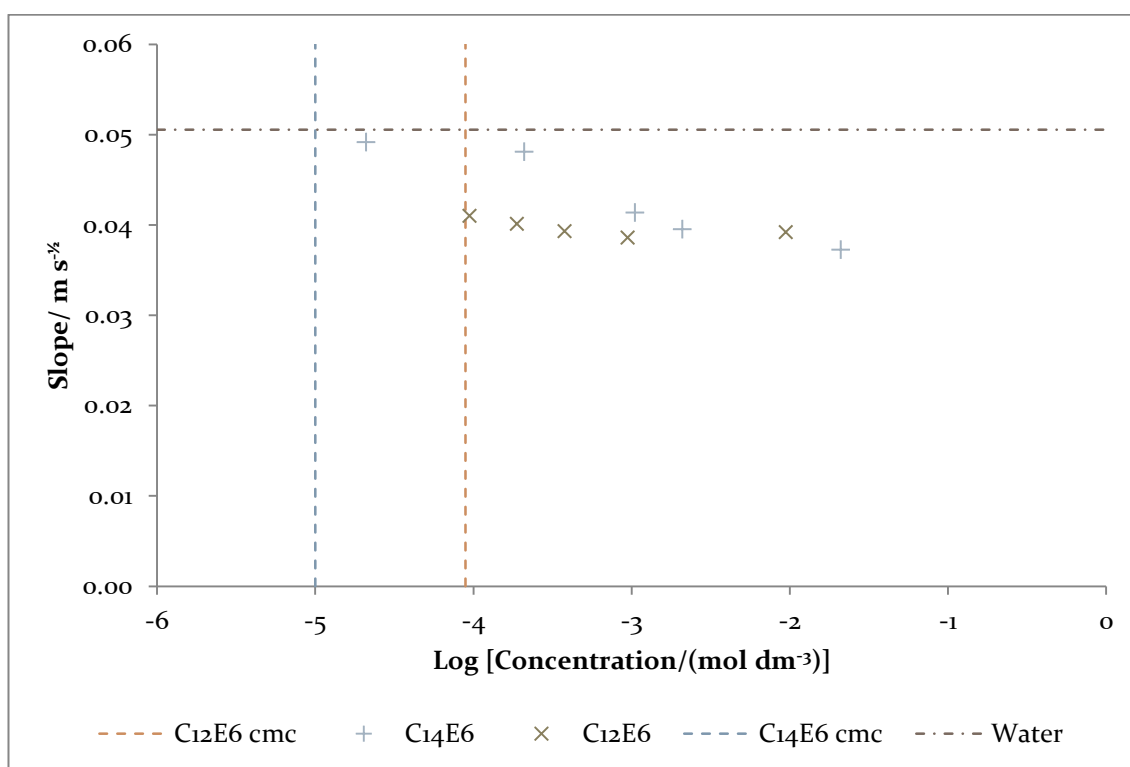


Figure 3.16 – Log concentration plots for  $\text{C}_{14}\text{E}_6$  and  $\text{C}_{12}\text{E}_6$

As all solutions were recorded above the cmc, all the concentration should have equal speeds if the surface is equilibrated. This appears to be true for  $\text{C}_{12}\text{E}_6$ . However, this is not consistent with the fit for  $\text{C}_{14}\text{E}_6$ , which might suggest the presence of kinetic barriers to adsorption at the air-water interface for this surfactant.

The longer alkyl chain  $C_{14}E_6$  surfactant is generally slower to penetrate than  $C_{12}E_6$ , which is consistent with the results found by Tiberg *et al.*<sup>10</sup> This is likely because micelles move slower than monomers and the micelle break up will be slower with the larger chain, due to  $C_{14}E_6$  having greater micellar stability.

### 3.7 Hydrophobic Capillaries

To determine the behaviour of surfactant solutions in hydrophobic capillaries, similar methods to the above hydrophilic case were used. However, there were problems obtaining reproducible and sufficient data. Many data points had to be discarded due to the program failing to identify the meniscus; even manually trying to identify the position was difficult. This is mostly likely due to the contact angle being near  $90^\circ$  and hence the meniscus would have been parallel the camera and difficult to see. The laser would have reflected off the meniscus poorly. Experiments using diffuse illumination from the sides still were hard to analyse due to the lack of contrast. Having the camera at an angle to the capillary to improve light levels would have made analysis difficult, as the scale would have not been linear.

One contribution to the poor reproducibility may be the lack in uniformity of the hydrophobic layer. By thoroughly washing the capillaries after they were silanised, and using a silane with only one reactive site, the presence of silane dimers in the capillary was greatly reduced. Additionally, using a dried desiccator to silanise and store the capillaries reduced the chance of hydrolysis removing the hydrophobic layer. However, it may have been better to have silanised the capillaries at a higher temperature to ensure that all the sites on the glass reacted. Tests were done using capillary depression experiments to see how uniform the layer was and no changes were observed, so there may have been other problems. The process used was described by Tiberg and his results were consistent. The silane may have reacted more uniformly at higher temperatures.

Although the meniscus was often hard to detect, the program often chose distances far from the meniscus, such as dim reflections off the end of the mount and so these invalid results were easy to remove, and hence had little effect other than to remove the number of data points available.

The size of the water droplet, affecting the Laplace pressure at the end of the PTFE tube and hence affecting the pressure at the end of the capillary may have had a greater effect for hydrophobic than for the hydrophilic capillaries. This could be due to the reduced driving force. However, the syringe was adjusted before moving the capillary, to minimise the curvature (to make the drop approximately flat with the end of the tube). Additionally,

the much larger internal diameter of the tube compared to the capillary will have reduced the effect of the droplet size.

Tests were performed on hydrophobised capillaries kindly provided by the Prof. Jas Pal S. Badyal group. These capillaries were made hydrophobic by exposing them to a monomer (PFAC8 – perfluorooctyl acrylate – from Flurochem) with a plasma discharge under very low pressure. These capillaries were found to be too hydrophobic for any surfactant solution used to penetrate them, and hence no data could be obtained.

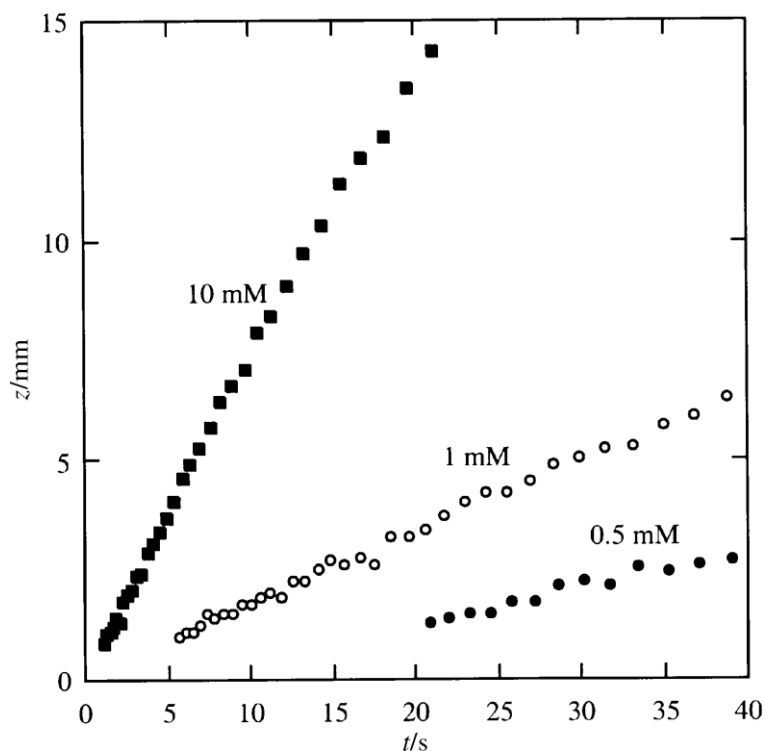


Figure 3.17 – “Short time” dynamics of capillary rise observed for  $C_{14}E_6$  surfactant solutions with varying bulk concentration (hydrophobic capillary radius 0.1 mm)

From Tiberg *et al.*<sup>10</sup>

Tiberg *et al.*<sup>10</sup> studied the penetration of surfactant solutions into vertical hydrophobic capillaries. He found that an increased surfactant concentration resulted in a higher rate of penetration. His data are displayed in Figure 3.17. His results show much slower imbibition rates, than for the hydrophilic capillaries, for example Figure 3.8. His results are linear with time, which demonstrates that the penetration is not following Lucas-Washburn behaviour.

Figure 3.18 and Figure 3.19 show some sample results obtained for SDS penetrating hydrophobic capillaries at about the cmc.

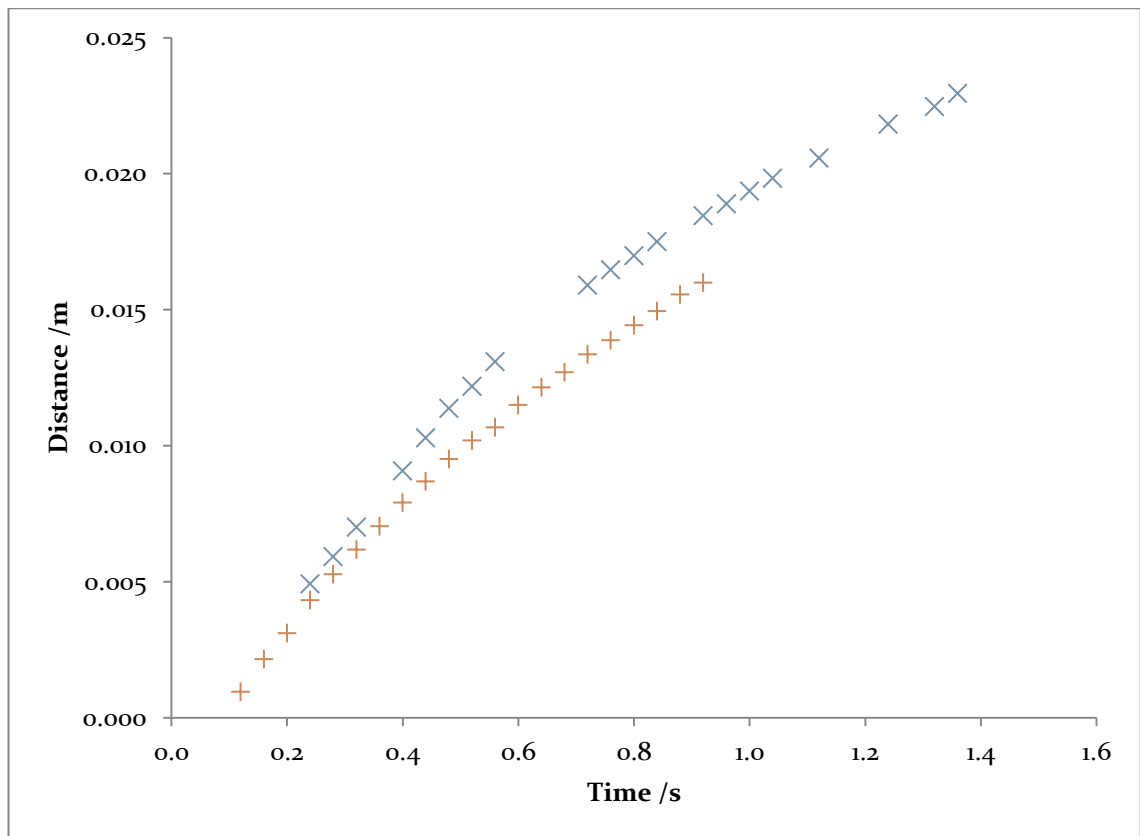


Figure 3.18 – Distance vs. time plot for SDS into 1  $\mu\text{l}$  hydrophobic capillaries at the cmc ( $0.00814 \text{ mol dm}^{-3}$ )

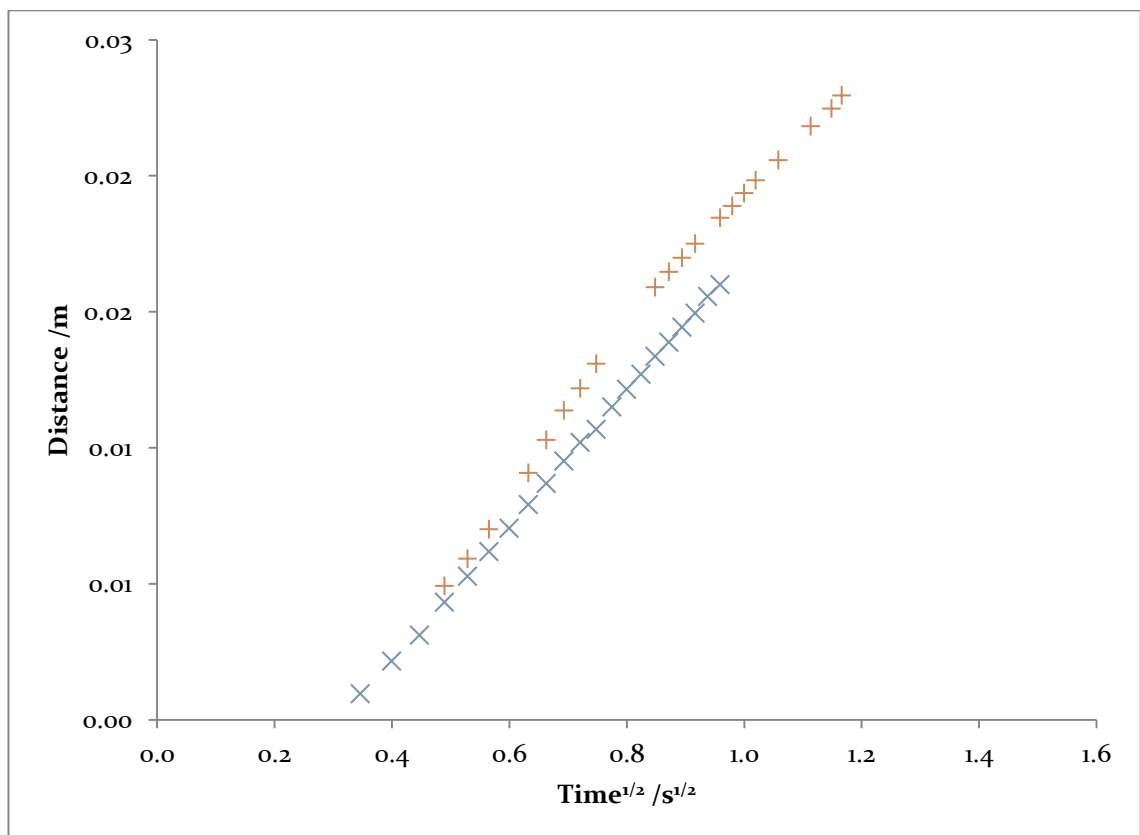


Figure 3.19 – Distance vs. square-root time plot for SDS into 1  $\mu\text{l}$  hydrophobic capillaries at the cmc ( $0.0081 \text{ mol dm}^{-3}$ )

The results obtained in these experiments (Figure 3.18) are inconsistent with the results of Tiberg, much faster rates are observed here and the distance time plots are more similar to Lucas-Washburn behaviour – distance linear to  $t^{1/2}$  – at least for part of the capillary. The slope in Figure 3.19 can be used to calculate  $\theta_d$  from the Lucas-Washburn equation, assuming an equilibrium value of  $\gamma \approx 0.04 \text{ N m}^{-1}$ . Working from the slope of the straightest line of Figure 3.20, the contact angle can be calculated to be  $90^\circ$  (to 3 s.f.) which agrees with predictions and explains why the meniscus was hard to view.

There were not enough reliable data to determine the effect of concentration on velocity above the cmc.

At concentrations below the cmc, the speed appears to be constant with distance, in agreement with Tiberg; Figure 3.20 is a sample of these data. Higher surfactant concentrations are imbibed faster, which can be related to increase in rate of adsorption of surfactant to the glass surface. A reduction in  $\gamma_{sl}$  is required to make  $\theta_d < 90^\circ$ , which is a prerequisite for imbibition.

These results could suggest that that overflowing cylinder model might apply as the kinetics are time independent and may be limited by rate of adsorption and not viscous dissipation.

There have been arguments in the literature for surfactant to diffuse ahead of the tpc, and it is possible that there is some contribution from this effect. More investigation of the flow patterns involved is needed.

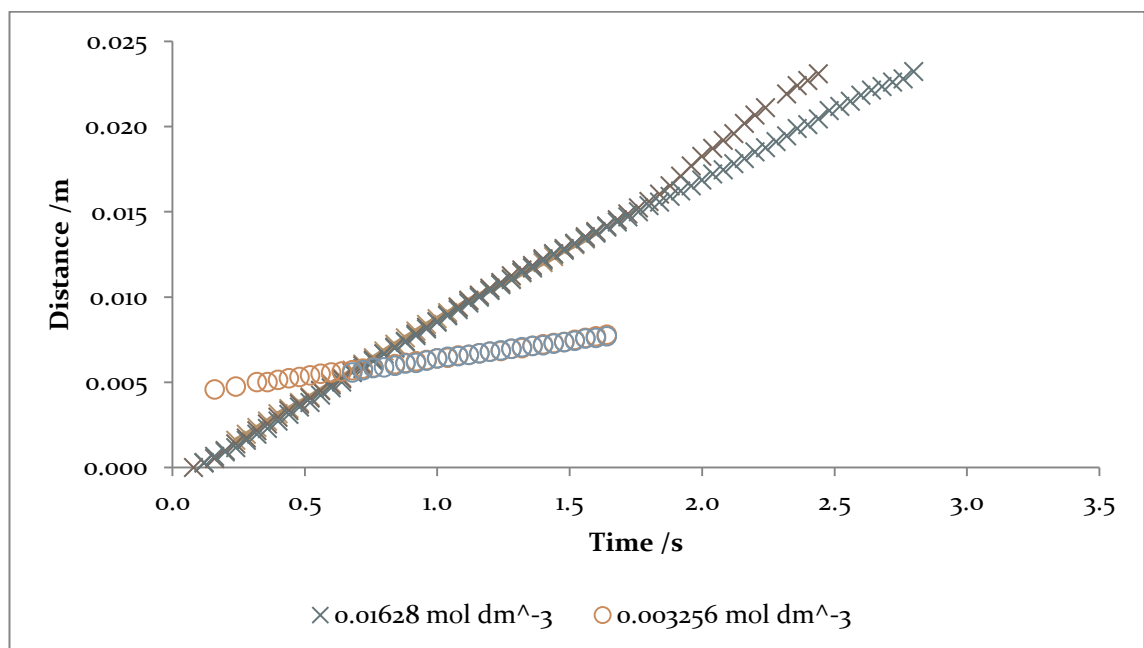


Figure 3.20 – Distance-time plot for SDS penetrating hydrophobic capillaries ( $[\text{SDS}] = 0.0001628 \text{ mol dm}^{-3}$ )

The circles do show similar behaviour to Tiberg, being linear and relatively slow.

The change in imbibition rate, after 2 seconds for one sample might reflect a change in hydrophobicity of the capillary.

### 3.8 Oil Filled Capillaries

Filling the capillaries with oil of equal viscosity to that of water means that the viscous dissipation is constant and so the velocity of penetration should be constant.

Figure 3.21 and Figure 3.22 show possible flow patterns inside a capillary, at the oil-water interface.

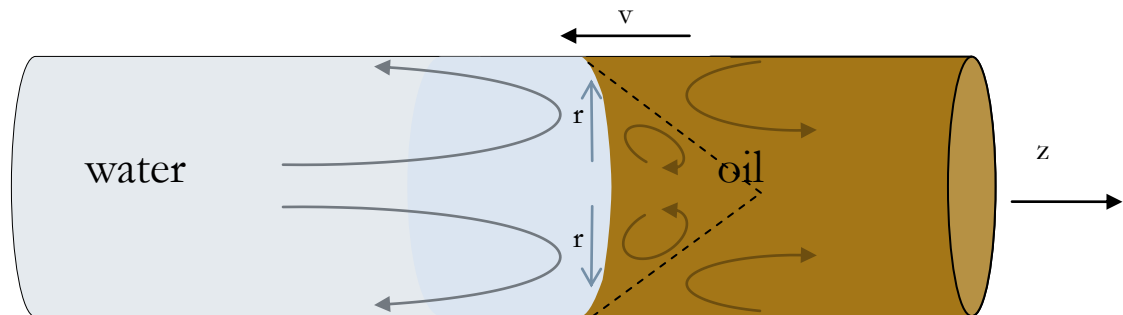


Figure 3.21 – Water with “overflowing cylinder” (split ejection) model

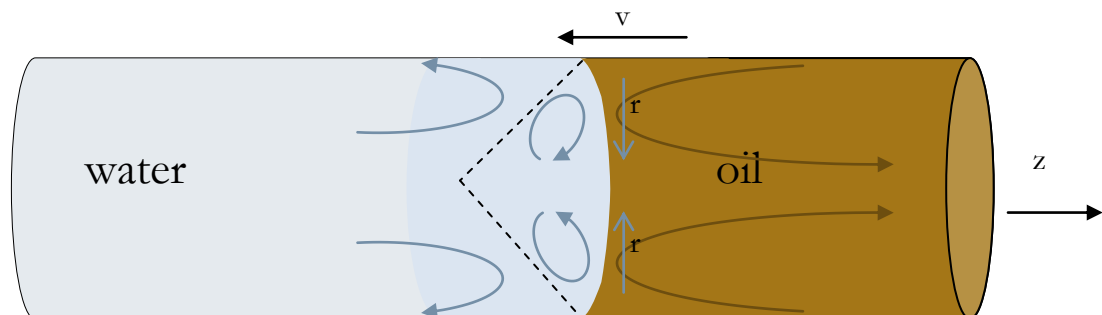


Figure 3.22 – Split injection model

Choosing two fluids with similar viscosities also eliminates inertial effects at the beginning of penetration. Decane was selected as the oil, since it has a similar viscosity to water. This idea is shown to work well by the linearity of Figure 3.23. SDS is not soluble in decane.

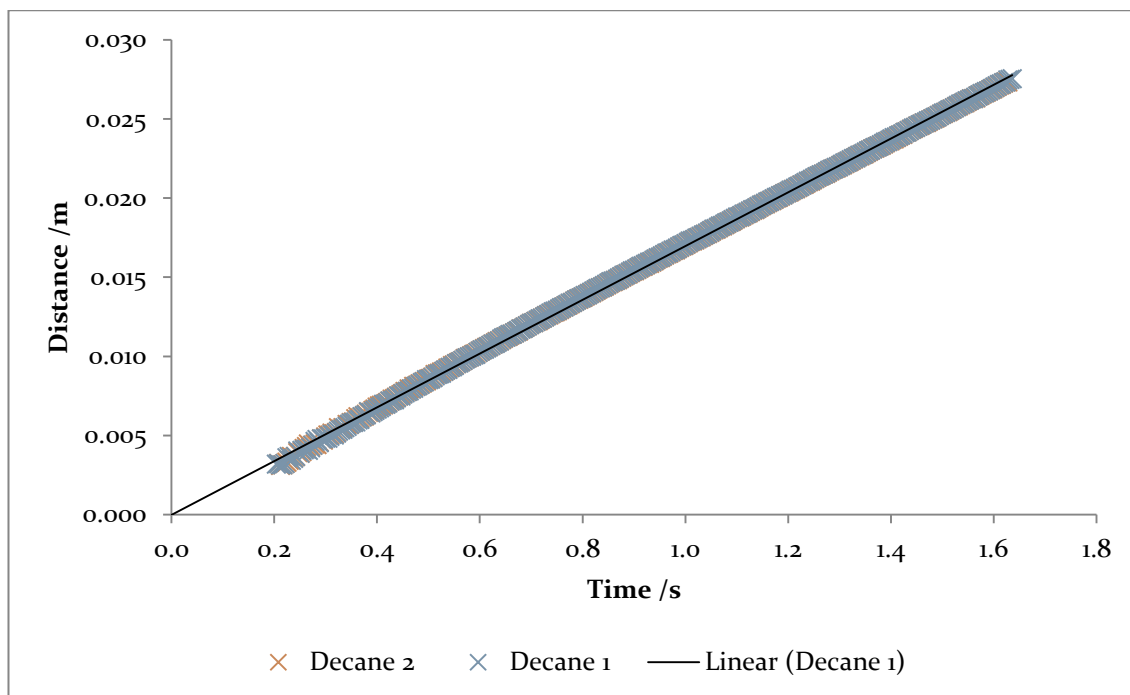


Figure 3.23 – Distance- time plot for water entering decane filled 1 $\mu$ l capillaries

Therefore we can seek a steady-state solution in which the capillary moves at speed  $v_0$  and the meniscus is stationary (Figure 3.21 and Figure 3.22).

Some of the data obtained with SDS present showed two different flow regimes (Figure 3.24). This is possibly due to the flow alternating between the overflowing cylinder model Figure 3.21 and the split injection Figure 3.22 model. The alternation between the two processes could be due to depletion of surfactant from the area near the meniscus, similar to what was seen by Tibergh *et al.*<sup>10</sup>, with their long-time studies on hydrophobic capillaries. Additionally, due to the suggested flow pattern with the split injection model, immediately behind the meniscus is a rotating torus of liquid, flowing against the flow of bulk solution. This rotating torus of liquid may also prevent diffusion of surfactant from the bulk. Further information about the flow patterns involved is required to gain a better understanding of the processes involved.

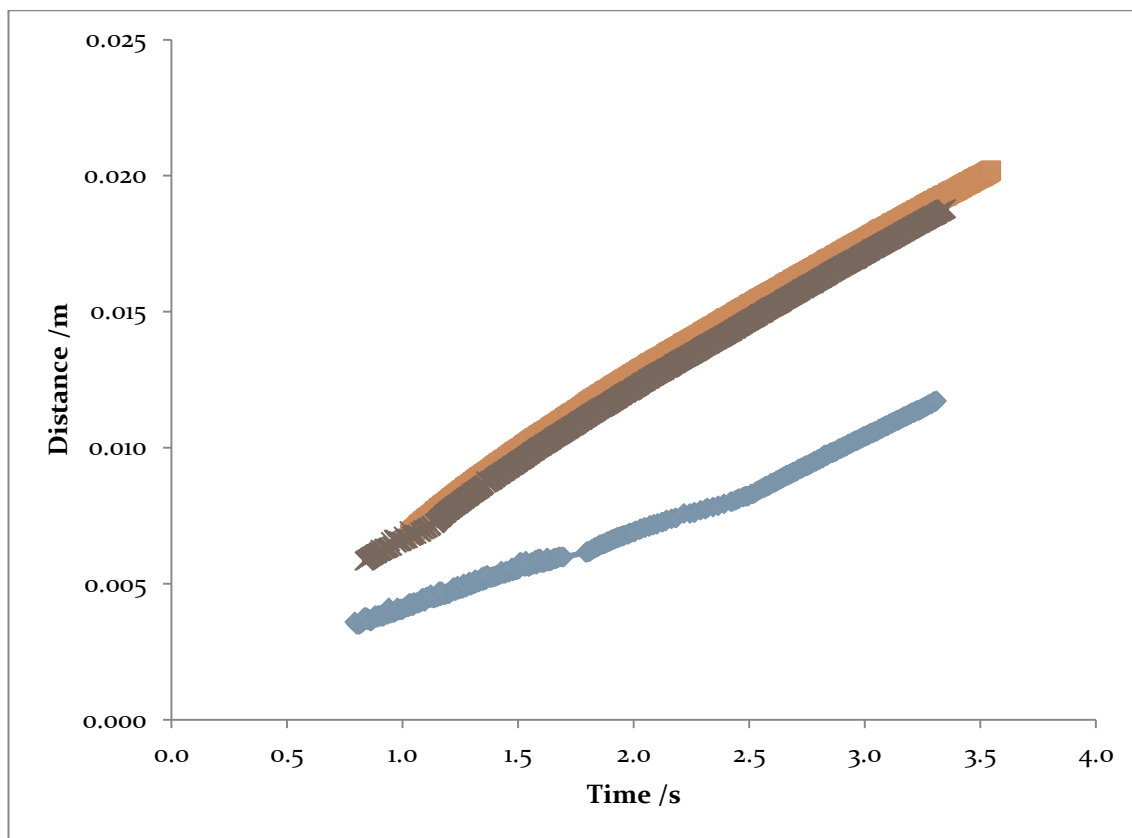


Figure 3.24 –  $0.00065 \text{ mol dm}^{-3}$  SDS penetrating oil filled  $1\mu\text{l}$  capillaries; two different flow rates are sometimes seen

Investigations to attempt to see if an air bubble between the oil and water affected results, in case air was also drawn into the capillary. Attempts to introduce a bubble between the two liquids intentionally, by only partially filling the capillary with oil were unsuccessful, as the water would not spontaneously enter the capillary.

It was noted that, during the experiments with oil and water, it was hard to see the meniscus both directly and from the scattered light. This was due to the similar refractive indexes of the two liquids, compared to air and water.

### 3.9 Further Experiments

Andy McKeague in the Bain group has begun investigating flow patterns in capillary flows using holographic particle image velocimetry (PIV). This technique should allow the determination of the flow patterns inside the capillary; particularly of interest is the case of water penetrating oil filled capillaries as the viscosities are very similar.

A new camera, the Photron Fastcam APX-RS capable of recording  $1024 \times 1024$  pixels at 10,000 frames per second was purchased and arrived in the last month of the project. This camera could be used to study these, and larger capillaries. This would help develop further understanding of the processes of capillary penetration on microsecond timescales and

investigation of faster processes such as the high speeds at the capillary entrance. The camera will also be useful for PIV studies into the flow patterns inside the capillaries.

### 3.10 Conclusion

This project has developed a good experimental method for optically studying the penetration of surfactant solutions into hydrophilic capillaries, which produces reliable, consistent results.

For hydrophilic capillaries, three models, the Lucas-Washburn, Young (i.e. driven by  $\gamma_{sv} - \gamma_{sl}$ ) and overflowing cylinder model, have been used and compared to experimental results. Although Lucas-Washburn type behaviour has been found, the model did not account for the rate of penetration, due to its neglect of dissipative mechanisms other than those in the bulk. The model also did not explain the effect of surfactant concentration on the rate of imbibition. The overflowing cylinder analogy was also not consistent with experimental results for hydrophilic capillaries, but could possibly apply for hydrophobic ones.

Experiments on hydrophobic capillaries did not agree with earlier work by Tiberg. Reproducibility was poor and it is necessary to improve the uniformity of the hydrophobic layer.

The method of using oil-filled capillaries to give constant viscous dissipation was successful but more work is required to fully utilise this technique.

Dynamic contact angle determination needs to be improved, possibly using better optical techniques, such as confocal microscopes and oil immersion lenses. The uniformity of hydrophobic coatings could be determined by capillary rise experiments using less penetrating liquids, such as hexadecane, or longer capillaries.

Although no firm conclusions may have been obtained on the mechanisms of capillary penetration of surfactant solutions, the field of work has been set for further investigation. Not all questions have been answered, but some direction as to the questions that need to be answered has been found. An important technical development is PIV, to determine the actual flow patterns involved.

## Bibliography

1. CRC. CRC Handbook of Chemistry and Physics, 74th ed.; CRC Press, 1994.
2. Atkins, P.; de Paula, J. *Atkins' Physical Chemistry*, 8th ed.; Oxford University Press: Oxford, 2006.
3. Yang, L. *Surface Tension Measurements; Laboratory Work (Unpublished)*; University of Durham: Durham, 2010.
4. Valkovska, D. S.; Shearman, G. C.; Bain, C. D.; Darton, R. C.; Eastoe, J. Adsorption of Ionic Surfactants at an Expanding Air–Water Interface. *Langmuir* **2004**, *20* (11), 4436–4445.
5. Weinheimer, R. M.; Evans, D. F.; Cussler, E. L. Diffusion in surfactant solutions. *Journal of Colloid and Interface Science* **1981**, *80* (2), 357-368.
6. Purcell, I.; Thomas, R.; J. Penfold, A. H. Adsorption of SDS and PVP at the air/water interface. *Colloids and Surfaces A: Physicochemical and Engineering Aspects* **1995**, *94* (2-3), 125-130.
7. Savelski, M. J.; Shetty, S. A.; Klob, W. B.; Cerro, R. L. Flow Patterns Associated with the Steady Movement of a Solid/Liquid/Fluid Contact Line. *Journal of Colloid and Interface Science* **1995**, *176*, 117-127.
8. Fuentes, J.; Cerro, R. L. Flow patterns and interfacial velocities near a moving contact line. *Experiments in Fluids* **2005**, *38*, 503-510.
9. Eastoe, J.; Dalton, J. S.; Rogueda, P. G. A.; Crooks, E. R.; Pitt, A. R.; Simister, E. A. Dynamic Surface Tensions of Nonionic Surfactant Solutions. *Journal of Colloid and Interface Science* **1997**, *188* (2), 423-430.
10. Tiberg, F.; Zhmud, B.; Hallstensson, K.; von Bahr, M. Capillary rise of surfactant solutions. *Physical Chemistry Chemical Physics* **2000**, *2*, 5189-5196.

## Appendices

### Appendix A Nomenclature

Other than where defined elsewhere, the following symbols are used:

$v$	Velocity
$\gamma_{lv, sv \text{ or } sl}$	Surface tension (liquid-vapour, solid-vapour or solid-liquid)
$R$	Radius
$\theta_{eq}$	Equilibrium contact angle
$\theta_d$	Dynamic contact angle
$g$	Acceleration due to gravity
$\eta$	Dynamic viscosity
$\nu$	Kinematic viscosity
$\rho$	Density
$l$	Length
$h$	Capillary rise height
$\Gamma$	Surface excess

## Appendix B Defined Terms

### Capillary Number

$$Ca \stackrel{\text{def}}{=} \frac{\mu v}{\gamma} \quad (\text{A.1})$$

A dimensionless quantity relating the balance of viscous stresses against interfacial tension stress

E.g. capillary number where speed is  $3.5 \text{ cm s}^{-1}$

$$Ca = \frac{10^{-3} \times 3.5 \times 10^{-2}}{0.07} = 5 \times 10^{-4} \quad (\text{A.2})$$

### Reynolds Number

$$Re = \frac{\rho R V}{\eta} \quad (\text{A.3})$$

The ratio of inertial to viscous forces

### Capillary Length

$$\lambda_c = \sqrt{\frac{\gamma}{\rho g}} \quad (\text{A.4})$$

Characteristic length scale of the meniscus due to gravity and surface tension<sup>1</sup>

### Capillary Pressure

$$p_c = \frac{2\gamma_{lv} \cos \theta}{R} \quad (\text{A.5})$$

The difference in pressure across the interface between two immiscible liquids

### Capillary Force

$$F_c = 2\pi R(\gamma_{sv} - \gamma_{sl}) \quad (\text{A.6})$$

The force by which water penetrates a capillary

### Drag

$$F_d = \int \left(\frac{dv}{dr}\right)^2 \eta dV \quad (\text{A.7})$$

### Péclet number

$$Pe_L = \frac{lv}{D} \quad (\text{A.9})$$

A dimensionless parameter for the ratio of the rate of advection (the transport of material by a moving fluid) to the rate of diffusion of the fluid driven by an appropriate gradient<sup>2</sup>

$L$  is the characteristic length and  $D$  the mass diffusion coefficient.

### Young-Laplace Equation

$$\Delta p = \frac{2\gamma}{r} \quad (\text{A.10})$$

### Lucas-Washburn Equation

$$h = \frac{2\gamma_{lv} \cos \theta}{\rho g r} \quad (\text{A.11})$$

### Weber Number

The inertial forces compared to the surface tension

$$We = \frac{\rho v^2 l}{\sigma} \quad (\text{A.12})$$

### Quéré Equation

For a constant rise velocity:

$$h = t \sqrt{\frac{1\sigma \cos \theta}{\rho R}} \quad (\text{A.13})^3$$

### Bibliography

1. Aarts, D. G. A. L. 1.Capillary Length in a Fluid–Fluid Demixed Colloid–Polymer Mixture. *The Journal of Physical Chemistry B* **2005**, *109* (15), 7407-7411.
2. Weisstein, E. W. Péclet Number.  
<http://scienceworld.wolfram.com/physics/PecletNumber.html> (accessed Sept 8, 2010).
3. Quéré, D. Inertial capillarity. *Europhysics Letters* **1997**, *39* (5), 533-538.

## rulerfft Function

### Contents

- [Rotation](#)

```
function [] = rulerfft(rulerfile)
    %{
    Image ruler on 1/2mm scale ans in m
    %}
    pic=imread(rulerfile);
```

### Rotation

```
    figure(1);
    imagesc(abs(pic(:,:,1)));
    colormap gray; %axis off;
    disp('Just press middle button if you dont want rotation. ');
    disp('Left-click two points on axis. Right-click to undo; middle
button to accept. ');

    crds = getRotation(pic);

    if size(crds,1)==2
        pic=my_intilt(pic,crds,'pic'); % do rotation
        imagesc(pic);
    else
        disp('Rotation function bypassed');
    end
    trans=fft2(pic(60:80,:));
    vab=abs(mean(trans));
    stop=round(length(vab)/2);

    truncateby = 6; % how many lines to miss off the start , to avoid
big peak
    rulerfreq=vab(truncateby:stop);

    % plot(abs(mean(trans))); % plot the transform

    freq=max(rulerfreq);

    [maxno index] = max(rulerfreq);
    freq=index+truncateby-2; % remove 2 because index in pic (start 0)
is different to fft (start 1)

    %1/2mm to mm
    freq=freq/2;
    disp(['mm per pic: ', num2str(freq)]);
    global mmdist;
    mmdist=freq/size(pic,2);

    disp(['mm per px: ', num2str(mmdist), ' mm']);
end
```

## imageprocess Function

```
function [ result ] =
imageprocess(folder_to_data,current_folder,first_pic,end_pic,fps,bgrem
ove>manual_mode,lp)
```

### %% Set variables

```
fileprefix=[folder_to_data,current_folder];
clear folder_to_data;
sobelx1 = [-1 0 1; -2 0 +2; -1 0 1];
```

### %% Check rulerfft has been run

```
global mmdist;
if isempty(mmdist)
    error('AD:nofft','You need to run rulerfft first!');
end
px=1e-3*mmdist; % the pixel size is now in m
```

### %% Check file existence

```
if exist([fileprefix,num2str(first_pic),'.tif'],'file')
    pic=imread([fileprefix,num2str(first_pic),'.tif']);
    type='pic';
    picsize=size(pic);

elseif exist([fileprefix, '.avi'],'file')
    vid = mmreader([fileprefix, '.avi']);
    fps = vid.FrameRate; %the frame rate in frames per second
    picsize = [vid.Height,vid.Width];
    type='mov';
    if strcmp(end_pic,'end')
        end_pic=vid.NumberOfFrames;
    end

else
    error('imageprocess:noexist','File doesnt exist');
end

pausetime=1/fps;

no_pics=end_pic-first_pic+1;
```

### %% Different code for pictures and movies

```
pics=zeros(picsize(1),picsize(2),no_pics); %set initial size for speed
tic;
switch type
    case 'pic'
        for x= first_pic:end_pic
            pics(:, :, x-
first_pic+1)=mean(imread([fileprefix,num2str(x),'.tif']),3);
        end
    case 'mov'
        for x= first_pic:end_pic
            pics(:, :, x-first_pic+1)=mean(read(vid,x),3);
        end
end
```

```

        clear vid x;
    otherwise
        error('AD:notype','Type not set. Silly boy');
end
time=toc;
disp(['Loaded ',num2str(no_pics),' images in ',num2str(time),'
seconds']);

```

## %% Rotation

```

figure(1);
image(abs(pics(:,:,1)));
colormap gray;
disp 'Just press middle button if you dont want rotation.';
disp 'Left-click two points on axis. Right-click to undo; middle
button to accept.';

crds = getRotation(pics); %get the coords for rotation

if size(crds,1)==2
    pics=my_imtilt(pics,crds,type); % do rotation
else
    disp('Rotation function bypassed');
end

```

## %% End Trimming

```

trim = [];
figure(1);
image(pics(:,:,1)); colormap gray;
disp('select left trim, click outisde for no trim');
[x,y] = ginput(1);
trim.left=round(x);

if trim.left < 1 || trim.left > size(pics,2) || y < 1 || y >
size(pics,1)
    trim.left = 1;
end

image(pics(:,trim.left:end,1)); colormap gray; axis off;
disp('select right trim, click outisde for no trim');
[x,y] = ginput(1);
if x < 1 || x > size(pics,2) || y < 1 || y > size(pics,1)
    trim.right=0;
else
    sizepic=size(pics);
    trim.right=-(round(x)-sizepic(2));
end
pics = pics(:,trim.left:end-trim.right+trim.left,:);

```

## %% Meniscus location

```

image(pics(:,:,1)); colormap gray; axis off;
disp('Select Middle of Capillary');
[blank,menmiddle] = ginput(1);
menmiddle=round(menmiddle);

if lp>0
    menmiddle=round(menmiddle*lp); % need to scale ypic for lp_filtery
end

```

## %% Low pass filter

```

if lp>0
    if lp==1
        error('lp_filter:less1','lp needs to be less than one');
    end
    pics=lp_filter(pics,lp);
end

```

## %% Background subtraction

```

if bgremove
    bgsub=mean(pics,3);

    for x= 1:no_pics
        pics(:,:,x)=pics(:,:,x)-bgsub;
    end
    image(pics(:,:,1)); pause(1);
    clear bgsub;
end

```

## %% Manual Mode

```

dist=zeros(no_pics,1);

if manual_mode

    for x= 1:no_pics

        image(pics(:,:,x)); colormap gray; axis off; axis equal;
        if ~all(dist)==0
            disp('Click on meniscus, outside if not visible');
        end

        [xplic,yplic] = ginput(1);
        xplic=round(xplic);

        if xplic < 1 || xplic > size(pics,2) || ypic < 1 || ypic >
size(pics,1)
            xplic=0;
        end

        dist(x)=xplic;

    end

else % automatically
    dist2=zeros(no_pics,1);
    dist=zeros(no_pics,1);
    for x= 1:no_pics % loop over matrix
        pic=pics(:,:,x);

```

## %% Addition sobel

```

totals=sum(pic);

sumedge = conv2(totals,[-1 0 1],'same');

sumedge(1)=0;
sumedge(end)=0;

sumedge=abs(sumedge);

```

```
[blank, d2]=max(sumedge);
dist2(x) = d2;
```

## %% Edge finding algorithm

```
edge = conv2(pic, sobelx1, 'same');
edge(:,1:2)=0;
edge(:,end-1:end)=0;
line = double(pic(menmiddle,:));
edge=mean(edge(2:end-1,:));
[blank, dist(x)] = max(edge.*line);
image(pic); colormap gray; axis off;
hold on;
plot(dist(x), menmiddle, '-ob'); %Plot location on image as
green circle
plot(dist2(x), menmiddle, '-og');
hold off;
pause(pausetime);
end
end
frametime=1/fps; % get time length of each frame
timestep=0:frametime:(frametime*(no_pics-1));
figure(2);
dism=dist*px;
if manual_mode
    plot(timestep, dism);
    timesqrt=sqrt(timestep);
    result=[timestep.', dism, timesqrt.'];
    result = num2cell(result);
    result = [ {current_folder, fps, 'manual_mode'; 'time',
'distance', 'sqrt time' }; result ];
else
    dism2=dist2*px;
    plot(timestep, dism, timestep, dism2); legend('sobel', 'sobel sum')
    timesqrt=sqrt(timestep);
    result=[timestep.', dism, dism2, timesqrt.'];
    result = num2cell(result);
    result = [ {current_folder, fps, ' ', ' '; 'time',
'distance', 'distance(sum)', 'sqrt time' }; result ];
end
```

```
xlabel('Time (s)');
ylabel('Distance');

clear pics bgsb;
end
```

Published with MATLAB® 7.9

## lp\_filtery Function

```
% Low Pass filter to pixelate in y
function [low_passed_pic]= lp_filtery(pic, ratio)

sp = size(pic);

diff=sp(1)*ratio;

n=ceil((sp(1)/2)-diff/2);

m=floor((sp(1)/2)+diff/2);

fpic=fft2(pic);
fpic=fftshift(fpic);

fpic2=fpic(n:m,1:end,:);

fpic2=fftshift(fpic2);

pic2=ifft2(fpic2);
pic2=abs(pic2); %if pic real - line needed
low_passed_pic=pic2;
end
```

Published with MATLAB® 7.9

## my\_intilt Function

Code kindly adapted from Andy McKeague's rotation function

```
function [newpic] = my_intilt(pic, crds, type)
% This program takes a picture... allows you to select two points...
these two points define the new x axis... the program then rotates the
picture so that the new axis becomes the axis - geddit??
% I've ceiled it up cos to facilitate you turning it into two
functions. As I imagine you will only want to run the "Find the new
axis bit once per set".
clear all;
```

### %% Read in the image.

```
% Takes in... [filename] and spits out... [pic] - filename is the path
to the file, pic is the array forming your picture
s = size(pic);
intp = 'y'; %% !LOOK! Pick 'y' for nearest neighbour, 'n' for none,
or 'a' for an average fill in blank points.
```

## %% Perform the rotation

```

% This bit takes in... [pic, crds, s, intp] and spits out... [newpic]
Where... pic and crds are described above s is size(pic) intrp allows
you to chose what happens to the gaps in the rotated picture newpic is
the rotated picture
[x y] = meshgrid(1:s(2),1:s(1));           % Define original coordinates

A = [crds(1,2)-crds(1,1); crds(2,2)-crds(2,1)]; % Define vector of new
axis

Alen = sqrt( A(1).^2 + A(2).^2 );
A = A/Alen;                               % Make A a unit vector

B = [0 ; -1];                             % Define the old axis

tta = asin(dot(B,A)); % Define the angle between

x2 = x*cos(tta) - y*sin(tta); % Rotate xs and ys in the usual way.
y2 = x*sin(tta) + y*cos(tta);

x2 = round(x2); % Round so that they fall on pixels
y2 = round(y2);

% from here...
miny2 = min(min(y2));
maxy2 = max(max(y2));
minx2 = min(min(x2));
maxx2 = max(max(x2));
xshift = 0;
yshift = 0;
if miny2<0
    yshift = -1*miny2;
end
if minx2<0
    xshift = -1*minx2;
end
s2 = [(maxy2-miny2+2) (maxx2-minx2+2) size(pic,3)];
% to here... is all making this 's2' which will
% define the size of the square the rotated image will
% fit onto - going to be called 'newpic'

% The below batch of logic deals with the spaces left between pixels
in the rotated image. We do this by cunning choice of background
colour. If we define the new background, newpic, to be zeros then the
gaps are all black. ('n')
% If we define the newpic to be all the average colour of pic then the
gaps may blend in a little better. ('a')
% If we give the background a distinctive value - eg. pi - we can
later fill the cells with the value pi with an average value from the
adjacent cells. ('y')
if intp == 'y'
    newpic = ones(s2)*pi;
elseif intp == 'a'
    newpic = ones(s2)*mean(mean(pic));
else
    newpic = zeros(s2);
end

% This loop fills the pixels from pic into newpic according to their
new x and y values. (x2 and y2)
for m = 1:s(1)
    for n = 1:s(2)

```

```

        newpic(y2(m,n)+yshift+1,x2(m,n)+xshift+1,:) = pic(m,n,:);
    end

end

s = size(newpic);

% The much talked about filler-inner.
if intp == 'y'
    for loop=1:size(pic,3)
        for m = 2:s(1)-1
            for n = 2:s(1)-1
                if newpic(m,n,loop) == pi;
                    c1 = [newpic(m+1,n,loop),newpic(m-
1,n,loop),newpic(m,n+1,loop),newpic(m,n-1,loop)];
                    c2 = 0;
                    l = 0;
                    for ct2 = 1:4
                        if c1(ct2) ~= pi
                            c2=c2+c1(ct2);
                            l = l+1;
                        end
                    end
                    mc2 = c2/l;
                    if mc2>0
                        newpic(m,n,loop) = mc2-pi;
                    end
                end
            end
        end
    end
end
newpic(newpic==pi) = 0; % Set the outsides back to 0;

```

Published with MATLAB® 7.9

## getRotation Function

Code extracted from my\_intilt function

```

function [crds] = getRotation(pics)

    but=0;
    ct = 1;
    crds = [];
    while but ~= 2 || size(crds,2)<2 && ~strcmp(crds, 'no')
        clear a b;
        [a,b,but] = ginput(1);
        if but == 1 && size(crds,2)<2
            crds(1,ct) = a;
            crds(2,ct) = b;
            ct = ct+1;
        end
        if but == 2 && size(crds,2)==0;
            crds='no'; % bypass rotation
        elseif but == 3 && size(crds,2)>1
            ct = 2;
            crds = crds(:,1);
        elseif but == 3 && size(crds,2)==1
            crds = [];
            ct = 1;
        end
    end

```

```
end
image(abs(pics(:,:,1))); colormap gray;
hold on;
try
    plot(crds(1,:),crds(2:,:), '-g')
    plot(crds(1,:),crds(2:,:), 'og')
catch ploterror;
end
hold off;
end
```

*Published with MATLAB® 7.9*